

**DOT/FAA/AR-05/23**

Office of Aviation Research  
Washington, D.C. 20591

# **Development of a Reference Liquid Water Content Probe**

August 2005

Final Report

This document is available to the U.S. public  
through the National Technical Information  
Service (NTIS), Springfield, Virginia 22161.



U.S. Department of Transportation  
**Federal Aviation Administration**

## **NOTICE**

This document is disseminated under the sponsorship of the U.S. Department of Transportation in the interest of information exchange. The United States Government assumes no liability for the contents or use thereof. The United States Government does not endorse products or manufacturers. Trade or manufacturer's names appear herein solely because they are considered essential to the objective of this report. This document does not constitute FAA certification policy. Consult your local FAA aircraft certification office as to its use.

This report is available at the Federal Aviation Administration William J. Hughes Technical Center's Full-Text Technical Reports page: [actlibrary.tc.faa.gov](http://actlibrary.tc.faa.gov) in Adobe Acrobat portable document format (PDF).

1. Report No. <b>DOT/FAA/AR-05/23</b>		2. Government Accession No.		3. Recipient's Catalog No.	
4. Title and Subtitle <b>DEVELOPMENT OF A REFERENCE LIQUID WATER CONTENT PROBE</b>				5. Report Date <b>August 2005</b>	
				6. Performing Organization Code	
7. Author(s) <b>J. Tan, M. Papadakis, and S. Muthuswamy</b>				8. Performing Organization Report No.	
9. Performing Organization Name and Address <b>Department of Aerospace Engineering Wichita State University Wichita, KS 67260</b>				10. Work Unit No. (TRAIS)	
				11. Contract or Grant No.	
12. Sponsoring Agency Name and Address <b>U.S. Department of Transportation Federal Aviation Administration Office of Aviation Research Washington, DC 20591</b>				13. Type of Report and Period Covered <b>Final Report</b>	
				14. Sponsoring Agency Code <b>AIR-100</b>	
15. Supplementary Notes <b>The FAA William J. Hughes Technical Center Technical Monitor was Manny Rios.</b>					
16. Abstract <p>This study reports on the development and calibration of a proof-of-concept reference probe for measuring the liquid water content (LWC) as defined in Title 14 Code of Federal Regulations Part 25, Appendix C and in supercooled large droplet icing cloud conditions. The conceptual design was based on a total pressure probe, water collector, and suction fan. Water droplets were collected iso-kinetically by the probe and weighed to determine the LWC. The initial effort concentrated on the evaluation of different methods of capturing and storing water droplets that entered the probe. Different types of adsorbent materials were installed into a detachable water collector to remove water droplets from an ingress water cloud via adsorption, e.g., with water adsorbent and blotter papers, silica gel and molecular sieve desiccants, and hydrophobic B-Gon fiber mesh. The basic test methodology was to inject a known amount of water directly into the probe inlet and then compare this to the amount adsorbed by the water collector. Tests conducted in a laboratory showed that collection efficiencies of <math>100.8 \pm 8\%</math> for LWC between 0.5 and <math>3.0\text{g/m}^3</math> were obtainable with the water collector configuration 11 Mod-I design. This design used a combination of blotter paper, silica gel, and B-Gon fiber to adsorb and trap incoming water droplets. However, silica gel desiccants adsorb ambient moisture (as well as water droplets from the spray cloud) that is difficult to quantify; therefore, the test data contained some measurement errors. In order to overcome this problem, the silica gel desiccant was removed from the Mod-I design, and instead, the ambient moisture was measured with an accurate humidity sensor, which was installed inside the probe. The modified probe was renamed the configuration 11 Mod-II design. Limited laboratory test results showed that collection efficiencies of <math>92 \pm 8\%</math> were obtainable with the Mod-II design. The iso-kinetic performance of the probe was successfully tested in the wind tunnel at velocities between 105 and 130 mph, where the iso-kinetic condition was attained within 3 seconds of engaging the suction fan of the probe. In summary, the study has successfully demonstrated a proof-of-concept reference probe in a laboratory and wind tunnel. However, further developments are required before it can be used as a production probe to measure LWC in Appendix C and large median volumetric diameter spray clouds.</p>					
17. Key Words <b>Aircraft icing, Liquid water content probe, Iso-kinetic conditions</b>			18. Distribution Statement <b>This document is available to the public through the National Technical Information Service (NTIS) Springfield, Virginia 22161.</b>		
19. Security Classif. (of this report) <b>Unclassified</b>		20. Security Classif. (of this page) <b>Unclassified</b>		21. No. of Pages <b>135</b>	22. Price

## ACKNOWLEDGEMENTS

This work was supported by a grant from the Federal Aviation Administration (FAA). The authors would like to thank Mr. Manny Rios and Dr. James T. Riley of the FAA William J. Hughes Technical Center; Mr. Eugene Hill, the FAA Icing National Resource Specialist; and Tom Bond, the Chief of the Icing Branch at the NASA Glenn Research Center for their support. The authors acknowledge the efforts of the following Wichita State University (WSU) personnel: Hsiung-Wei Yeong and the wind tunnel crew for their assistance with the wind tunnel tests; Mark Murrell and Art Porter of the WSU Machine Shop for their efforts in fabricating the probe.

## TABLE OF CONTENTS

	Page
EXECUTIVE SUMMARY	xiii
1. INTRODUCTION	1-1
2. DESIGN OF AN ISO-KINETIC PROBE	2-1
2.1 Technical Design	2-2
2.2 Probe Fabrication	2-4
2.3 Computational Fluid Dynamics Analysis	2-7
2.3.1 Computational Fluid Dynamics Simulation of the LWC Probe in a Wind Tunnel	2-7
2.3.2 Computational Fluid Dynamics Simulation of the Water Collector	2-10
3. EXPERIMENTAL INVESTIGATION IN A LABORATORY	3-1
3.1 Experimental Setup	3-1
3.2 Water-Adsorbent Materials	3-4
3.3 Preliminary Tests	3-6
3.4 Water Collector Configuration Tests	3-8
3.5 Tests With Water Collector Configuration 11 Mod-I	3-20
3.5.1 Findings	3-28
3.5.2 Conclusions	3-28
4. EXPERIMENTAL INVESTIGATION IN A WIND TUNNEL WITH THE WATER COLLECTOR CONFIGURATION 11 MOD-I DESIGN	4-1
4.1 Test Facility	4-1
4.2 Probe Installation	4-1
4.3 Iso-Kinetic Flow Control System	4-3
4.3.1 Throttling Valve	4-4
4.3.2 The ISFC Software and Data Acquisition System	4-5
4.4 Test Procedure	4-9
4.5 Test Measurements	4-10
4.6 Results and Discussions	4-14
5. EXPERIMENTAL INVESTIGATION WITH THE WATER COLLECTOR CONFIGURATION 11 MOD-II DESIGN	5-1

5.1	Method of Computing LWC With Relative Humidity Measurements	5-1
5.2	Test Measurements	5-2
5.3	Data Reduction	5-9
5.4	Results and Discussion	5-11
6.	SUMMARY	6-1
7.	CONCLUSIONS	7-1
8.	RECOMMENDATIONS	8-1
9.	REFERENCES	9-1
APPENDICES		
A—Characteristics of Silica Gel and Molecular Sieve Desiccants		
B—Water Collector Configuration Tests		
C—Test Procedure for Configuration 11 Mod-I		
D—Mod-I Test Data—Wind Tunnel		
E—Mod-II Test Data—Laboratory		
F—Fundamental Humidity Equations		

## LIST OF FIGURES

Figure		Page
2-1	Schematic Layout of LWC Reference Probe in a Wind Tunnel	2-1
2-2	Technical Drawing of the Reference Probe	2-3
2-3	Sealing Joint DRGW 1	2-3
2-4	Coannular Sectional View of the Water Collector	2-3
2-5	Flange 2	2-4
2-6	Flange 3	2-4
2-7	Flange 4	2-4
2-8	Flange 5	2-4
2-9	Components of the Probe	2-4
2-10	Probe Assembly	2-4
2-11	Probe Inlet—Side View	2-5
2-12	Probe Inlet—Bottom View	2-5
2-13	Probe With Total and Static Ports	2-5
2-14	Probe Main Body and Convergent Outlet Nozzle	2-6
2-15	Coannular Water Collector Container	2-6
2-16	Assembly of Water Collection System	2-6
2-17	Computational Grid of the Wind Tunnel and Probe	2-8
2-18	Solid Model of the Reference Probe	2-8
2-19	Predicted Streamlines—Side View	2-9
2-20	Predicted Velocity Vectors and Streamlines—Isometric View	2-9
2-21	Predicted Velocity Vectors and Streamlines—Top View	2-9
2-22	Computational Grid of the Reference Probe	2-10
2-23	Predicted Velocity Vectors Inside the Probe	2-12

2-24	Streamlines Distribution Inside the Probe	2-12
2-25	Velocity Contour Across Collector—Top View	2-12
2-26	Pressure Distribution Across Collector—Top View	2-12
2-27	Streamlines Distribution Inside Probe—Probe Main Body Removed	2-13
2-28	Streamlines Distribution Inside Probe—Top View	2-13
3-1	Experimental Setup	3-1
3-2	Schematic Setup	3-1
3-3	Aerodynamic Performance of Suction Fan	3-2
3-4	Direct Method of Water Injection With the Spray Brush	3-3
3-5	Water Collector Assembly	3-3
3-6	Various Components of the Collector	3-3
3-7	Method of Installing Silica Gel and Molecular Sieve	3-4
3-8	Water-Adsorbent Paper Wrapped Around Inner Container	3-4
3-9	B-Gon Wrapped Around Inner Container of Collector	3-4
3-10	Blotter Paper Attached to the Divergent Nozzle	3-4
3-11	Silica Gel	3-5
3-12	Molecular Sieve	3-5
3-13	DRIMOP	3-5
3-14	B-Gon Fiber Mesh	3-5
3-15	Water-Adsorbent Paper	3-6
3-16	Blotter Paper	3-6
3-17	Pressure Loss Devices With Three Different Opening Sizes	3-20
3-18	Installation of a Pressure Loss Device Downstream of the Suction Fan	3-20
3-19	Liquid Water Content (Water Collected) Versus LWC (Water Sprayed)	3-21
3-20	Liquid Water Content (Water Collected) Versus Collection Efficiency	3-21

3-21	Contributions to Collection Efficiency by Blotter Paper and Silica Gel	3-21
4-1	The WSU 7- by 10-ft Wind Tunnel Facility	4-1
4-2	Installation of the Reference Probe in the WSU 7- by 10-ft Wind Tunnel— Front View	4-2
4-3	Position of the Spray Brush in Front of the Probe Inlet	4-2
4-4	Water Supply for the Spray Brush	4-2
4-5	Humidity Sensor Vaisala	4-3
4-6	Humidity Sensor Inside the Reference Probe	4-3
4-7	Extension Hose Connects Probe to Suction Fan	4-3
4-8	Suction Fan Exhaust to Throttle Valve	4-3
4-9	Throttle Valve	4-4
4-10	Probe Inlet Pressure Versus Valve Driving Current	4-4
4-11	Data Acquisition System (SCXI-1001)	4-5
4-12	Iso-Kinetic Flow Control Software	4-6
4-13	Static Pressure Plots—Laboratory	4-8
4-14	Relative Humidity Plots—Laboratory	4-8
4-15	Temperature Plots—Laboratory	4-8
4-16	Preparation of the Reference Probe and ISFC Control	4-10
4-17	Comparison Between LWCs Based on Water Collected and Sprayed	4-11
4-18	Liquid Water Content Versus Collection Efficiency	4-11
4-19	Probe and Tunnel RH Distribution—Wind Tunnel in Operation	4-14
4-20	Probe and Tunnel Temperature Distribution—Wind Tunnel in Operation	4-14
4-21	Probe and Tunnel RH Distribution—Static Spray Test	4-15
4-22	Probe and Tunnel Temperature Distribution—Static Spray Test	4-15
4-23	Probe and Tunnel Pressure Distribution—Wind Tunnel in Operation	4-16

4-24	Probe and Tunnel Pressure Distribution—Static Spray Test	4-16
5-1	Humidity Sensor Inside the Reference Probe	5-3
5-2	Fisherbrand Humidity Sensor	5-3
5-3	Throttle Valve Installed in a Fume Cupboard	5-3
5-4	Iso-Kinetic Flow Control System	5-3
5-5	Method of Creating a Multilayered Blotter Tube	5-4
5-6	Comparison Between LWCs Based on Water Collected and Water Sprayed	5-4
5-7	Liquid Water Content Based on Water Collected Versus Collection Efficiency	5-4
5-8	Contribution to the LWC by Blotter, B-Gon, and Evaporated Water	5-5
5-9	Distribution of Probe Volumetric Mass Flow Ratio	5-5
5-10	Probe RH Distribution	5-10
5-11	Probe Static Pressure Distribution	5-10
5-12	Probe Temperature Distribution	5-10
5-13	Static Pressure Distribution—Test 2	5-12
5-14	Static Pressure Distribution—Test 7	5-12

## LIST OF TABLES

Table		Page
3-1	Test Results for Configuration 1	3-9
3-2	Test Results for Configuration 2	3-10
3-3	Test Results for Configuration 3	3-11
3-4	Test Results for Configuration 4	3-11
3-5	Test Results for Configuration 5	3-12
3-6	Test Results for Configuration 6	3-13
3-7	Test Results for Configuration 7	3-13
3-8	Test Results for Configuration 8	3-14
3-9	Test Results for Configuration 9	3-15
3-10	Test Results for Configuration 10	3-16
3-11	Test Results for Configuration 11	3-17
3-12	Test Results for Configuration 11 Mod-I	3-19
3-13	Test Results for Configuration 11 Mod-I (Laboratory)	3-22
4-1	Test Results for Configuration 11 Mod-I (Wind Tunnel)	4-12
5-1	Test Results for Configuration 11 Mod-II (Laboratory)	5-6

## EXECUTIVE SUMMARY

A proof-of-concept reference probe was fabricated from Perspex and high-density molecular weight polyethylene material to demonstrate the iso-kinetic technique of measuring liquid water content (LWC) in Title 14 Code of Federal Regulations (CFR) Part 25 Appendix C and in supercooled large-droplet icing cloud. The probe consisted of a 90 degree elbow inlet, water collector, external main body, and suction fan. Tests were conducted in a laboratory and wind tunnel to assess the probe's performance, such as the range of applicable LWC, tunnel velocities and water mass, and its measurement accuracy. The conceptual design was based on a total pressure probe that was connected to a water collector and suction fan. Iso-kinetic condition (i.e., capture area ratio of 1.0) was obtained by setting the static pressure at the probe inlet to the static pressure in the free stream. This was achieved by varying the volumetric flow rate through the probe with a metering valve so that the probe inlet velocity matched the tunnel free-stream velocity. Water droplets that entered the probe were collected in a removable container that was lined with water-adsorbent paper and desiccant material. The container was weighed (before and after a spray test) to determine the amount of water collected in a given duration. The LWC was determined from the collected water mass and volumetric air drawn into the probe.

The initial effort concentrated on the selection of the best performing water collector configuration, based on its collection efficiency, which was carried out mainly in a laboratory. The method of assessment involved injecting a known amount of water in the form of a water droplet cloud directly into the probe and then compare this to the amount collected by the water collector. The ratio between these two measurements defines the collection efficiency for a particular water collector configuration. Tests conducted in a laboratory showed that collection efficiencies of  $100.8 \pm 8\%$  for LWC between 0.5 and  $3.0\text{g/m}^3$  were obtainable with the water collector configuration 11 Mod-I design. This design used a combination of blotter paper, silica gel, and B-Gon fiber to adsorb and trap incoming water droplets. Lower collection efficiencies were obtained in the (limited) tests conducted in the Wichita State University 7- by 10-ft wind tunnel. It is believed that the dry conditions in the wind tunnel led to excessive evaporative loss in the water collector, hence, the poor measurements. The temperatures (in the test section) were approximately 100°F, and humidity ranged from 20% to 35%. The evaporative loss was detected with a humidity sensor that was installed inside the reference probe. However, the iso-kinetic performance of the probe was successfully tested in the wind tunnel at velocities between 105 and 130 mph, where the (iso-kinetic) condition was attained within 3 seconds of engaging the suction fan of the probe.

Although the conceptual workings of the Mod-I design was quite successful, there were some inherent measurement errors caused by the environment moisture that was adsorbed into the silica gel desiccant, which cannot be easily accounted for. To overcome this, the (silica gel) desiccant was removed from the Mod-I design, and instead, the ambient moisture was measured with an accurate humidity sensor that was installed inside the probe. The modified probe was renamed the configuration 11 Mod-II design. Limited laboratory tests showed that collection efficiencies of about  $92 \pm 8\%$  were obtained with the Mod-II design. The results were encouraging as it overcomes the significant drawback in the Mod-I design, and it provides a direct development path for converting this conceptual probe to a production design suitable for measuring LWC in 14 CFR Part 25 Appendix C and large MVD spray clouds.

## 1. INTRODUCTION.

This work was part of an ongoing effort to develop instrumentation for total liquid water content (LWC) measurements in supercooled large droplet (SLD) icing conditions. SLD splashing effects pose significant problems for current instrumentation used for measuring LWC. The icing blade and rotating cylinder, which are commonly used to measure LWC in icing wind tunnels, can provide accurate measurements in an icing spray cloud with a median volume diameter (MVD) less than 50 microns. However, it was reported that their accuracies tend to degrade with increasing MVD spray cloud [1]. Hot-wire probes also showed significant drop-off in response with large MVD cloud; therefore, some measurements have been known to vary by more than 20% from the mean values [2]. Limited experimental data showed that large droplets tend to splash on impact with solid surfaces [3 and 4], and it is believed that some of the original water mass may have been lost from the process, hence, poorer LWC measurements. Since a significant proportion of the droplet sizes in an SLD icing cloud are greater than 50 microns, there is a concern that current LWC instruments may not be able to provide accurate LWC measurements. It is important that accurate measurements in icing tunnels can be obtained for SLD conditions due to the need to develop experimental data that is directly applicable to certification and also for developing and validating icing codes, which can adequately predict ice shapes in these conditions.

To address this, a proof-of-concept iso-kinetic probe was developed to measure LWC in an SLD icing cloud. The advantage of an iso-kinetic probe is that it is less sensitive to droplet splashing; therefore, it can cope with large droplets or mixed-phase icing conditions. Unlike an icing blade or hot-wire LWC probes, droplets were drawn iso-kinetically into the probe and caught by a barrier filter. The amount (of water mass) collected was then weighed to provide a direct LWC measurement. The iso-kinetic condition defines a cylindrical stream tube in a spray cloud with a cross-sectional area equal to the probe's inlet area, hence, each measurement represents a discrete point in a spray cloud distribution. This (iso-kinetic) condition was achieved by nulling (or simply equalizing) the wall static pressures between the flows inside and outside of the probe, hence, equal velocities prevailed (inside and outside of the probe) [5].

The development of the probe required a considerable effort; therefore, it was undertaken in the following phases:

1. To construct and demonstrate the concept of iso-kinetic measurement of LWC.
2. To compare the LWC measured by the reference probe and an existing LWC instrument in a wind tunnel.
3. To fabricate a new airfoil-shaped reference probe suitable for wind tunnel.
4. To assess the probe's performance in an icing wind tunnel.

The current study included the following research steps:

- Conceptual design of the probe.
- Computational fluid dynamics (CFD) analysis of the probe.
- Fabrication and installation of the probe.
- Evaluation of different water collection techniques using a range of water absorption and hydrophobic materials.
- Selection of a collection technique and calibration tests in a laboratory.
- Development of software and instrumentation for iso-kinetic measurement.
- Testing in the Wichita State University (WSU) 7- by 10-ft wind tunnel.
- Report preparation.

This report describes the work performed and findings from the above steps. Significant effort was focused on the selection of an efficient water collector configuration in the icing laboratory. The method of assessment was based on the injection of a known amount of water directly into the probe and then measuring the amount collected by the water collector. The ratio between these two measurements defines the collection efficiency of the water collector. The water spray was created with a painter's brush that was placed near the probe's inlet nozzle. The iso-kinetic performance of the probe was evaluated in the WSU 7- by 10-ft wind tunnel. During the wind tunnel tests, a number of LWC measurements was also performed to evaluate the probe performance under more realistic conditions.

The report is arranged in the following manner:

- Section 1 introduces the topic of research and defines the needs for a probe that can accurately measure LWC in a SLD spray cloud.
- Section 2 describes the design and fabrication of the conceptual reference probe. It also describes the CFD simulations of the conceptual probe in a wind tunnel and the flow distribution through the water collector inside the probe.
- Section 3 describes the experimental tests that were conducted in a laboratory including 11 different water collector configurations. It also describes an extended test program with the selected water collector configuration that has the highest collection efficiency.
- Section 4 describes the experimental tests that were conducted in the WSU 7- by 10-ft wind tunnel with the selected water collector configuration. It also describes the development and performance of the iso-kinetic flow control (ISFC) system. A

discussion on the performance of the probe in terms of the water collection efficiencies based on a limited number of experimental data is also provided.

- Section 5 describes the performance of a modified probe in a laboratory. The highly efficient water collector from section 3, which had been tested in a laboratory and a wind tunnel, was modified to include a humidity sensor. This section describes the relevant humidity equations and discusses the results based on the limited water collection efficiency measurement data.
- Section 6 gives a summary of the work that led to the successful development of the reference probe.
- Section 7 provides conclusions on the performance of the probe based on the experimental tests conducted. It also provides data on the collection efficiencies and standard deviations of the probe with the selected water collector configurations.
- Section 8 lists recommendations for further work that aim to develop this proof-of-concept probe into an LWC instrument for Title 14 Code of Federal Regulations Part 25, Appendix C and SLD clouds.

## 2. DESIGN OF AN ISO-KINETIC PROBE.

Figure 2-1 shows a schematic layout of a reference (or iso-kinetic) probe in a wind tunnel that was conceived at the beginning of the study. It shows the probe mounted on the tunnel floor and connected to a suction pump. The difference in the static pressures from the probe inlet and the tunnel wall was fed to a computer system that was programmed to control a flow-metering valve. The software was developed to determine the amount of valve movement required to achieve iso-kinetic condition at the probe inlet. When this condition was set, the water spray was activated for a predefined duration and the water from the droplets entering the probe was deposited on a water collector inside the probe. The amount of water collected by the probe collector was then used to derive the LWC using the following expression:

$$LWC (g/m^3) = \frac{\text{Mass of water collected per unit time (g/s)}}{\text{Volume of air drawn by the probe inlet per unit time (m}^3\text{/s)}}$$

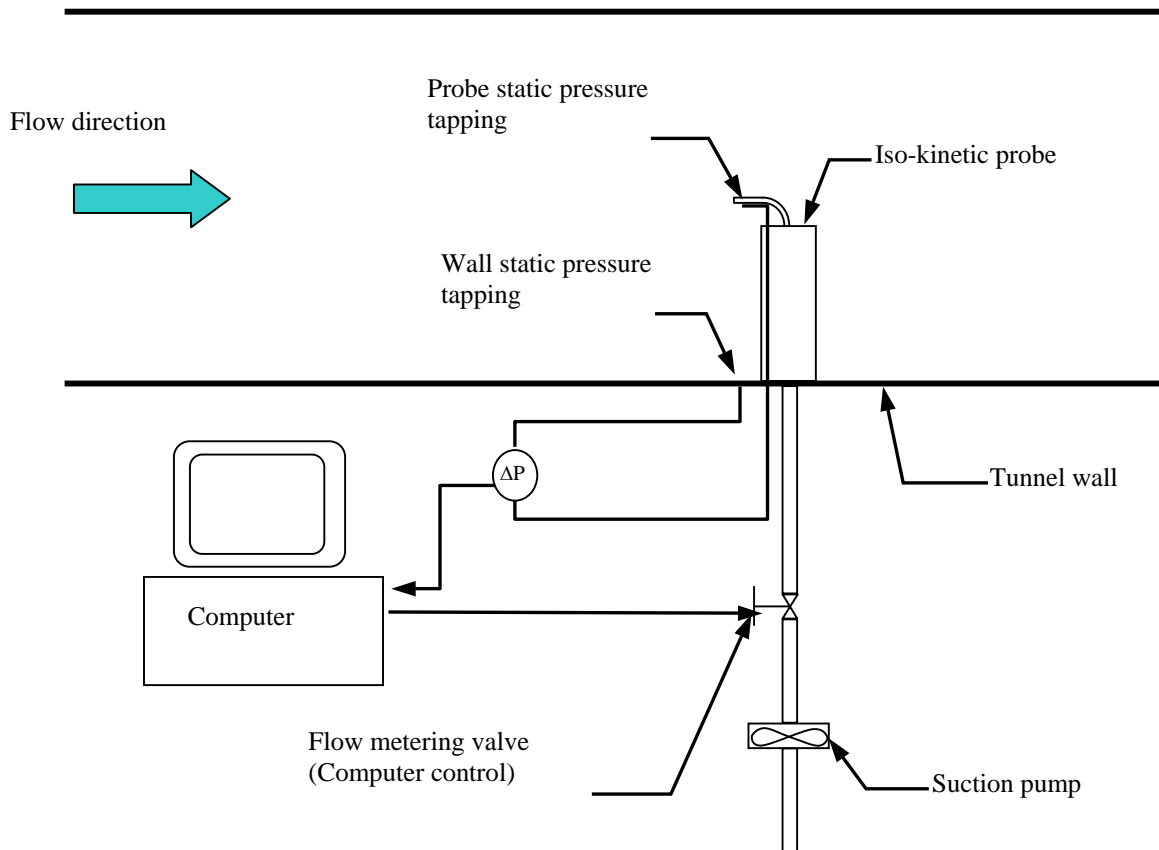


FIGURE 2-1. LAYOUT OF LWC REFERENCE PROBE IN A WIND TUNNEL

Limited information available from published literature [5] showed that a conceptual probe design could be based on a total pressure probe with a water collection (or filtration) system and suction fan to provide the necessary vacuum pressure. The basic design concept was adopted in

the current application for an icing wind tunnel. The anticipated performance of the probe is listed below.

- Capable of measuring LWC of up to  $3.0 \text{ g/m}^3$ .
- Capable of tunnel velocities of up to 200 mph (limited by the performance of the suction fan and probe inlet diameter of 1 inch).
- Low pressure loss across the water collector system to maximize probe inlet velocity.

Preliminary tests showed that desiccant materials such as silica gel and molecular sieve were able to adsorb water effectively; therefore, the conceptual water collector used these desiccant materials to adsorb the incoming water droplets. The tests also identified an industrial suction fan that could be used in the design. However, for operations at high tunnel speeds, the pressure loss across the probe must be kept to a minimum due to the limited vacuum power of the fan. This (low pressure loss) was achieved by having large internal volume to reduce the internal flow velocity through the water collector. In addition, lower flow velocities tend to enhance the water collection process. These probe design requirements were used to set nominal dimensions for the probe and water collector. To minimize fabrication costs, commercially available materials such as Perspex and polyethylene were selected for the construction of the probe.

The following section describes the technical design and fabrication of a conceptual probe. A CFD analysis was also conducted to support the design and development of the probe.

## 2.1 TECHNICAL DESIGN.

The design effort was directed mainly on the water collector whose primary function was to extract the water from a spray cloud. The conceptual design involved using two coannular (inner and outer) cylindrical containers that would be filled with water-adsorbent material.

After several technical discussions with the WSU machine shop personnel, a technical drawing of the conceptual design was produced, as shown in figure 2-2. This figure shows a 90 degree elbow tube attached to a solid base with a machined divergent nozzle. The water collector was attached to this divergent nozzle end, and the assembly was fitted onto a hollow tube that formed the probe's main body. Figure 2-3 shows the method of sealing the joints between the water collector assemblies and the tube. The probe's main body was attached to a solid base with a machined convergent nozzle for connection to a suction fan. The probe is 7 inches in height and 27 inches in diameter. Figure 2-4 shows a coannular sectional view of the water collector. Figures 2-5 to 2-8 show the supporting rings and structures needed to hold wire meshes that would form the walls of the coannular containers. The cross-sectional shapes of all the components were circular. The fabricated components of the reference probe are described in section 2.2.

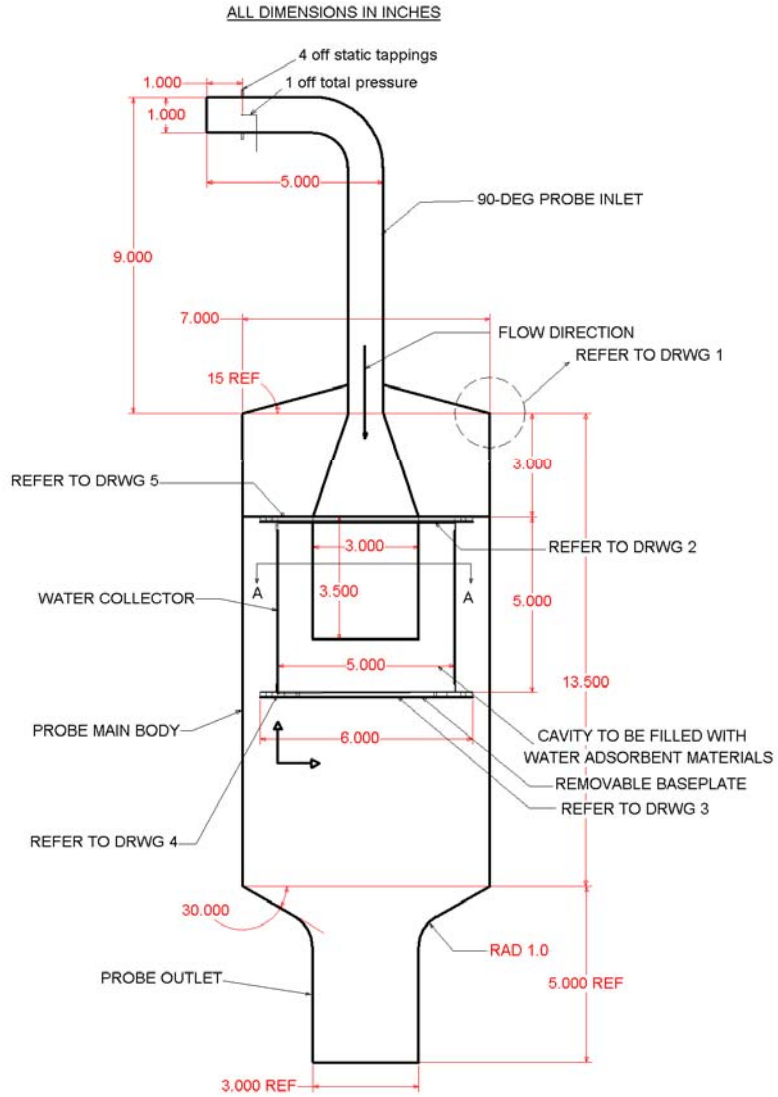


FIGURE 2-2. TECHNICAL DRAWING OF THE REFERENCE PROBE

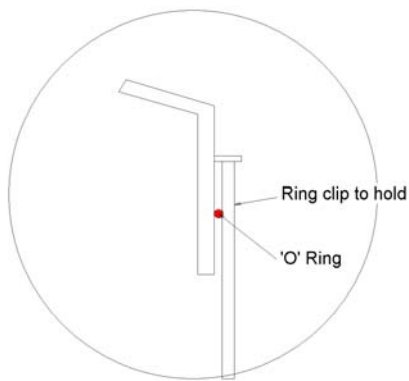


FIGURE 2-3. SEALING JOINT DRGW 1

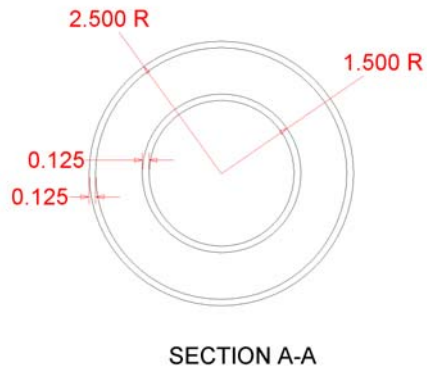


FIGURE 2-4. COANNULAR SECTIONAL VIEW OF THE WATER COLLECTOR

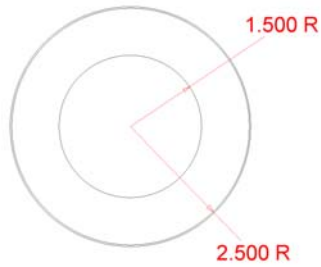


FIGURE 2-5. FLANGE 2

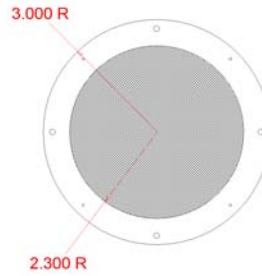


FIGURE 2-6. FLANGE 3

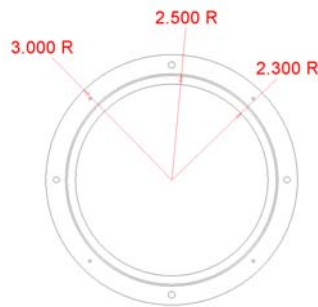


FIGURE 2-7. FLANGE 4

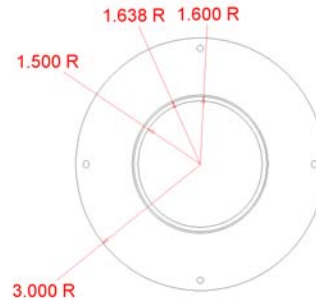


FIGURE 2-8. FLANGE 5

**2.2 PROBE FABRICATION.**

Most of the components shown in figures 2-2 to 2-8 were fabricated in-house. However, certain components such as the suction fan, metering valve, and desiccant materials were bought from external suppliers. The probe materials used included Ultra-High-Molecular Weight Polyethylene, which has a characteristic white plastic appearance and clear Perspex tube. Figure 2-9 shows the various components of the reference probe, and figure 2-10 shows the final assembly of the reference probe. A brief description of the various parts follows.

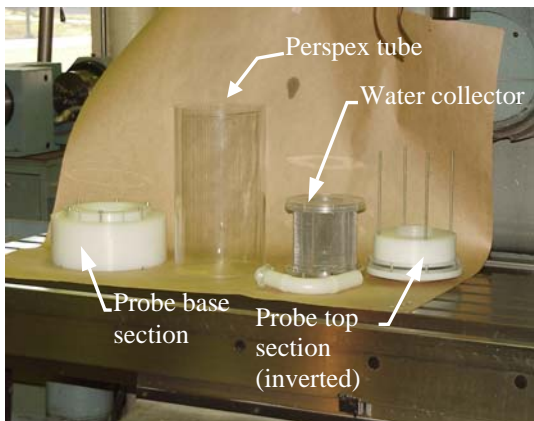


FIGURE 2-9. COMPONENTS OF THE PROBE



FIGURE 2-10. PROBE ASSEMBLY

The probe top section, figures 2-11 and 2-12, consisted of a 90 degree elbow tube (TNOS-90-100, Sani-Tech Canada) that was attached to a solid base section with the divergent nozzle (figure 2-11). The outer diameter of the tube was 1 inch, the tube thickness was 1/16 inch, and the tube dimensions were approximately 5.5 by 5.5 inches. (These tube dimensions were different from the technical drawing shown in figure 2-2 because, during the design phase, it was not known whether this would be fabricated or purchased from an external company). The 90 degree elbow tube was detachable from the solid base so that another elbow tube, which had been fitted with a total and static pressure ports, as shown in figure 2-13, could be used for inlet velocity measurement. The divergent nozzle (of the top section) was 3 inches in diameter at the base and extended for about 3 inches to join with the 90 degree elbow tube. The nozzle end was machined with an overhang lip (figure 2-12) to prevent surface water (in the probe interior) from being blown backward, a phenomenon that can occur when there are strong recirculating flows in the water collector chamber.

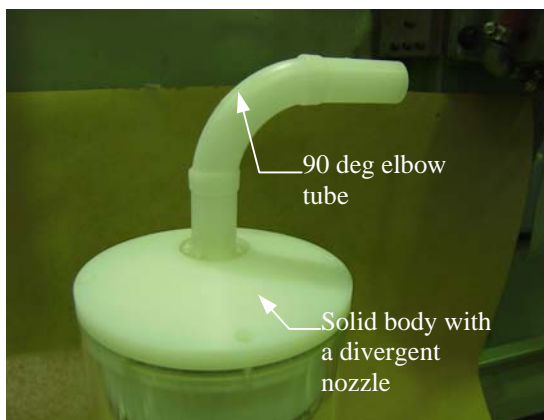


FIGURE 2-11. PROBE INLET—SIDE VIEW

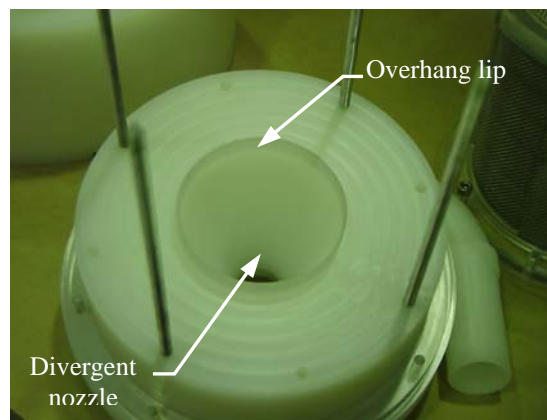


FIGURE 2-12. PROBE INLET—BOTTOM VIEW

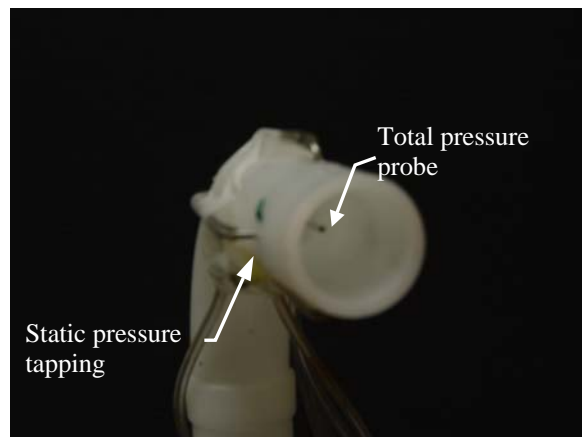


FIGURE 2-13. PROBE WITH TOTAL AND STATIC PORTS

The main body of the probe, shown in figure 2-14, consisted of a single clear Perspex tube that was attached to a solid base with a convergent nozzle. The inner diameter of this nozzle was 3 inches. The outer diameter of the tube was 7 inches, the tube thickness was 5/8 inch, and the tube length was approximately 14 inches. Clear Perspex was used because of the need for visual examination of the water collector during testing. The probe top section (with the 90 degree elbow) was attached to this body and was sealed with an O-ring, as shown in figure 2-3.

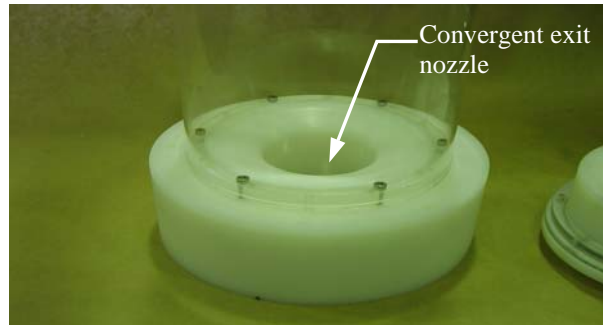


FIGURE 2-14. PROBE MAIN BODY AND CONVERGENT OUTLET NOZZLE

The removable water collection system (figure 2-15) was constructed from two coannular cylindrical containers. The diameter and length of the inner container were 3 and 3.5 inches, respectively, and the dimensions of the outer container were 5 and 5 inches respectively. This gave a void clearance of 1 1/2 inches at the bottom and 1 inch on the side. This (void) would be filled either with desiccant materials or hydrophobic fiber. Stainless steel wire mesh with 0.020 inch in diameter, 0.030 inch opening, and 36% porosity was used to form the sidewalls and base of the containers. The bottom wire mesh was removable for the filling of the water-adsorbent materials into the void clearance. Figure 2-16 shows the assembled water collector attached to the base of the probe top section with four elongated rods. It also shows the external supports for the wire mesh, which were machined from Perspex material.

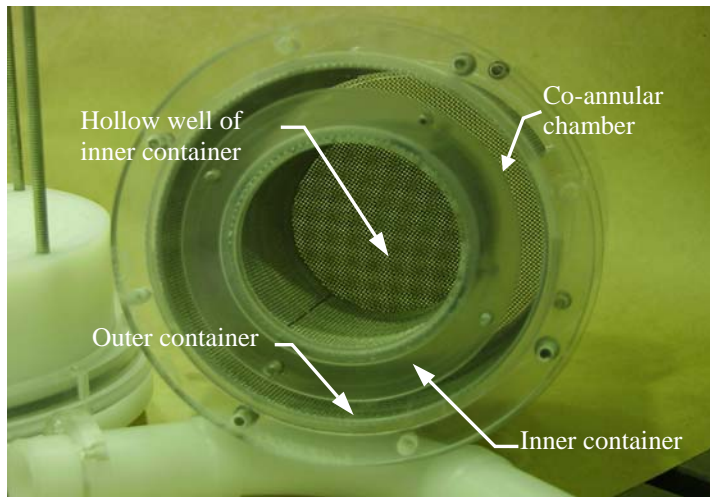


FIGURE 2-15. COANNULAR WATER COLLECTOR CONTAINER



FIGURE 2-16. ASSEMBLY OF WATER COLLECTION SYSTEM

During the operation of the probe, water droplets (from a spray cloud) that entered the probe inlet initially splashed and filmed on the 90 degree elbow tube. The inlet flow slowed down when it entered the divergent nozzle, which enhanced the process of water filming and runback on the internal surfaces. The slow moving air entered the hollow well of the water collector before going through the collector filter where the flow velocity was further reduced. This filter (or collector) consisted of desiccant materials such as silica gel or molecular sieve that adsorbed the water droplets during the transition (passage through the water-adsorbent layer) phase.

## 2.3 COMPUTATIONAL FLUID DYNAMICS ANALYSIS.

A CFD study was performed to assess the effect of the large probe main body on the flow distribution near the inlet nozzle and to investigate the flow behavior inside the probe. The analysis would be used to support the design and development of the probe. It was also hoped that the analysis would reveal the aerodynamic features of the probe prior to the experimental tests in a laboratory and wind tunnel. The commercially available FLUENT software (version 5.4) was used for this study. It must be noted that the CFD analysis was carried out during the fabrication phase, and the final 90 degree elbow tube dimensions, described in section 2.2, were not used in the analysis. As will be shown in section 3, the selected configuration of the water collector was also quite different from the current design.

The following CFD analysis was carried out:

- Simulation of the probe in the WSU 3- by 4-ft wind tunnel. The smaller tunnel was initially selected for experimental tests based on tunnel schedule and cost constraints. The final tests, however, were conducted in the larger 7- by 10-ft tunnel because of probe installation issues in the smaller tunnel facility. Although the CFD analysis was conducted with the smaller tunnel, it was felt that the results will be applicable to the larger tunnel facility because the tunnel blockage due to the probe was less than 10 percent based on the 3- by 4-ft test section. The blockage for the larger tunnel was about 2%.
- Simulation of the water collector. The main objective of this analysis was the flow distribution inside the water collector and the passage through the water absorption medium. This medium was simulated in FLUENT as a packed bed using an empirically specified pressure loss.

The reason for the separate internal and external flow analyses was to reduce the computer effort that would have been required to create a single large computational grid for the internal and external probe geometry and the wind tunnel. The coupling of the external flow and internal flow analyses was accomplished by using the iso-kinetic flow condition at the inlet of the probe for a specified tunnel speed.

### 2.3.1 Computational Fluid Dynamics Simulation of the LWC Probe in a Wind Tunnel.

The WSU 3- by 4-ft facility is an open loop wind tunnel and is powered by a 200-horsepower (hp) electric motor that drives a four-bladed, 11-ft-diameter propeller. It can generate flow velocities up to 200 mph (90 m/s) in a 3- by 4- by 4-ft-long test section. A computational grid

was created to simulate the test section of the wind tunnel. The upstream end of the test section was extended by 5 ft, whereas the downstream end was extended by 3 ft. The final dimensions of the grid were 3 by 4 by 12 ft. The probe was located in the middle of the wind tunnel floor and about 7 ft from the inlet. The extended inlet section ensured a fully developed velocity profile at the inlet, while the elongated downstream section ensured complete mixing of any flow separation occurring aft of the probe.

Figure 2-17 shows a three-dimensional computational grid of the test section including the reference probe. A total of 800,000 tetrahedral cells were used to create the grid. Figure 2-18 shows a close-up view of the reference probe. Grid refinement was applied around the probe and tunnel walls. The inlet velocity was set to 110 mph (50 m/s) and turbulent intensity was set to 1%. The inlet velocity profile was assumed to be uniform. The tunnel exit was simulated as a pressure boundary and was set to an absolute pressure of 14.46 psi. To simulate iso-kinetic flow, the probe inlet nozzle was also simulated as a pressure boundary, but the gauge pressure was set to the tunnel exit pressure. The reasons for this were (1) the initial probe inlet pressure was not known a priori and (2) the short distance between the probe and tunnel exit, and the assumption of smooth wall conditions (hence, low wall frictional losses), implied that their static pressures be similar. Therefore, the tunnel wall static pressure, at the location of the probe inlet, can also be assumed to be equal to the free-stream static pressure at the test section outlet.

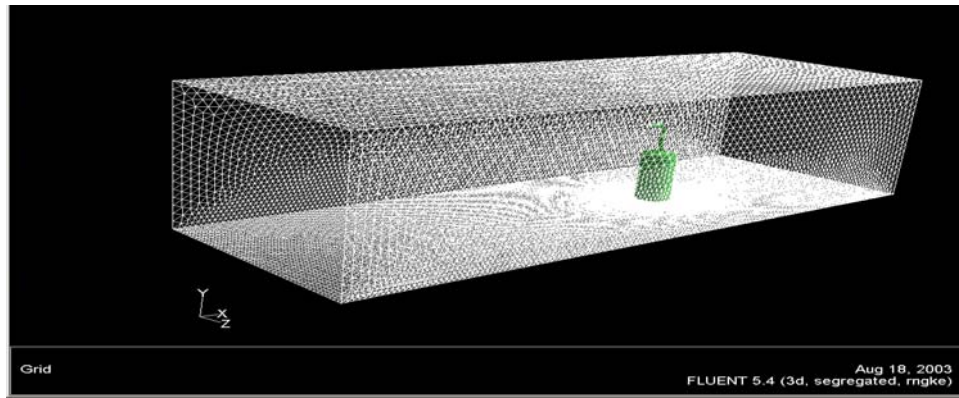


FIGURE 2-17. COMPUTATIONAL GRID OF THE WIND TUNNEL AND PROBE

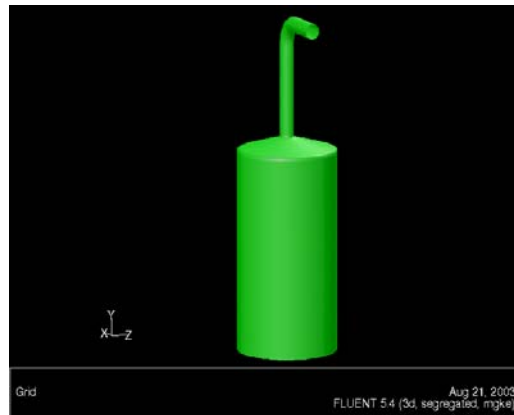


FIGURE 2-18. SOLID MODEL OF THE REFERENCE PROBE

The analysis employed the SIMPLE algorithm in the FLUENT software because the pressure-velocity dependency was negligible since the tunnel velocity was quite low. The  $k-\epsilon$  RNG turbulence model and near-wall functions were also applied to simulate turbulent flow.

Figures 2-19 and 2-21 show the predicted streamlines and velocity vectors around the reference probe (velocity magnitudes are indicated by the color distributions). The streamlines in figure 2-19 indicate a small upturn in flow direction near the edge of the top section (of the probe) where the free stream approaches the probe. However, this small upturn flow has no significant effect on the free stream near the probe inlet. Close-up views of the flow field in figures 2-20 and 2-21 indicate that the streamlines entering the probe inlet were parallel, demonstrating that the flow at the probe inlet was iso-kinetic flow (i.e., same velocity as the free stream). The separated flow regions aft of the main body of the probe and the 90 degree elbow tube, shown in figure 2-21, were also quite small and had no significant effect on the probe inlet flow.

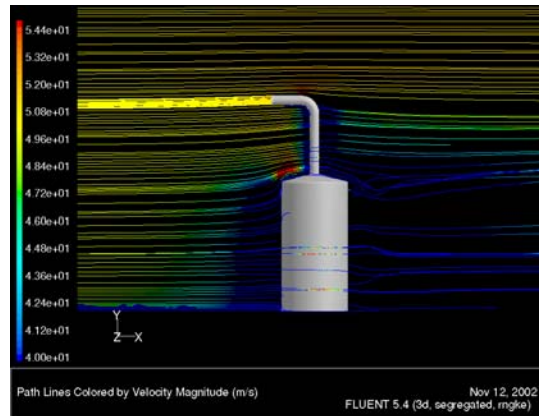


FIGURE 2-19. PREDICTED STREAMLINES—SIDE VIEW

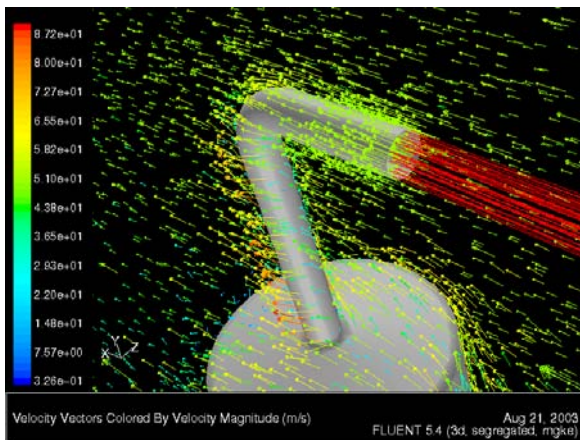


FIGURE 2-20. PREDICTED VELOCITY VECTORS AND STREAMLINES— ISOMETRIC VIEW

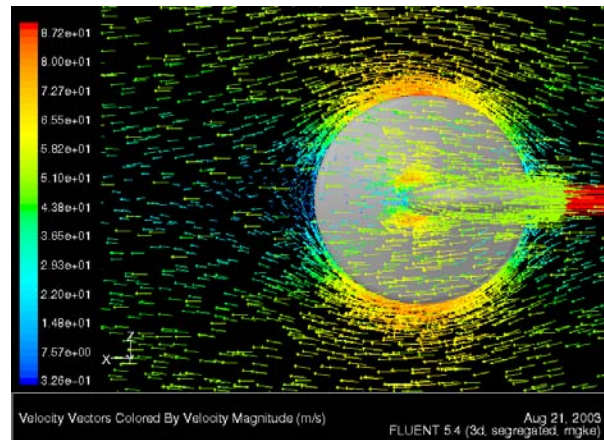


FIGURE 2-21. PREDICTED VELOCITY VECTORS AND STREAMLINES— TOP VIEW

### 2.3.2 Computational Fluid Dynamics Simulation of the Water Collector.

The technical design, shown in figure 2-2, was used to create a computational grid of the reference probe shown in figure 2-22. The coannular water collector was modeled as two thin cylindrical shells. The inner container (or shell) has a hollow well (3 inches in diameter) that was attached to the divergent nozzle of the probe top section. Figure 2-22 shows the computational grid of the probe including the water collector. A total of 100,000 tetrahedral cells were used to model the probe geometry. No grid refinement was used because it was not possible to define the pressure drop across the porous medium with any degree of accuracy due to the lack of experimental data. Therefore, only approximate flow distributions inside the probe could be expected from the predicted results.

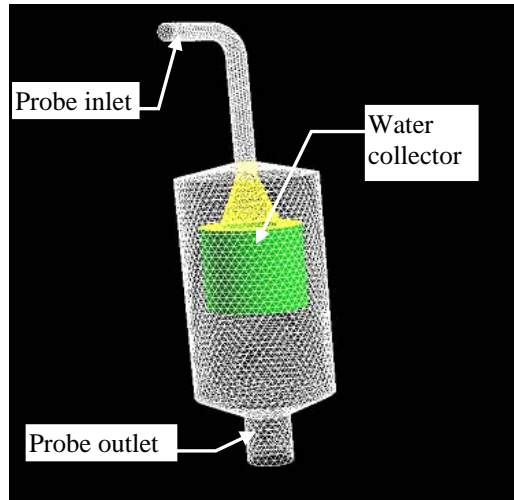


FIGURE 2-22. COMPUTATIONAL GRID OF THE REFERENCE PROBE

Pressure boundary conditions were applied at the probe inlet and outlet ports of the probe. The total pressure at the probe inlet was fixed to ambient total pressure. The probe inlet velocity was computed from the CFD analysis. The gauge pressure at the probe outlet was set to an absolute pressure of 14.55 psi to simulate suction. The pressure boundary condition at the probe outlet was intended to simulate realistic suction pressure that would have been provided by a suction fan.

The collector, simulated as a packed bed, consisted of silica gel pellets. Molecular sieve desiccants were not modeled due to time and cost constraints. The FLUENT software employs Ergun's correlation to simulate flows through a porous medium. The semiempirical correlation is applicable for a range of Reynolds numbers and types of packed beds, and is written as follows:

$$\frac{\nabla p}{L} = \frac{150\mu(1-\varepsilon)^2 v}{D_p^2 \varepsilon^3} + \frac{1.75\rho(1-\varepsilon) V^2}{D_p \varepsilon^3} \quad (2-1)$$

where

- $\nabla p$  = pressure drop across porous medium (Pa)
- $\rho$  = air density (kg/m<sup>3</sup>)
- $\mu$  = air viscosity (kg/ms)
- $\varepsilon$  = void fraction
- $D_p$  = mean particle diameter (m)
- $v$  = superficial velocity flowing through the medium (m/s)
- $L$  = thickness of the porous medium (m)

The FLUENT software requires the above terms to be entered as the pressure loss coefficients,  $\alpha$  and  $\beta$ , which are written as follows:

$$\frac{\nabla p}{L} = \frac{\mu v}{\alpha} + \frac{\rho v^2}{2} \beta \quad (2-2)$$

When the flow through the porous medium is turbulent, which was assumed in the present analysis, the first term in equation 2-1 is usually zero. (For laminar flow, the second term tends to zero.) Therefore, ignoring the first term and comparing equation 2-2 with 2-1 gives

$$\beta = \frac{3.5(1 - \varepsilon)}{D_p \varepsilon^3} \quad (2-3)$$

The mean diameter of silica gel was 0.050 inch (1.27e-3m). The void fraction (in equation 2-3) was estimated since no data could be found in published literature. Through a process of trial and error, the void fraction value of 0.4 ( $\beta \sim 26,000$ ) was found to provide a probe inlet velocity of approximately 110 mph (50m/s). Higher velocity range was not investigated due to time and cost constraints. The probe inlet turbulent intensity was set to 1%, which was similar to the value previously set for the wind tunnel computations. The analysis employed the SIMPLE algorithm in FLUENT, together with the k- $\varepsilon$  RNG turbulence model and near-wall functions. The predicted results are shown in figures 2-23 to 2-28.

Figure 2-23 shows that the flow velocity remained fairly constant along the 90 degree elbow tube until it reached the divergent section where a nonuniform decelerating flow was found. The core flow depicted in figure 2-24 is biased towards one side of the divergent section and the hollow well of the inner container. The inlet velocity of 110 mph (50 m/s) was reduced to about 4 mph (2 m/s) inside the hollow well. To assess the pressure distribution inside the collector, a contour plane was created at about 2.3 inches from the top edge of the water collector, as shown in figure 2-27. Contour plots of the Y-velocity component and static pressure distributions are shown in figures 2-25 and 2-26, respectively. These figures show two distinct flow patterns, which suggest that a recirculating flow has developed inside the inner container. Figures 2-27 and 2-28 show the flow streamlines through the water collector (or porous medium). These streamlines indicate that the flow was uniformly distributed around the collector.

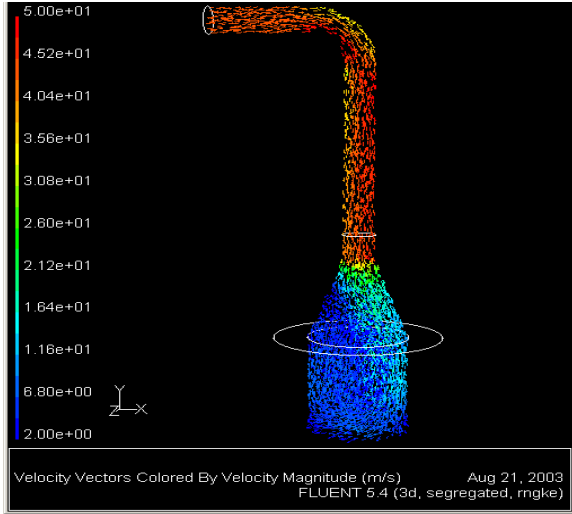


FIGURE 2-23. PREDICTED VELOCITY VECTORS INSIDE THE PROBE

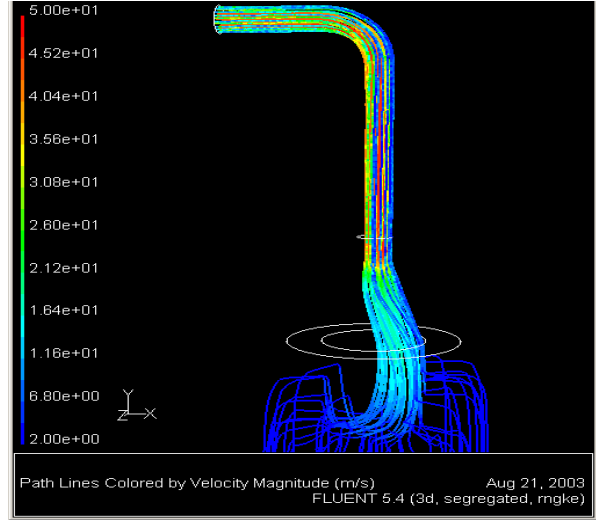


FIGURE 2-24. STREAMLINES DISTRIBUTION INSIDE THE PROBE

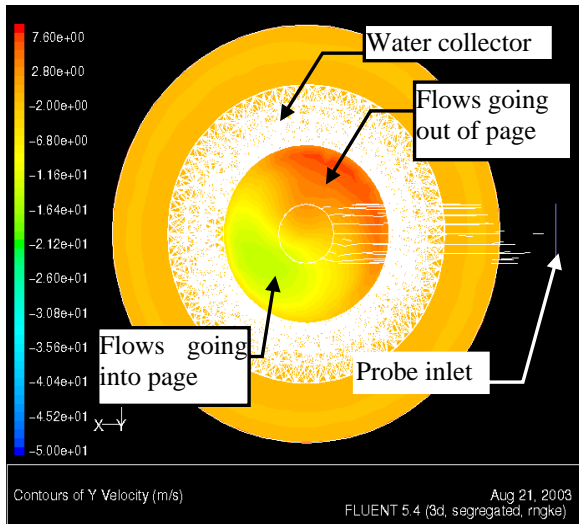


FIGURE 2-25. VELOCITY CONTOUR ACROSS COLLECTOR—TOP VIEW

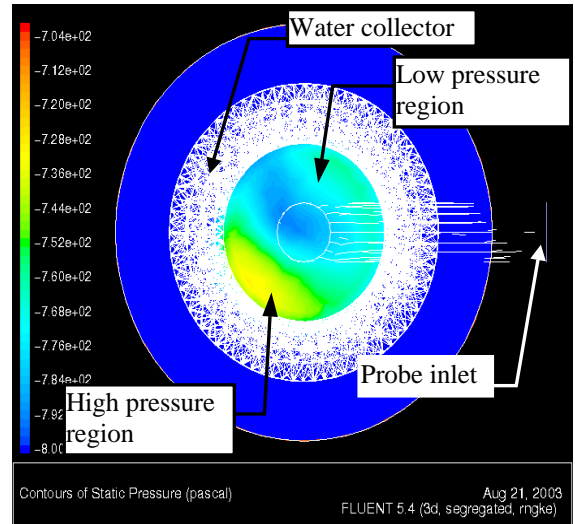


FIGURE 2-26. PRESSURE DISTRIBUTION ACROSS COLLECTOR—TOP VIEW

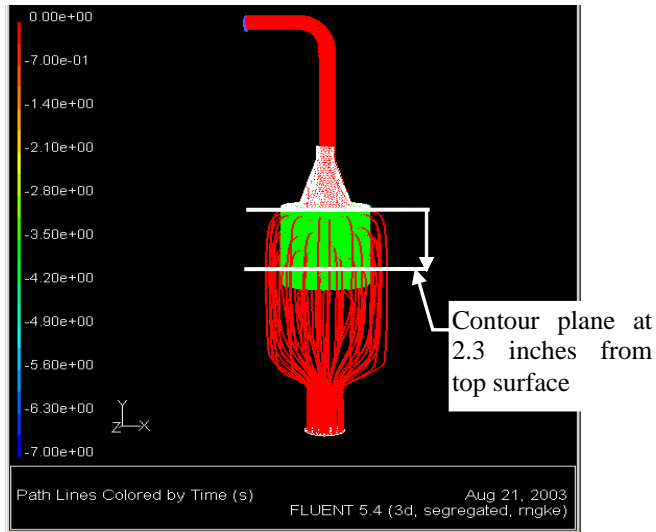


FIGURE 2-27. STREAMLINES DISTRIBUTION INSIDE PROBE— PROBE MAIN BODY REMOVED

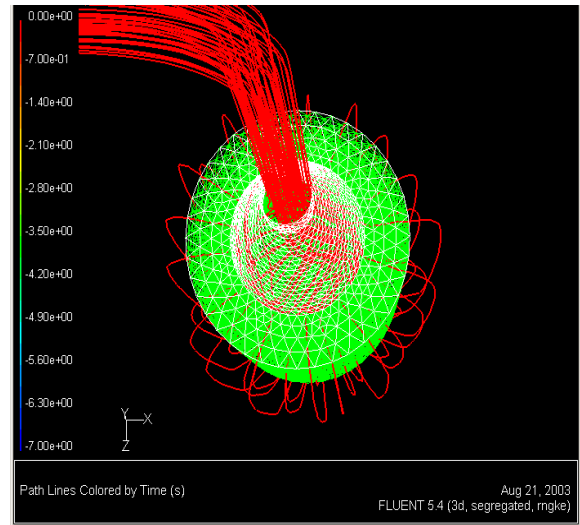


FIGURE 2-28. STREAMLINES DISTRIBUTION INSIDE PROBE— TOP VIEW

In summary, the CFD analysis performed indicate the following trends:

- The large probe main body has negligible effects on the iso-kinetic flow at the probe inlet.
- The flow separation aft of the probe was quite small; therefore, the effects on the iso-kinetic flow were also negligible.
- The flows inside the probe were biased towards one side of the divergent nozzle that continued into the inner container.
- A recirculating flow might have developed inside the hollow well of the inner container.
- The flow distribution through the porous medium had exhibited an even distribution around the outer container. However, this (effect) may be due to the boundary conditions that were used to simulate the porous medium.

### 3. EXPERIMENTAL INVESTIGATION IN A LABORATORY.

This section describes the experimental tests with the reference probe that was conducted in the laboratory. It also describes the experimental setup, characteristics of the water-adsorbent materials used, and the different methods of water collection employed during the investigation. The basic test methodology was to weigh the water collector that contained the adsorbent materials (and adsorbed water) and compare this to the amount of water injected directly into the probe. The main experimental effort involved the selection of a water collector configuration capable of high collection efficiencies over a range of LWC intensities. The selected collector configuration was subjected to an extended test program to define its collection efficiency. The equipment used in the tests included the reference probe, suction fan, U-tube water manometer, and an air-spray brush.

#### 3.1 EXPERIMENTAL SETUP.

Figure 3-1 shows the basic experimental setup, which was designed to conduct water collection efficiency tests on the reference probe. Figure 3-2 shows a similar schematic layout of the reference probe, suction fan and a U-tube water manometer. Figure 3-1 shows the reference probe attached to a wooden base, which was used to raise the probe above the floor so that the flexible hose connecting the probe outlet to the suction fan could be attached to the probe. The 90 degree elbow tube of the probe was equipped with four static pressure ports; however, only one port was connected to the single-channel water manometer during the early tests because the pressure differences between the four ports was minimal. No flow control was used to set isokinetic conditions at the inlet since the initial effort was directed at selecting an efficient method of water collection.

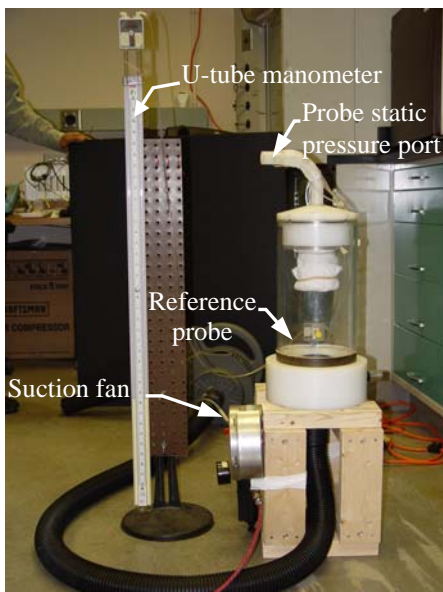


FIGURE 3-1. EXPERIMENTAL SETUP

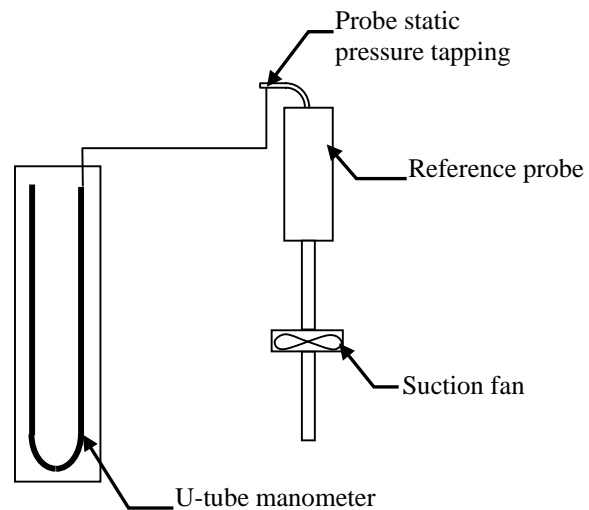


FIGURE 3-2. SCHEMATIC SETUP

A description of the main components of the experimental setup (figure 3-1) is given below.

- Suction Fan—The suction fan was part of a standard 6.5-hp industrial wet and dry vacuum system (RIDGID WD#1735, Emerson Tool Company). The vacuum system consisted of a storage base tank, two extension wands, two 6-ft flexible hoses, and several hose couplings. The suction fan had an inlet and an outlet port, and was normally attached to the base tank. However, this (tank) was removed to optimize the vacuum produced by the fan. The aerodynamic performance of the fan was determined by slowly increasing the flow resistance at the inlet port (blocking with increasing number of porous layers) while the outlet port was opened to the atmospheric conditions. By taking the ratio of the static pressures of the inlet ( $P_1$ ) and outlet ports ( $P_2$ ) over a range of volumetric flows, the pressure ratios ( $P_2/P_1$ ) as a function of volumetric flow rate were obtained, as shown in figure 3-3.

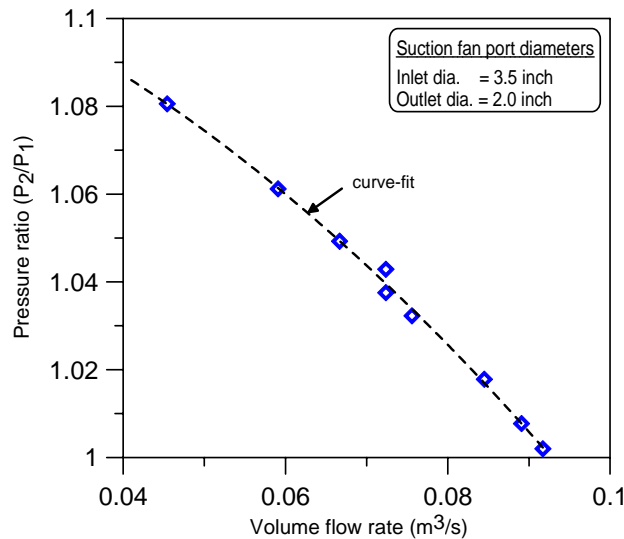


FIGURE 3-3. AERODYNAMIC PERFORMANCE OF SUCTION FAN

- Spray Brush—An air-spray brush (Paasche double action airbrush, #VL-SET, Passche Airbrush Company) was used to generate water droplets in the form of a spray cloud. The brush (figure 3-4) was approximately 6 inches long by 5/8 inches in diameter (measured at 3 inches from exit nozzle). Water from a small glass bottle was drawn into the brush nozzle via a vacuum created by a high-pressure air supply that was connected near the brush exit nozzle. The cloud plume size and penetration length depended on the spray pressure and a lever that controlled the water flow rate, e.g., at 30 psig and midlevel lever setting, the plume size was approximately 12 inches long and 3 inches in diameter (measured at about 6 inches from the spray nozzle exit). The droplet sizes produced by the spray brush were not measured (due to time and cost constraints), but it was estimated that at a spray pressure of 30 psig, the droplet size generated was approximately 20 to 30 microns. During experimental tests, the spray brush was placed at about 1 1/2 inches from the reference probe's inlet, as shown in figure 3-4. This ensured that all water droplets from the spray plume would enter the probe.

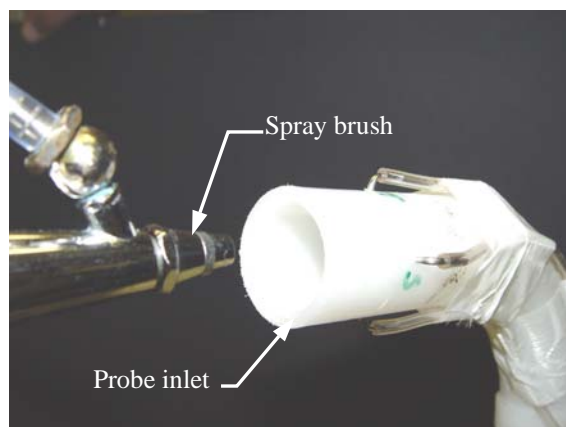


FIGURE 3-4. DIRECT METHOD OF WATER INJECTION WITH THE SPRAY BRUSH

- Water Collector System—The basic water collector was fabricated from two coannular containers with wire-meshed walls, as shown in figure 3-5. The water collector was attached to the divergent nozzle of the probe top section by four elongated screws. Figure 3-6 shows the various components of the water collector and their association to the inner and outer container.

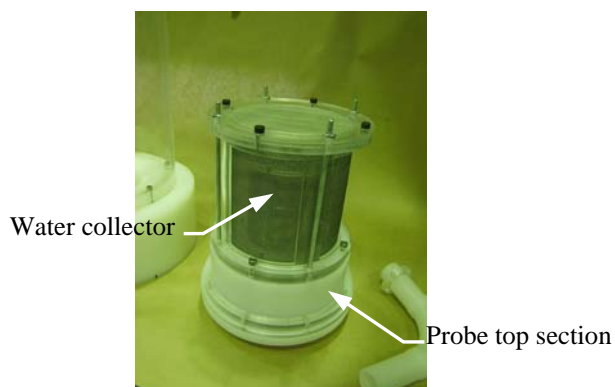


FIGURE 3-5. WATER COLLECTOR ASSEMBLY

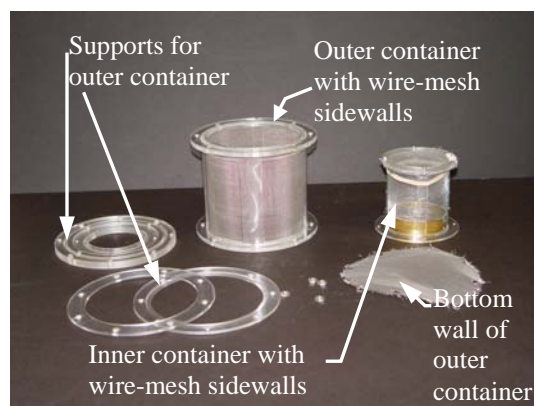


FIGURE 3-6. VARIOUS COMPONENTS OF THE COLLECTOR

The void between the inner and outer container was filled with either silica gel or molecular sieve pellets mixed with polystyrene foam cuttings (figure 3-7). The filling process involved turning the collector upside down and then removing the wire mesh that formed the bottom wall of the outer container (figure 3-6). The addition of polystyrene cuttings helped to increase the porosity of the filling and disperse the desiccant pellets in the large void space. The collector was initially designed for silica and molecular sieve pellets but it was later modified to include other materials such as water-adsorbent paper, B-Gon fiber mesh, and blotter paper. The paper and B-Gon fiber mesh were wrapped around the inner container, as shown in figures 3-8 and 3-9, respectively. Blotter paper was rolled into a tube and installed at the exit end of the diverging nozzle, as shown in figure 3-10.

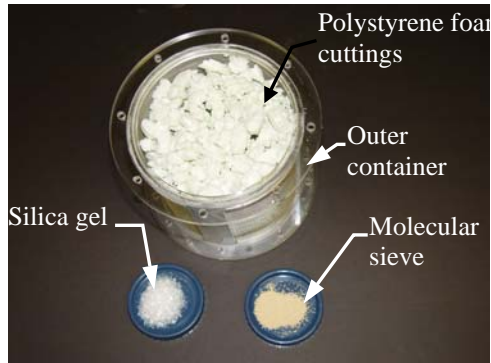


FIGURE 3-7. METHOD OF INSTALLING SILICA GEL AND MOLECULAR SIEVE

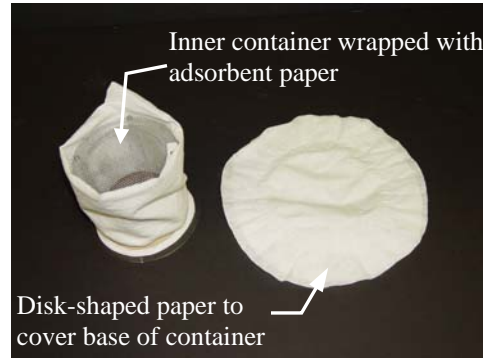


FIGURE 3-8. WATER-ADSORBENT PAPER WRAPPED AROUND INNER CONTAINER

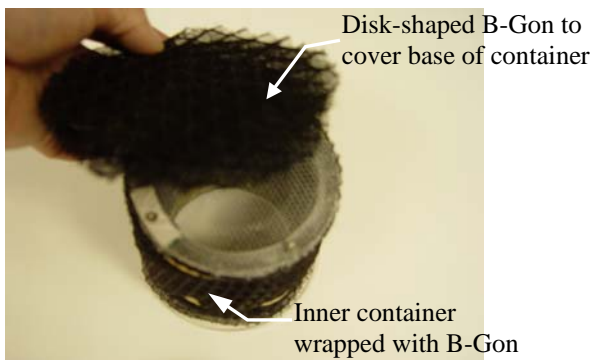


FIGURE 3-9. B-GON WRAPPED AROUND INNER CONTAINER OF COLLECTOR

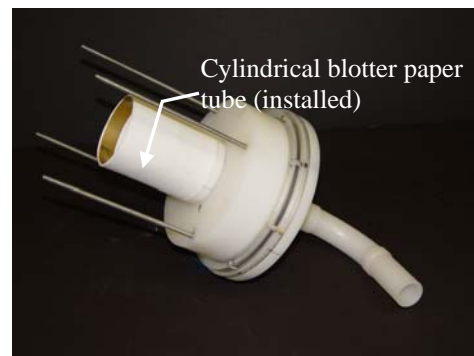


FIGURE 3-10. BLOTTER PAPER ATTACHED TO THE DIVERGENT NOZZLE

### 3.2 WATER-ADSORBENT MATERIALS.

The types of water-adsorbent materials that were tested included the following:

- Silica gel desiccant (figure 3-11)—Silica gel is silicon dioxide ( $\text{SiO}_2$ ), which is a naturally occurring mineral that has been purified and processed into either granular or beaded form. It has an average pore size of 24 angstroms and has a strong affinity for moisture. The silica gel will adsorb moisture at temperatures up to 220°F (105°C). Silica gel performs best at room temperatures (70° to 90°F) and high humidity (60% to 90% relative humidity (RH)). Silica gel has a characteristic white crystalline structure, and the sizes of the beads are normally between 0.020 and 0.079 inch (0.5 and 2 mm).
- Molecular sieve desiccant (figure 3-12)—Molecular sieve is a porous crystalline aluminosilicate, a synthetic desiccant that has a very strong affinity for moisture. The distinctive feature of the molecular sieve structure, compared to other desiccants, is the uniformity of the pore size openings in the crystal lattice structure. Based on the product literature, the most commonly used pore size is 4 angstroms (4A), although pore sizes of 3 angstroms (3A), 5 angstroms (5A), and 10 angstroms (13X) are also available. A small pore size allows the selection of a molecular sieve product that can adsorb water, yet

exclude most other molecules, such as volatile organics. Molecular sieve desiccants have a characteristic brown-colored, spherical-shaped pellet with sizes that are normally between 0.028 and 0.039 inch (0.7 and 1.0 mm).

- DRIMOP desiccant (figure 3-13)—DRIMOP is a super liquid absorber that can adsorb water or other fluids up to 300 times its own weight. In the presence of any fluid (based on product literature), a DRIMOP packet quickly bursts open, releasing a superadsorbent polymer powder, which quickly absorbs and immobilizes the fluid. DRIMOP type desiccants have a characteristic white powdery substance.
- B-Gon fiber mesh (figure 3-14)—B-Gon filaments are normally aligned perpendicular to the airflow for maximum droplet removal efficiency. B-Gon filament has a unique interlacing knitted structure oriented into a ladder arrangement, hence, it can cause a change in direction of vapor flow. This effect enhances droplet removal by impaction, interception, and centrifugal actions. The material removes water droplets by trapping them between the interlaced mesh, which is hydrophobic.
- Domestic paper (figure 3-15)—These are industrial strength domestic water-adsorbent papers that are readily available from most grocery stores.
- Blotter paper (figure 3-16)—This type of paper (Verigood #100 Blotter paper) was used in the water impingement tests with the dye tracer technique, which had been reported by Papadakis, et al. [6].



FIGURE 3-11. SILICA GEL

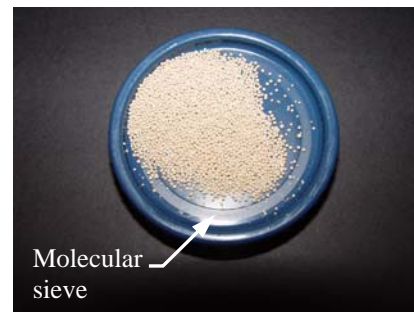


FIGURE 3-12. MOLECULAR SIEVE



FIGURE 3-13. DRIMOP

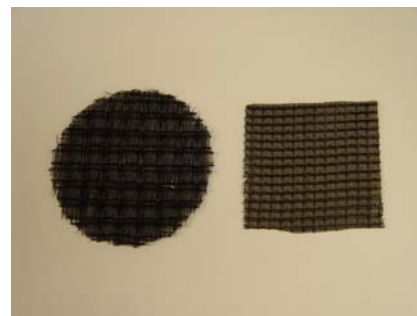


FIGURE 3-14. B-GON FIBER MESH



FIGURE 3-15. WATER-ADSORBENT PAPER

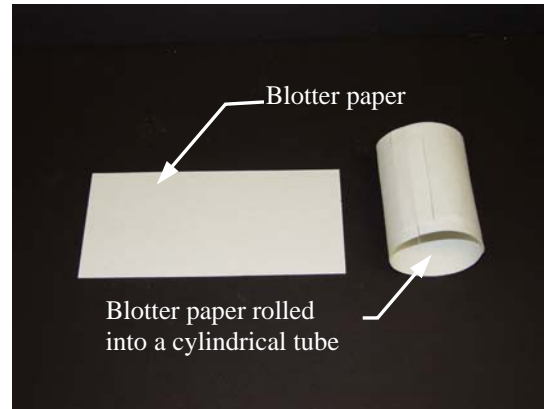


FIGURE 3-16. BLOTTER PAPER

The amount of adsorbent materials required for a test depends on the material type and amount of water to be injected into the probe. In the case of silica gel or molecular sieve, the amount required also depends on the RH and temperature of the test condition. For example, at a RH of 50% and 77°F, silica gel adsorbs approximately 25% of its own weight, but at 100°F, it can only adsorb about 15% of its own weight. The desiccant's water absorption capacity with respect to the RH and temperature are shown in appendix A, figures A-1 and A-2 respectively. In the case of the adsorbent paper, blotter paper, and B-Gon fiber mesh, no data could be found; therefore, the degree of water penetration is the only method of assessment. B-Gon fiber is hydrophobic, hence, it does not adsorb water, instead, water droplets are trapped between the fiber layers. Therefore, collection efficiency is dependent on the number of layers used.

### 3.3 PRELIMINARY TESTS.

The objective of the preliminary tests was to define and select an efficient method of water collection. The basic test methodology was to inject a known amount of water (stored in a glass container) directly into the probe and then compare this to the amount caught by the water collector. A spray nozzle was used to deliver a measured amount of water in the form of a cloud consisting of a range of droplet sizes. These tests were conducted in the WSU laboratory. Test procedures were established (based on preliminary tests) for conducting this kind of gravimetric measurements. This involved weight measurements of the silica gel and molecular sieve pellets together with polystyrene cuttings (figure 3-7). These efforts led to the development of the following test procedure:

- Place collector in a plastic bag to minimize evaporation, weigh, and record data (mg).
- Weigh and record water bottle of the spray brush (mg).
- Set spray brush volume control lever and record supply air pressure (psig).
- Clear out any remaining water in the spray brush with compressed air. Then using another water bottle, refill the spray brush and connecting tube with water, ensuring there are no visible air bubbles in the tube.

- Replace the water bottle with the one to be used for testing, taking care to ensure that no water was lost during the transfer.
- Set the distance between the probe inlet and spray brush to approximately 1.5 inches using a specially designed fixture.
- Start suction fan and allow airflow to settle for at least 3 seconds.
- Start water spray and record start time.
- Spray for a fixed time period.
- Remove water collector and place inside a plastic bag to prevent evaporation. Weigh and record (mg).
- Weigh and record remaining water in the glass container (mg). Again, ensure the full length of the nozzle plastic tube is filled with water and there are no visible air bubbles.
- Compute the collection efficiency using the following equation:

$$\text{Collection efficiency (\%)} = \frac{\text{Mass of water collected by probe per unit time (g/s)} \times 100}{\text{Mass of water injected locally into the probe per unit time (g/s)}}$$

$$\text{Water spray rate (g/s)} = \frac{\text{Mass of water injected locally into the probe (g)}}{\text{Spray duration (s)}}$$

A number of water collection efficiency tests were also conducted during the process of defining the above test procedure. However, the probe collection efficiencies were quite low and the data was scattered due to the following:

- The resolution of the electronic balance used in the tests did not have sufficient accuracy for performing gravimetric measurements. The balance had a load capacity of 1 kg and resolution of 0.1 g. Although higher resolution balances such the Denver Instrument P-214 and Mettler Toledo AG204 (load capacity 210 mg, resolution 0.1 mg) were available, they were not used because the dry weight of the water collector alone (586 mg) was greater than the maximum load capacity of these balances.
- The desiccant pellets that were trapped in the wire mesh at the end of a test could not be easily removed, therefore, subsequent tests often included the weight of the trapped pellets.
- Some desiccants might have been lost through the wire-meshed walls of the water collector. The sizes of molecular sieve pellets ranged from 0.028 to 0.039 inch (silica gel sizes varied from 0.020 to 0.079 inch), whereas the size of the wire opening was 0.030 inch.

- The process of having to replace wetted polystyrene cuttings with dried materials after a test was time-consuming and tedious. This effort was necessary to minimize the measurement errors caused by the remaining surface water in the polystyrene foam.

In conclusion, it was difficult to ascertain the probe collection efficiency with the current conceptual design that relied solely on desiccant materials; therefore, it was decided to seek an alternative method of capturing the water mass.

### 3.4 WATER COLLECTOR CONFIGURATION TESTS.

As a result of the problems experienced with the conceptual water collector design, a number of different methods of configuring the water collector were conceived and tested. These methods used a higher-resolution electronic balance (load capacity 210 mg, resolution 0.1 mg) by discarding the wire mesh from the water collector. The previous objectives were adopted: to define and select an efficient method of water collection.

A total of 11 different water collector configurations were investigated with the test procedures defined in section 3.3. Some configurations involved minor modifications to the collector while others required considerable modifications. Descriptions of the various collectors tested and related test findings are given in appendix B. The tabulated results are shown in tables 3-1 to 3-12. The following water-adsorbent materials were tested:

- Silica gel desiccant
- Molecular sieve desiccant
- DRIMOP liquid adsorber
- Water-adsorbent paper
- Blotter paper
- B-Gon fiber mesh

The findings presented in appendix B indicate that configuration 11 Mod-I had the highest water collection efficiency, which was approximately 100%. The configuration 11 Mod-I design used a plastic container with a straight exit tube, a circular B-Gon pouch filled with silica gel desiccant and a cylindrical blotter paper tube (figures B-11a and B-11b, appendix B). The maximum probe inlet static pressures recorded in the tests were approximately 0.94 psig (26" H<sub>2</sub>O). In summary, this design was selected for further experimental tests to better define its measurement accuracy and resolution.

TABLE 3-1. TEST RESULTS FOR CONFIGURATION 1

Test No.	Weight of B-Gon and Inner Container		Amount of Water Collected (g)	Weight of Spray Water Used		Amount of Water Used (g)	Spray Pressure (psig)	Spray Duration (s)	Run Duration (s)	Rate of Spray (g/s)	Collection Efficiency (%)	Water Lost/Gain (g)
	Before	After		Before	After							
1	80.0947	85.0182	4.9235	95.2665	87.3204	7.9461	20.0	15.0	45.0	0.530	62.0	(3.0226)
2	81.3960	91.8323	10.4363	94.2515	80.2109	14.0406	20.0	20.0	40.0	0.702	74.3	(3.6043)
3	81.6971	88.5511	6.8540	97.3618	87.4796	9.8822	20.0	20.0	40.0	0.494	69.4	(3.0282)
4	81.1567	91.2813	10.1246	93.5384	79.0897	14.4487	20.0	30.0	50.0	0.482	70.1	(4.3241)
5	78.9429	81.9474	3.0045	93.3290	87.2922	6.0368	30.0	40.0	40.0	0.151	49.8	(3.0323)
6	79.2922	82.2144	2.9222	98.8672	92.8455	6.0217	30.0	40.0	40.0	0.151	48.5	(3.0995)
7	78.9537	81.1839	2.2302	90.3139	85.8489	4.4650	30.0	30.0	30.0	0.149	49.9	(2.2348)
8	79.1789	81.2924	2.1135	91.0674	86.6082	4.4592	30.0	30.0	30.0	0.149	47.4	(2.3457)
9	79.0789	80.3859	1.3070	92.7830	89.9203	2.8627	30.0	20.0	20.0	0.143	45.7	(1.5557)
10	79.4126	81.2306	1.8180	95.0960	91.1005	3.9955	30.0	30.0	30.0	0.133	45.5	(2.1775)
11	79.2058	80.8335	1.6277	91.8306	86.3616	5.4690	30.0	60.0	60.0	0.091	29.8	(3.8413)
12	78.9968	80.1795	1.1827	92.9018	88.8964	4.0054	30.0	45.0	45.0	0.089	29.5	(2.8227)
13	79.2070	80.6418	1.4348	92.8970	87.7963	5.1007	30.0	60.0	60.0	0.085	28.1	(3.6659)
14	78.8421	79.9259	1.0838	93.4174	89.4899	3.9275	30.0	45.0	45.0	0.087	27.6	(2.8437)
15	78.8747	79.6471	0.7724	93.3208	90.7845	2.5363	30.0	30.0	30.0	0.085	30.5	(1.7639)
16	79.0391	79.6475	0.6084	95.4638	92.9663	2.4975	30.0	30.0	30.0	0.083	24.4	(1.8891)

TABLE 3-2. TEST RESULTS FOR CONFIGURATION 2

Test No.	Weight of Adsorbent Paper and Inner Container		Amount of Water Collected (g)	Weight of Spray Water Used		Amount of Water Used (g)	Spray Pressure (psig)	Spray Duration (s)	Rate of Spray (g/s)	Collection Efficiency (%)	Water Lost/Gain (g)
	Before	After		Before	After						
1	73.3305	76.0834	2.7529	90.8320	85.5910	5.2410	30.0	30.0	0.175	52.5	(2.4881)
2	72.3537	75.0586	2.7049	90.4083	85.1937	5.2146	30.0	30.0	0.174	51.9	(2.5097)
3	73.3763	76.6164	3.2401	92.9054	86.7185	6.1869	30.0	40.0	0.155	52.4	(2.9468)
4	73.7878	76.0171	2.2293	92.6764	88.0524	4.6240	30.0	30.0	0.154	48.2	(2.3947)
5	73.5581	74.9976	1.4395	94.0638	91.0642	2.9996	30.0	20.0	0.150	48.0	(1.5601)
6	73.6162	75.6668	2.0506	95.4575	91.0520	4.4055	30.0	30.0	0.147	46.5	(2.3549)
7	73.8104	75.1116	1.3012	92.2182	89.2717	2.9465	30.0	20.0	0.147	44.2	(1.6453)
8	73.3724	74.2440	0.8716	89.0420	86.8317	2.2103	30.0	20.0	0.111	39.4	(1.3387)
9	73.1410	74.6429	1.5019	92.5413	87.1217	5.4196	30.0	60.0	0.090	27.7	(3.9177)
10	72.4733	73.9074	1.4341	93.8633	88.4915	5.3718	30.0	60.0	0.090	26.7	(3.9377)
11	72.9550	73.9924	1.0374	93.6235	89.6990	3.9245	30.0	45.0	0.087	26.4	(2.8871)
12	73.2227	73.9091	0.6864	88.4445	85.8528	2.5917	30.0	30.0	0.086	26.5	(1.9053)
13	72.9897	73.6444	0.6547	94.5960	92.0730	2.5230	30.0	30.0	0.084	25.9	(1.8683)
14	72.2985	73.2107	0.9122	92.0232	88.2262	3.7970	30.0	45.0	0.084	24.0	(2.8848)
15	78.8421	80.3202	1.4781	92.4853	87.2714	5.2139	30.0	60.0	0.087	28.3	(3.7358)
16	77.6879	78.4457	0.7578	95.0779	92.5265	2.5514	30.0	30.0	0.085	29.7	(1.7936)

TABLE 3-3. TEST RESULTS FOR CONFIGURATION 3

Test No.	Weight of Adsorbent Paper and Inner Container		Amount of Water Collected (g)	Weight of Spray Water Used		Amount of Water Used (g)	Spray Pressure (psig)	Spray Duration (s)	Rate of Spray (g/s)	Collection Efficiency (%)	Water Lost/Gain (g)
	Before	After		Before	After						
1	72.6993	74.6695	1.9702	84.2895	81.1602	3.1293	30.0	20.0	0.156	63.0	(1.1591)
2	73.2607	76.3671	3.1064	86.7599	81.7507	5.0092	30.0	40.0	0.125	62.0	(1.9028)
3	73.4383	76.5352	3.0969	88.5750	83.6392	4.9358	30.0	40.0	0.123	62.7	(1.8389)
4	73.3785	74.8550	1.4765	86.8056	84.3507	2.4549	30.0	20.0	0.123	60.1	(0.9784)
5	73.2213	74.9275	1.7062	87.6242	84.5531	3.0711	30.0	30.0	0.102	55.6	(1.3649)
6	73.0702	74.8106	1.7404	88.1487	85.1508	2.9979	30.0	30.0	0.100	58.1	(1.2575)
7	72.9659	73.4394	0.4735	82.7816	81.6168	1.1648	30.0	30.0	0.039	40.7	(0.6913)

TABLE 3-4. TEST RESULTS FOR CONFIGURATION 4

Test No.	Weight of Adsorbent Paper, Inner Container, and External Layer		Amount of Water Collected (g)	Weight of Spray Water Used		Amount of Water Used (g)	Spray Pressure (psig)	Spray Duration (s)	Rate of Spray (g/s)	Collection Efficiency (%)	Water Lost/Gain (g)
	Before	After		Before	After						
1	78.7019	80.0280	1.5026	86.9154	84.1593	2.7561	30.0	30.0	0.092	54.5	(1.2535)
	8.8295	9.0060	0.1765								
2	72.2771	72.4005	1.3282	87.7268	85.0075	2.7193	30.0	30.0	0.091	48.8	(1.3911)
	8.6252	8.6566	0.0314								
	17.3701	18.5435	1.1734								

TABLE 3-5. TEST RESULTS FOR CONFIGURATION 5

Test No.	Weight of B-Gon Fiber		Amount of Water Collected (g)	Weight of Spray Water Used		Amount of Water Used (g)	Spray Pressure (psig)	Spray Duration (s)	Rate of Spray (g/s)	Collection Efficiency (%)	Water Lost/Gain (g)
	Before	After		Before	After						
1	85.2527	86.7602	1.5075	85.1426	82.3332	2.8094	30.0	30.0	0.094	53.7	(1.3019)
2	74.8078	75.3882	0.5804	87.4788	84.7010	2.7778	30.0	30.0	0.093	20.9	(2.1974)
3	78.4893	79.6624	1.1731	79.8775	76.1733	3.7042	30.0	40.0	0.093	31.7	(2.5311)
4	72.7063	73.7122	1.0059	82.4832	78.7968	3.6864	30.0	40.0	0.092	27.3	(2.6805)
5	87.6121	89.6425	2.0304	90.5121	85.1727	5.3394	30.0	60.0	0.089	38.0	(3.3090)
6	86.5964	88.7319	2.1355	89.1114	83.7457	5.3657	30.0	60.0	0.089	39.8	(3.2302)
7	78.0692	80.1724	2.1032	85.7223	82.2259	3.4964	30.0	40.0	0.087	60.2	(1.3932)
8	78.4445	80.1853	1.7408	86.2377	82.8072	3.4305	30.0	40.0	0.086	50.7	(1.6897)
9	78.2206	79.6005	1.3799	86.7059	84.1339	2.5720	30.0	30.0	0.086	53.7	(1.1921)
10	72.3130	75.1992	2.8862	86.0644	80.9438	5.1206	30.0	60.0	0.085	56.4	(2.2344)
11	72.7655	74.8718	2.1063	80.1412	76.7232	3.4180	30.0	40.0	0.085	61.6	(1.3117)
12	99.5902	100.9363	1.3461	90.2754	87.7521	2.5233	30.0	30.0	0.084	53.3	(1.1772)
13	72.9355	73.9991	1.0636	82.7389	80.1412	2.5977	30.0	40.0	0.065	40.9	(1.5341)
14	72.3013	73.3302	1.0289	88.1174	86.2886	1.8288	30.0	30.0	0.061	56.3	(0.7999)

TABLE 3-6. TEST RESULTS FOR CONFIGURATION 6

Test No.	Weight of Adsorbent Material and Plastic Container		Amount of Water Collected (g)	Weight of Spray Water Used		Amount of Water Used (g)	Spray Pressure (psig)	Spray Duration (s)	Rate of Spray (g/s)	Collection Efficiency (%)	Water Lost/Gain (g)
	Before	After		Before	After						
1	99.0056	100.7548	1.7492	88.5719	85.3426	3.2293	30.0	30.0	0.108	54.2	(1.4801)
2	104.5306	106.5054	1.9748	92.1606	89.1310	3.0296	30.0	30.0	0.101	65.2	(1.0548)
3	102.7610	104.6033	1.8423	94.9042	92.1925	2.7117	30.0	30.0	0.090	67.9	(0.8694)
4	124.3563	125.6231	1.2668	90.7507	88.5982	2.1525	30.0	30.0	0.072	58.9	(0.8857)

TABLE 3-7. TEST RESULTS FOR CONFIGURATION 7

Test No.	Weight of Adsorbent Paper and Inner Container		Amount of Water Collected (g)	Weight of Spray Water Used		Amount of Water Used (g)	Spray Pressure (psig)	Spray Duration (s)	Rate of Spray (g/s)	Collection Efficiency (%)	Water Lost/Gain (g)
	Before	After		Before	After						
1	72.7848	73.4981	1.8635	83.6655	80.6981	2.9674	30.0	30.0	0.099	62.8	(1.1039)
	27.5824	28.7326	1.1502								
2	73.7672	74.6169	1.7944	86.4554	83.6698	2.7856	30.0	30.0	0.093	64.4	(0.9912)
	29.5675	30.5122	0.9447								
3	72.5520	72.8521	1.5631	80.7365	77.9319	2.8046	30.0	30.0	0.093	55.7	(1.2415)
	21.4213	22.6843	1.2630								
4	78.2328	78.3774	1.3855	85.1927	82.4825	2.7102	30.0	30.0	0.090	51.1	(1.3247)
	21.3306	22.5715	1.2409								
5	72.9413	72.9870	0.4935	82.9388	80.7454	2.1934	30.0	30.0	0.073	22.5	(1.6999)
	21.4078	21.8556	0.4478								

TABLE 3-8. TEST RESULTS FOR CONFIGURATION 8

Test No.	Weight of Adsorbent Paper and Inner Container		Amount of Water Collected (g)	Weight of Spray Water Used		Amount of Water Used (g)	Spray Pressure (psig)	Spray Duration (s)	Rate of Spray (g/s)	Collection Efficiency (%)	Water Lost/Gain (g)
	Before	After		Before	After						
1	93.0045	94.8051	1.8006	89.3605	85.7555	3.6050	30.0	30.0	0.120	49.9	(1.8044)
2	79.0591	80.7054	1.6463	86.3550	83.6713	2.6837	30.0	30.0	0.089	61.3	(1.0374)
3	86.2514	88.0427	1.7913	83.6609	81.0265	2.6344	30.0	30.0	0.088	68.0	(0.8431)
4	91.9878	93.3791	1.3913	85.7491	83.1269	2.6222	30.0	30.0	0.087	53.1	(1.2309)

TABLE 3-9. TEST RESULTS FOR CONFIGURATION 9

Test No.	Weight of Adsorbent Paper and Inner Container		Amount of Water Collected (g)	Weight of Spray Water Used		Amount of Water Used (g)	Spray Pressure (psig)	Spray Duration (s)	Rate of Spray (g/s)	Collection Efficiency (%)	Water Lost/Gain (g)
	Before	After		Before	After						
1	95.9549	97.9392	1.9843	152.1853	149.4555	2.7298	30.0	0.091	72.7	(0.7455)	
2	95.9874	97.7410	1.7536	156.0295	153.5257	2.5038	30.0	0.083	70.0	(0.7502)	
3	97.9875	99.4920	1.5045	148.7345	146.3160	2.4185	30.0	0.081	62.2	(0.9140)	
4	95.7001	97.4659	1.7658	150.6670	148.2512	2.4158	30.0	0.081	73.1	(0.6500)	
5	98.3654	100.1135	1.7481	158.3974	155.9930	2.4044	30.0	0.080	72.7	(0.6563)	
6	96.8822	98.5971	1.7149	151.8985	149.5498	2.3487	30.0	0.078	73.0	(0.6338)	
7	97.9982	99.5223	1.5241	154.9552	152.6982	2.2570	30.0	0.075	67.5	(0.7329)	
8	96.5970	98.1719	1.5749	153.4981	151.2565	2.2416	30.0	0.075	70.3	(0.6667)	
9	95.9860	97.4319	1.4459	151.5290	149.3179	2.2111	30.0	0.074	65.4	(0.7652)	
10	95.2894	96.8729	1.5835	158.1864	156.0017	2.1847	30.0	0.073	72.5	(0.6012)	
11	96.0744	97.6534	1.5790	151.2011	149.0385	2.1626	30.0	0.072	73.0	(0.5836)	
12	95.8827	97.4501	1.5674	147.2483	145.1044	2.1439	30.0	0.071	73.1	(0.5765)	
13	95.6692	97.1475	1.4783	154.1017	152.0109	2.0908	30.0	0.070	70.7	(0.6125)	
14	95.9419	97.1635	1.2216	152.6958	150.7086	1.9872	30.0	0.066	61.5	(0.7656)	
15	96.0332	97.2277	1.1945	155.9939	154.1273	1.8666	30.0	0.062	64.0	(0.6721)	
16	96.0090	97.1090	1.1000	153.8696	152.2021	1.6675	30.0	0.056	66.0	(0.5675)	
17	94.1096	95.1113	1.0017	153.0828	151.4900	1.5928	30.0	0.053	62.9	(0.5911)	
18	96.1963	97.4050	1.2087	155.4613	153.8812	1.5801	30.0	0.053	76.5	(0.3714)	

TABLE 3-10. TEST RESULTS FOR CONFIGURATION 10

Test No.	Weight of Blotter Paper		Amount of Water Collected (g)	Weight of Spray Water Used		Amount of Water Used (g)	Max. Inlet Pres. ("H <sub>2</sub> O)	Min. Inlet Pres. ("H <sub>2</sub> O)	Inlet Pres. ("H <sub>2</sub> O)	Spray Pressure (psig)	Spray Duration (s)	Rate of Spray (g/s)	Collection Efficiency (%)	Water Lost/Gain (g)
	Before	After		Before	After									
1	13.4142	15.9662	2.5520	89.1792	85.7363	3.4429	11.3	-10.8	22.1	30.0	30.0	0.115	74.1	(0.8909)
2	12.7970	15.3091	2.5121	91.0011	87.5954	3.4057	11.2	-10.6	21.8	30.0	30.0	0.114	73.8	(0.8936)
3	13.4556	15.7246	2.2984	89.7038	86.3151	3.3887	11.7	-11.3	23.0	30.0	30.0	0.113	67.8	(1.0903)
4	12.7851	15.2288	2.4437	90.5060	87.2306	3.2754	11.8	-11.3	23.1	30.0	30.0	0.109	74.6	(0.8317)
5	12.7578	14.9700	2.4220	94.3897	91.0230	3.3667	11.2	-10.6	21.8	30.0	30.0	0.112	71.9	(0.9447)
6	12.8112	15.2537	2.4425	91.7995	88.4635	3.3360	11.5	-11.1	22.6	30.0	30.0	0.111	73.2	(0.8935)
7	12.8031	15.2263	2.4232	88.1160	84.8276	3.2884	11.3	-11.1	22.4	30.0	30.0	0.110	73.7	(0.8652)

TABLE 3-11. TEST RESULTS FOR CONFIGURATION 11

Test No.	Weight of Blotter Paper		Amount of Water Collected (g)	Weight of Spray Water Used		Amount of Water Used (g)	Max. Inlet Pres. ("H <sub>2</sub> O)	Min. Inlet Pres. ("H <sub>2</sub> O)	Inlet Pres. ("H <sub>2</sub> O)	Spray Pressure (psig)	Spray Duration (s)	Rate of Spray (g/s)	Collection Efficiency (%)	Water Lost/Gain (g)
	Before	After		Before	After									
1	12.7233	15.2759	3.4545	87.1259	90.4544	3.3285	9.4	-9.1	18.5	30.0	30.0	0.111	103.79	0.1260
	31.4780	32.3799	0.9019											
2	12.7865	15.2026	3.1425	91.9151	95.2973	3.3822	9.9	-9.5	19.4	30.0	30.0	0.113	92.91	(0.2397)
	32.9290	33.4448	34.1712	0.7264										
3	12.7897	15.2007	2.7768	88.4753	91.8721	3.3968	9.6	-9.1	18.7	30.0	30.0	0.113	81.75	(0.6200)
	31.2636	31.4627	31.8285	0.3658										
4	12.0063	14.3466	2.5793	85.0991	88.4553	3.3562	9.6	-9.1	18.7	30.0	30.0	0.112	76.85	(0.7769)
	31.8300	32.0690	0.2390											
5	12.5784	14.8952	2.5773	91.3118	94.7245	3.4127	9.6	-9.1	18.7	30.0	30.0	0.114	75.52	(0.8354)
	32.0454	32.3059	0.2605											
6	12.7919	15.2340	2.4899	87.8380	91.2668	3.4288	9.6	-9.1	18.7	30.0	30.0	0.114	72.62	(0.9389)
	32.3044	32.3522	0.0478											
7	13.5364	15.9106	3.3628	89.0787	92.3908	3.3121	9.2	-9.1	18.3	30.0	30.0	0.110	101.53	0.0507
	31.9156	32.9042	0.9886											
8	13.2310	15.7681	3.0775	88.8557	92.2712	3.4155	9.2	-9.1	18.3	30.0	30.0	0.114	90.10	(0.3380)
	32.9135	33.4300	0.5165											
9	13.6218	16.0725	3.9985	87.2636	90.7020	3.4384	7.2	-7.1	14.3	30.0	30.0	0.115	116.29	0.5601
	31.0876	32.6354	1.5478											
10	15.5247	17.5451	2.8492	90.5095	93.3074	2.7979	9.2	-9.1	18.3	30.0	30.0	0.093	101.83	0.0513
	25.4582	26.2870	0.8288											
11	15.5619	18.0647	3.4573	90.2215	93.6995	3.4780	9.2	-9.1	18.3	30.0	30.0	0.116	99.40	(0.0207)
	25.2990	26.2535	0.9545											

TABLE 3-11. TEST RESULTS FOR CONFIGURATION 11 (Continued)

Test No.	Weight of Blotter Paper		Amount of Water Collected (g)	Weight of Spray Water Used		Amount of Water Used (g)	Max. Inlet Pres. ("H <sub>2</sub> O)	Min. Inlet Pres. ("H <sub>2</sub> O)	Inlet Pres. ("H <sub>2</sub> O)	Spray Pressure (psig)	Spray Duration (s)	Rate of Spray (g/s)	Collection Efficiency (%)	Water Lost/Gain (g)
	Before	After		Before	After									
12	13.4264	15.8812	2.8993	92.7945	89.4416	3.3529	9.2	-9.1	18.3	30.0	30.0	0.112	86.47	(0.4536)
	21.6976	22.1421	0.4445											
13	22.3579	25.0711	3.0533	90.1501	86.4393	3.7108	7.3	-8.0	15.3	30	30	0.124	82.28	(0.6575)
	27.4553	27.7954	0.3401											
14	22.3884	25.0186	3.2813	91.2187	87.5604	3.6583	7.3	-8.0	15.3	30	30	0.122	89.69	(0.3770)
	27.9241	28.5752	0.6511											
15	28.5012	30.7736	3.1963	90.7473	87.0511	3.6962	7.5	-8.1	15.6	30	30	0.123	86.48	(0.4999)
	27.0338	27.8002	0.7664											
16	27.8787	30.5173	2.9763	91.1969	87.5831	3.6138	7.0	-7.9	14.9	30	30	0.120	82.36	(0.6375)
	27.7738	28.1115	0.3377											
17	22.3622	24.7696	2.8153	91.5502	87.6187	3.9315	6.6	-7.6	14.2	30	30	0.131	71.61	(1.1162)
	27.5213	27.9292	0.4079											

TABLE 3-12. TEST RESULTS FOR CONFIGURATION 11 MOD-I

Test No.	Weight of Blotter Paper		Amount of Water Collected (g)	Weight of Spray Water Used		Amount of Water Used (g)	Max. Inlet Pres. ("H <sub>2</sub> O)	Min. Inlet Pres. ("H <sub>2</sub> O)	Inlet Pressure ("H <sub>2</sub> O)	Spray Pressure (psig)	Spray Duration (s)	Rate of Spray (g/s)	Collection Efficiency (%)	Water Lost/Gain (g)
	Before	After		Before	After									
1	15.5688	17.8289	3.1438	89.8168	86.5479	3.2689	12.4	-13.9	26.3	30.0	30.0	0.109	96.17	(0.1251)
	24.7006	25.5843	0.8837											
2	15.5860	18.0332	3.2881	92.3648	89.0383	3.3265	12.2	-13.6	25.8	30.0	30.0	0.111	98.85	(0.0384)
	24.6937	25.5346	0.8409											
3	15.6233	18.1434	3.4344	94.2287	90.8196	3.4091	12.0	-13.5	25.5	30.0	30.0	0.114	100.74	0.0253
	25.0776	25.9919	0.9143											
4	22.6262	25.2639	3.7169	91.6015	88.1430	3.4585	11.6	-12.8	24.4	20.0	30.0	0.115	107.47	0.2584
	25.0406	26.1198	1.0792											
5	15.5512	18.0412	3.3544	91.0175	87.6553	3.3622	12.5	-13.8	26.3	20.0	37.0	0.091	99.77	(0.0078)
	24.8587	25.7231	0.8644											
6	15.3753	17.8673	3.4518	91.1967	87.8597	3.3370	12.3	-13.6	25.9	20.0	37.0	0.090	103.44	0.1148
	25.6037	26.5635	0.9598											
7	15.6317	18.1301	3.3795	91.3433	87.9744	3.3689	12.2	-13.6	25.8	20.0	37.0	0.091	100.31	0.0106
	25.3452	26.2263	0.8811											

### 3.5 TESTS WITH WATER COLLECTOR CONFIGURATION 11 MOD-I.

The preliminary tests discussed in section 3.4 showed that collection efficiencies within 100% could be attained with configuration 11 Mod-I. However, the results were based on a small range of water spray rates; hence, accuracy of the technique could not be ascertained. Further tests were, therefore, conducted over a wider range of conditions, including those normally found in icing wind tunnels, i.e., LWC between 0.1 to 3 g/m<sup>3</sup>.

To relate the test measurements to icing cloud conditions, the water spray rate was converted into LWC with the following expression:

$$LWC \text{ (based on water sprayed or collected, g/m}^3\text{)} = \frac{\text{Rate of water sprayed or collected (g/s)}}{\text{Probe inlet volumetric flow (m}^3\text{/s)}} \quad (3-1)$$

The volumetric flow was calculated from the following equation:

$$\text{Probe inlet volumetric flow (m}^3\text{/s)} = \frac{\pi D^2}{4} \sqrt{\frac{2 \times \Delta P}{\rho}} \times \text{Discharge coefficient} \quad (3-2)$$

where

$D$  – inner diameter of the 90 degree elbow tube (0.022 m or 0.866 inch)

$\Delta P$  – inlet static pressure (Pa)

$\rho$  – flow density (kg/m<sup>3</sup>)

Discharge coefficient – 1.0 (assumes a uniform velocity profile at the probe inlet)

The LWC of the cloud entering the probe inlet was adjusted via changing the probe inlet air volumetric flow and amount of water sprayed. To reduce the probe air volumetric flow, a container with a small hole was installed downstream of the suction fan exhaust. Figure 3-17 shows three such containers with different hole sizes. Figure 3-18 shows the installation of a container into the extension wand of the suction fan.



FIGURE 3-17. PRESSURE LOSS DEVICES WITH THREE DIFFERENT OPENING SIZES

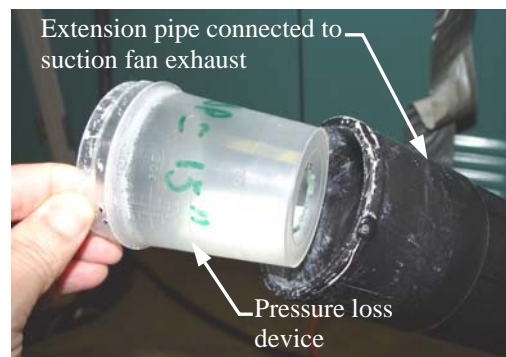


FIGURE 3-18. INSTALLATION OF A PRESSURE LOSS DEVICE DOWNSTREAM OF THE SUCTION FAN

The test procedure described in section 3.3 was altered to suit the probe efficiency tests with blotter paper tube and silica gel desiccants installed in the probe collector. The modified test procedures in section C.1 of appendix C describe the preparation of the container, water sample, blotter paper, silica gel, test methodology, and data analysis. A total of 65 tests were conducted and the results are shown in figures 3-19 to 3-21 and table 3-13. Tests 1 to 61 were conducted with approximately 3.3 g of water, and tests 62 to 65 were conducted with approximately 10.2 g of water. The following materials, settings, and test conditions were used:

- Silica gel 7 to 8 g
- Water used or sprayed 2.3 to 10.5 g
- Spray brush air pressure setting 10 to 30 psig
- Spray duration 30 to 130 s
- Spray rate 0.029 to 0.350 g/s
- LWC 0.54 to 8.5 g/m<sup>3</sup>
- Test duration 30 to 130 s

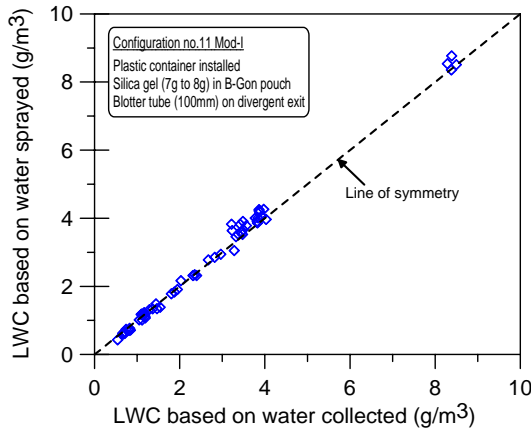


FIGURE 3-19. LIQUID WATER CONTENT (Water Collected) VERSUS LWC (Water Sprayed)

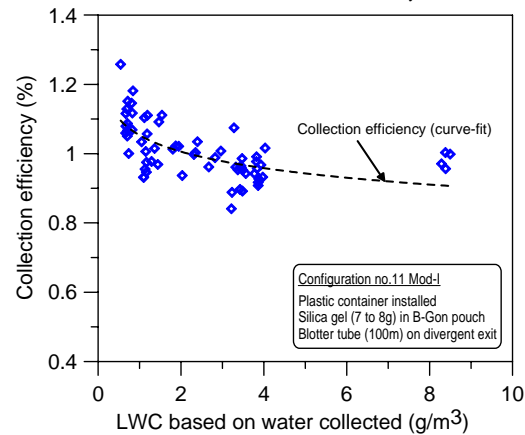


FIGURE 3-20. LIQUID WATER CONTENT (Water Collected) VERSUS COLLECTION EFFICIENCY

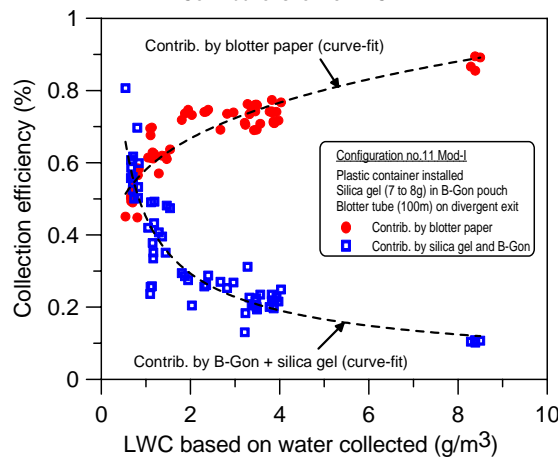


FIGURE 3-21. CONTRIBUTIONS TO COLLECTION EFFICIENCY BY BLOTTER PAPER AND SILICA GEL

TABLE 3-13. TEST RESULTS FOR CONFIGURATION 11 MOD-I (LABORATORY)

Test No.	Weight of Blotter Paper		Amount of Water Collected (g)	Weight of Spray Water Used		Amount of Water Used (g)	Maximum Inlet Pressure ("H <sub>2</sub> O)	Minimum Inlet Pressure ("H <sub>2</sub> O)	Inlet Pressure ("H <sub>2</sub> O)
	Before	After		Before	After				
1	15.5688	17.8289	3.1438	89.8168	86.5479	3.2689	12.4	-13.9	26.3
	24.7006	25.5843	0.8837						
2	15.5860	18.0332	3.2881	92.3648	89.0383	3.3265	12.2	-13.6	25.8
	24.6937	25.5346	0.8409						
3	15.6233	18.1434	3.4344	94.2287	90.8196	3.4091	12.0	-13.5	25.5
	25.0776	25.9919	0.9143						
4	22.6262	25.2639	3.7169	91.6015	88.1430	3.4585	11.6	-12.8	24.4
	25.0406	26.1198	1.0792						
5	15.5512	18.0412	3.3544	91.0175	87.6553	3.3622	12.5	-13.8	26.3
	24.8587	25.7231	0.8644						
6	15.3753	17.8673	3.4518	91.1967	87.8597	3.3370	12.3	-13.6	25.9
	25.6037	26.5635	0.9598						
7	15.6317	18.1301	3.3795	91.3433	87.9744	3.3689	12.2	-13.6	25.8
	25.3452	26.2263	0.8811						
8	22.3349	24.7527	3.0929	93.6698	90.3679	3.3019	14.5	-14.5	29.0
	25.9885	26.6636	0.6751						
9	22.3558	24.5944	3.0425	90.2834	87.0168	3.2666	14.7	-14.6	29.3
	25.4446	26.2165	0.7719						
10	22.2960	24.5680	3.1116	91.7500	88.4925	3.2575	14.4	-14.3	28.7
	25.2978	26.1374	0.8396						
11	22.2699	24.4771	3.0437	92.1807	88.9155	3.2652	14.5	-14.4	28.9
	25.7473	26.5838	0.8365						
12	22.3015	24.5598	2.8996	94.9600	91.7982	3.1618	5.5	-5.2	10.7
	25.3279	25.9692	0.6413						
13	22.2628	24.4916	2.9122	92.9389	89.7976	3.1413	5.5	-5.2	10.7
	25.4072	26.0906	0.6834						
14	22.2556	24.5488	2.9820	91.8690	88.6705	3.1985	5.5	-5.2	10.7
	25.5413	26.2301	0.6888						
15	22.3386	24.7124	3.1057	92.1532	88.9219	3.2313	5.6	-5.3	10.9
	25.7452	26.4771	0.7319						
16	22.6099	25.1166	3.2462	92.0454	88.7521	3.2933	5.6	-5.3	10.9
	25.5185	26.2580	0.7395						
17	22.5482	24.9960	3.1207	90.6261	87.3534	3.2727	5.5	-5.2	10.7
	25.9011	26.5740	0.6729						
18	22.4370	24.8238	3.2643	91.4187	88.2220	3.1967	5.5	-5.2	10.7
	25.7495	26.6270	0.8775						
19	22.5446	24.8305	3.1727	92.3731	89.2691	3.1040	5.6	-5.3	10.9
	25.5409	26.4277	0.8868						
20	22.3192	24.4856	3.0533	90.4450	87.4299	3.0151	5.6	-5.3	10.9
	25.2320	26.1189	0.8869						
21	22.3183	24.8441	3.2991	90.2764	86.8669	3.4095	6.7	-6.7	13.4
	25.6071	26.3804	0.7733						

TABLE 3-13. TEST RESULTS FOR CONFIGURATION 11 MOD-I  
(LABORATORY) (Continued)

Spray Pressure (psig)	Spray Duration (s)	Rate of Spray (g/s)	Collection Efficiency (%)	Water Lost/Gain (g)	LWC Water Collected (g/m <sup>3</sup> )	LWC Water Sprayed (g/m <sup>3</sup> )	LWC (Collected) Contributed by Blotter (%)	LWC (Collected) Contributed by Silica (%)
30.0	30.0	0.109	96.17	(0.1251)	2.6715	2.7778	69.14	27.03
30.0	30.0	0.111	98.85	(0.0384)	2.8211	2.8540	73.57	25.28
30.0	30.0	0.114	100.74	0.0253	2.9639	2.9421	73.92	26.82
20.0	30.0	0.115	107.47	0.2584	3.2792	3.0512	76.27	31.20
20.0	37.0	0.091	99.77	(0.0078)	2.3112	2.3166	74.06	25.71
20.0	37.0	0.090	103.44	0.1148	2.3966	2.3169	74.68	28.76
20.0	37.0	0.091	100.31	0.0106	2.3510	2.3436	74.16	26.15
20	37.0	0.089	93.67	(0.2090)	2.0294	2.1665	73.22	20.45
10	67.0	0.049	93.14	(0.2241)	1.0968	1.1776	69.51	23.63
10	67.0	0.049	95.52	(0.1459)	1.1334	1.1865	69.75	25.77
10	67.0	0.049	93.22	(0.2215)	1.1048	1.1852	67.60	25.62
30	30.0	0.105	91.71	(0.2622)	3.8630	4.2123	71.42	20.28
30	30.0	0.105	92.71	(0.2291)	3.8798	4.1850	70.95	21.76
30	30.0	0.107	93.23	(0.2165)	3.9728	4.2612	71.70	21.54
20	37.0	0.087	96.11	(0.1256)	3.3239	3.4583	73.46	22.65
20	37.0	0.089	98.57	(0.0471)	3.4743	3.5247	76.12	22.45
20	37.0	0.088	95.36	(0.1520)	3.3710	3.5352	74.79	20.56
10	67.0	0.048	102.11	0.0676	1.9473	1.9069	74.66	27.45
10	67.0	0.046	102.21	0.0687	1.8752	1.8346	73.64	28.57
10	67.0	0.045	101.27	0.0382	1.8046	1.7820	71.85	29.42
30	30.0	0.114	96.76	(0.1104)	3.9276	4.0590	74.08	22.68

TABLE 3-13. TEST RESULTS FOR CONFIGURATION 11 MOD-I (LABORATORY)  
(Continued)

Test No.	Weight of Blotter Paper		Amount of Water Collected (g)	Weight of Spray Water Used		Amount of Water Used (g)	Maximum Inlet Pressure ("H <sub>2</sub> O)	Minimum Inlet Pressure ("H <sub>2</sub> O)	Inlet Pressure ("H <sub>2</sub> O)
	Before	After		Before	After				
22	22.2962	24.6077	3.1680	91.0307	87.6700	3.3607	7.5	-7.5	15.0
	25.5680	26.3570	0.7890						
23	22.3629	25.0705	3.4673	91.1422	87.6435	3.4987	7.8	-7.8	15.6
	25.2942	26.0539	0.7597						
24	22.3611	25.0380	3.5454	91.5624	88.0732	3.4892	7.4	-7.3	14.7
	25.4527	26.3212	0.8685						
25	22.4764	25.1375	3.3985	92.2427	88.6357	3.6070	7.7	-7.7	15.4
	25.4726	26.1960	0.7234						
26	22.4701	24.7877	3.0977	90.9700	87.4971	3.4729	7.5	-7.5	15.0
	25.6101	26.3057	0.6956						
27	22.3974	24.8870	3.1237	93.0954	89.8173	3.2781	7.6	-7.6	15.2
	26.3957	27.0298	0.6341						
28	22.2380	24.5959	3.0635	93.5992	90.1830	3.4162	7.6	-7.6	15.2
	25.8044	26.5100	0.7056						
29	22.3100	24.7402	3.0844	91.4531	88.2566	3.1965	7.6	-7.6	15.2
	26.4779	27.1321	0.6542						
30	22.3623	24.7840	3.1299	93.0510	89.7886	3.2624	7.8	-7.8	15.6
	26.7926	27.5008	0.7082						
31	22.2598	24.5958	2.8965	93.8918	90.4473	3.4445	7.5	-7.9	15.4
	26.5838	27.0328	0.4490						
32	22.5484	24.8430	2.8907	90.0863	86.8320	3.2543	7.4	-7.8	15.2
	25.5120	26.1081	0.5961						
33	22.4556	25.0857	3.4622	91.4359	87.8933	3.5426	7.5	-8.1	15.6
	27.5893	28.4214	0.8321						
34	22.3454	24.9776	3.4117	90.8259	87.2619	3.5640	7.2	-7.8	15.0
	27.5796	28.3591	0.7795						
35	22.8182	25.4166	3.3176	92.0822	88.4285	3.6537	6.5	-7.5	14.0
	27.7525	28.4717	0.7192						
36	27.0432	28.7130	3.1549	91.9030	88.9507	2.9523	11.5	-13.7	25.2
	27.0615	28.5466	1.4851						
37	26.4434	28.1492	3.2608	91.1095	88.1906	2.9189	12.1	-14.5	26.6
	27.1909	28.7459	1.5550						
38	26.5722	28.0280	2.9137	91.6892	88.7763	2.9129	12.0	-14.5	26.5
	27.9431	29.4010	1.4579						
39	26.4329	28.2429	3.1656	91.5830	88.3442	3.2388	4.0	-6.3	10.3
	27.5388	28.8576	1.3188						
40	26.5560	28.7413	3.5377	92.2566	88.6053	3.6513	4.0	-6.3	10.3
	27.7740	29.0547	1.2807						
41	26.3664	28.5951	3.4837	91.8112	88.2383	3.5729	6.4	-8.8	15.2
	27.3045	28.5595	1.2550						
42	26.6254	28.8670	3.4947	93.2096	89.5179	3.6917	6.5	-8.9	15.4
	27.1811	28.4180	1.2369						
43	26.6950	28.9521	3.6575	92.8535	89.2188	3.6347	12.0	-15.0	27.0
	27.1707	28.5436	1.3729						

TABLE 3-13. TEST RESULTS FOR CONFIGURATION 11 MOD-I  
(LABORATORY) (Continued)

Spray Pressure (psig)	Spray Duration (s)	Rate of Spray (g/s)	Collection Efficiency (%)	Water Lost/Gain (g)	LWC Water Collected (g/m <sup>3</sup> )	LWC Water Sprayed (g/m <sup>3</sup> )	LWC (Collected) Contributed by Blotter (%)	LWC (Collected) Contributed by Silica (%)
30	30.0	0.112	94.27	(0.1927)	3.5647	3.7815	70.79	23.48
30	30.0	0.117	99.10	(0.0314)	3.8257	3.8603	77.39	21.71
30	30.0	0.116	101.61	0.0562	4.0298	3.9660	76.72	24.89
30	30.0	0.120	94.22	(0.2085)	3.7741	4.0056	74.16	20.06
30	30.0	0.116	89.20	(0.3752)	3.4856	3.9078	69.17	20.03
30	30.0	0.109	95.29	(0.1544)	3.4916	3.6642	75.95	19.34
30	30.0	0.114	89.68	(0.3527)	3.4243	3.8186	69.02	20.65
30	30.0	0.107	96.49	(0.1121)	3.4477	3.5730	76.03	20.47
30	30.0	0.109	95.94	(0.1325)	3.4534	3.5996	74.23	21.71
30	30.0	0.115	84.09	(0.5480)	3.2166	3.8251	71.06	13.04
30	30.0	0.108	88.83	(0.3636)	3.2312	3.6376	70.51	18.32
30	30	0.118	97.73	(0.0804)	3.8201	3.9088	74.24	23.49
30	30	0.119	95.73	(0.1523)	3.8389	4.0103	73.86	21.87
30	30	0.122	90.80	(0.3361)	3.8640	4.2555	71.12	19.68
30	100.0	0.030	106.86	0.2026	0.8217	0.7689	56.56	50.30
30	100.0	0.029	111.71	0.3419	0.8266	0.7399	58.44	53.27
30	100.0	0.029	100.03	0.0008	0.7400	0.7398	49.98	50.05
30	100.0	0.032	97.74	(0.0732)	1.2896	1.3194	57.02	40.72
30	100.0	0.037	96.89	(0.1136)	1.4411	1.4874	61.81	35.08
30	100.0	0.036	97.50	(0.0892)	1.1682	1.1981	62.38	35.13
30	100.0	0.037	94.66	(0.1970)	1.1643	1.2299	61.16	33.50
30	80.0	0.045	100.63	0.0228	1.1503	1.1431	62.86	37.77

TABLE 3-13. TEST RESULTS FOR CONFIGURATION 11 MOD-I  
(LABORATORY) (Continued)

Test No.	Weight of Blotter Paper		Amount of Water Collected (g)	Weight of Spray Water Used		Amount of Water Used (g)	Maximum Inlet Pressure ("H <sub>2</sub> O)	Minimum Inlet Pressure ("H <sub>2</sub> O)	Inlet Pressure ("H <sub>2</sub> O)
	Before	After		Before	After				
44	26.7202	28.6398	3.2964	91.6539	88.5355	3.1184	12.1	-15.0	27.1
	27.4055	28.7538							
45	26.7468	28.8388	3.7890	91.1942	87.7828	3.4114	12.0	-15.0	27.0
	27.0082	28.6876							
46	26.6600	28.6424	3.5677	90.9538	87.7214	3.2324	12.1	-15.2	27.3
	27.2038	28.7891							
47	26.6331	28.6353	3.3707	90.2473	86.9877	3.2596	12.3	-15.2	27.5
	27.4081	28.7766							
48	26.4837	28.4393	3.2617	92.2983	89.0852	3.2131	6.3	-9.0	15.3
	26.9412	28.2123							
49	26.6776	28.7844	3.7269	92.6550	89.3006	3.3544	6.4	-9.2	15.6
	26.9905	28.5808							
50	26.6448	28.5885	3.5464	93.6955	90.4469	3.2486	6.4	-9.2	15.6
	26.9318	28.4959							
51	26.8083	29.0137	4.3430	90.6180	86.6224	3.9956	12.1	-16.4	28.5
	45.5807	47.6782							
52	26.5445	28.4124	4.0124	91.8483	88.0613	3.7870	12.2	-15.5	27.7
	45.3925	47.5031							
53	26.6975	28.3902	3.6437	92.0927	88.8650	3.2277	12.3	-15.7	28.0
	45.3158	47.2668							
54	26.7345	28.3347	3.5155	92.7000	89.5489	3.1511	12.3	-15.7	28.0
	45.2429	47.1582							
55	26.7194	28.4632	3.7595	91.8851	88.6200	3.2651	12.3	-15.7	28.0
	45.8189	47.8346							
56	26.6343	27.6522	2.8393	90.1849	87.9273	2.2576	12.0	-15.7	27.7
	26.3984	28.2198							
57	26.4417	28.2730	3.7327	91.4531	87.9541	3.4990	14.4	-13.5	27.9
	26.4956	28.3970							
58	26.6189	28.2249	3.5154	90.6967	87.4389	3.2578	14.4	-13.5	27.9
	26.2628	28.1722							
59	26.6246	28.3311	3.6852	91.5442	88.0361	3.5081	14.4	-13.3	27.7
	26.4697	28.4365							
60	26.9945	28.5768	4.0426	91.9648	88.4357	3.5291	13.2	-12.1	25.3
	26.3998	28.8601							
61	26.6270	28.8145	4.4367	92.1136	88.3575	3.7561	14.5	-13.6	28.1
	26.3768	28.6260							
62	41.2349	50.2305	10.0745	94.8204	84.5303	10.0887	12.6	-14.1	26.7
	120.5952	121.6741							
63	46.2900	55.2753	10.0545	94.4919	83.9809	10.5110	12.8	-14.5	27.3
	120.9411	122.0103							
64	41.8369	50.7041	9.9351	95.3860	85.1505	10.2355	12.8	-14.5	27.3
	120.6013	121.6692							
65	39.5495	48.4962	10.031	95.5672	85.5684	9.9988	12.8	-14.4	27.2
	120.7592	121.8431							

TABLE 3-13. TEST RESULTS FOR CONFIGURATION 11 MOD-I  
(LABORATORY) (Continued)

Spray Pressure (psig)	Spray Duration (s)	Rate of Spray (g/s)	Collection Efficiency (%)	Water Lost/Gain (g)	LWC Water Collected (g/m <sup>3</sup> )	LWC Water Sprayed (g/m <sup>3</sup> )	LWC (Collected) Contributed by Blotter (%)	LWC (Collected) Contributed by Silica (%)
30	70.0	0.045	105.71	0.1780	1.1827	1.1188	62.47	43.24
30	80.0	0.043	111.07	0.3776	1.1917	1.0729	61.84	49.23
30	80.0	0.040	110.37	0.3353	1.1159	1.0110	61.33	49.04
30	80.0	0.041	103.41	0.1111	1.0504	1.0158	61.42	41.98
30	80.0	0.040	101.51	0.0486	1.3627	1.3424	61.95	39.56
30	80.0	0.042	111.10	0.3725	1.5420	1.3879	63.70	47.41
30	80.0	0.041	109.17	0.2978	1.4674	1.3441	61.02	48.15
30	150.0	0.027	108.69	0.3474	0.7091	0.6523	56.20	52.50
30	150.0	0.025	105.95	0.2254	0.6645	0.6271	50.22	55.73
30	130.0	0.025	112.89	0.4160	0.6925	0.6134	52.44	60.45
30	130.0	0.024	111.56	0.3644	0.6681	0.5989	50.78	60.78
30	130.0	0.025	115.14	0.4944	0.7145	0.6205	53.41	61.73
30	130.0	0.017	125.77	0.5817	0.5425	0.4314	45.09	80.68
30	130.0	0.027	106.68	0.2337	0.7107	0.6662	52.34	54.34
30	130.0	0.025	107.91	0.2576	0.6693	0.6203	49.30	58.61
30	130.0	0.027	105.05	0.1771	0.7042	0.6703	48.98	56.06
30	130.0	0.027	114.55	0.5135	0.8083	0.7056	44.84	69.71
30	130.0	0.029	118.12	0.6806	0.8417	0.7126	58.24	59.88
30	30	0.336	99.86	(0.0142)	8.4967	8.5087	89.17	10.69
30	30	0.350	95.66	(0.4565)	8.3861	8.7669	85.48	10.17
30	30	0.341	97.07	(0.3004)	8.2865	8.5371	86.63	10.43
20	30	0.333	100.32	0.0318	8.3815	8.3550	89.48	10.84

### 3.5.1 Findings.

The collection efficiencies obtained varied from 84% to 126%. The inlet static pressures recorded during the tests varied from 0.37 to 1.06 psig (10.3" to 29.3" Hg).

Figure 3-19 shows the comparison between the LWC based on the amount of water collected and used (sprayed). The results showed that most data laid on the line of symmetry, which represents equal amounts of water collected and sprayed. The test data for LWC in the range of 3.0 to 4.0g/m<sup>3</sup> indicate that relatively less water was collected compared to the amount of water sprayed. This can also be seen in figure 3-20 where for LWC values between 3.0 and 4.0g/m<sup>3</sup>; the probe collection efficiency was approximately 90%. Figure 3-21 shows the contributions of the blotter paper (indicated the red dots) and silica gel (indicated the blue squares) to the catch efficiency of the probe collector as a function of LWC (based on water collected). Each set of data was also curve-fitted with a log-based power curve, which shows good agreement with experimental data. The two fitted curves intersected at a collection efficiency of about 0.55. The results showed that the sum of the contributions (to the collection efficiency) of the blotter paper and silica gel (includes B-Gon fiber mesh) was nearly 1.0. In addition, the following characteristics were observed from the results in figure 3-21:

- At LWC values between 0.5 and 1.0g/m<sup>3</sup>, the amount of water adsorbed by blotter paper was less than 50%, whereas silica gel (and B-Gon) adsorbed more than 50%. The average collection efficiency was slightly higher than 100%.
- At LWC values between 1.0 and 2.0g/m<sup>3</sup>, the amount of water adsorbed by blotter paper was more than 65%, whereas silica gel (and B-Gon) adsorbed less than 30%. The average collection efficiency was slightly less than 100%.
- At LWC values between 3.0 and 4.0g/m<sup>3</sup>, the amount of water adsorbed by blotter paper was about 70%, whereas silica gel (and B-Gon) adsorbed about 20%. The average collection efficiency was 90%.
- At LWC values of approximately 8.5g/m<sup>3</sup>, the amount of water adsorbed by blotter paper was about 90%, whereas silica gel (and B-Gon) adsorbed about 10%. The average collection efficiency was 100%.

The mean collection efficiency based on the data presented in table 3-13 was 100.8% and the standard deviation was 7.89%.

### 3.5.2 Conclusions.

It was concluded that configuration 11 Mod-I was an efficient water collector, where efficiencies of nearly 100% were attainable for LWC values between 0.54 and 8.5g/m<sup>3</sup>. This configuration was installed in the WSU 7- by 10-ft wind tunnel for iso-kinetic tests, as described in section 4.

#### 4. EXPERIMENTAL INVESTIGATION IN A WIND TUNNEL WITH THE WATER COLLECTOR CONFIGURATION 11 MOD-I DESIGN.

This section describes the experimental tests that were conducted in the WSU 7- x 10-ft Beech Memorial Low-Speed Wind Tunnel. The objective was to evaluate the iso-kinetic operation of the probe and to conduct a limited number of water collection tests. Prior to the wind tunnel tests, an ISFC system was developed and tested in the laboratory. Descriptions of the development of the ISFC system, experimental setup in the wind tunnel, and experimental results are given below.

##### 4.1 TEST FACILITY.

The WSU wind tunnel is a single-return, closed circuit facility with a maximum speed of 160 mph (235 ft/s), corresponding to a Reynolds number of 1.46 million per foot. The test section is 7 ft high by 10 ft wide by 12 ft long. Four screens located in the plenum chamber upstream of the test section were used for flow conditioning. The contraction ratio between the plenum and test sections is 6 to 1. The tunnel is equipped with a four-bladed, 11-ft diameter, variable pitch propeller, which is driven by a 1000-hp electric motor. Figure 4-1 shows the planview of the facility.

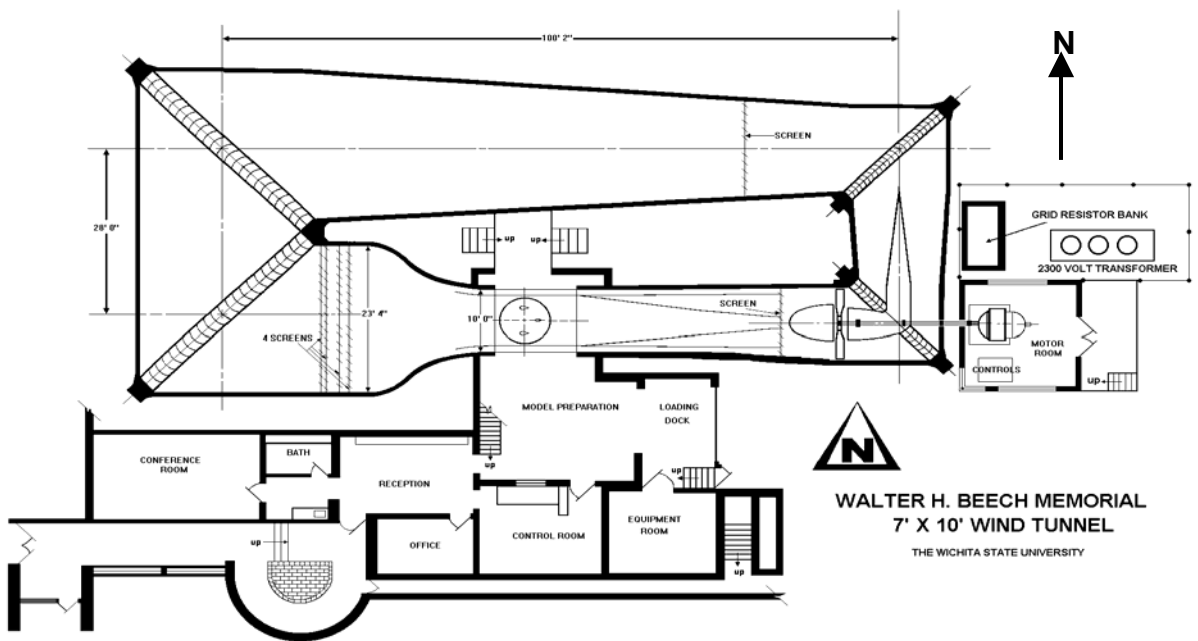


FIGURE 4-1. THE WSU 7- BY 10-ft WIND TUNNEL FACILITY

##### 4.2 PROBE INSTALLATION.

The reference probe was installed at the center of the test section, as shown in figure 4-2. The base of the probe was secured to a 3- by 2-ft by 3/4-inch-thick plywood platform, and the whole assembly was bolted onto the tunnel turntable. A 7- by 8-ft H-type hollow steel frame (diameter 1 inch) was attached to the tunnel floor and ceiling and was located upstream of the probe. The

water spray brush was secured to a steel bracket with two ring clips (figure 4-3), and they, in turn, were secured to the horizontal bar of the H-frame with an adjustable bolt clamp. The steel bracket (and brush) could be adjusted horizontally while vertical movements involved adjusting the H-bar itself. These lateral movements enabled the alignment of the spray brush with the center of the probe inlet. The distance between the spray brush nozzle and probe inlet was set to approximately 1 1/2 inches. The tubing that supplied water to the spray brush was secured to the H-frame and tunnel walls before exiting through a hole that was located next to the entry door of the test section (figure 4-2). Figure 4-4 shows the connection of this tubing to a water supply bottle. A humidity sensor (Vaisala HMP233, accuracy  $\pm 1\%$  RH) was also installed in the test section to record the RH in the air stream during experimental tests and was secured to the horizontal bar with a steel bracket, as shown in figure 4-5. Another humidity sensor (FisherBrand traceable hygrometer, cat.11-661-21, accuracy  $\pm 3\%$  RH) was installed inside the reference probe, as shown in figure 4-6. This was placed centrally at approximately mid-distance between the plastic container exit and reference probe outlet port.

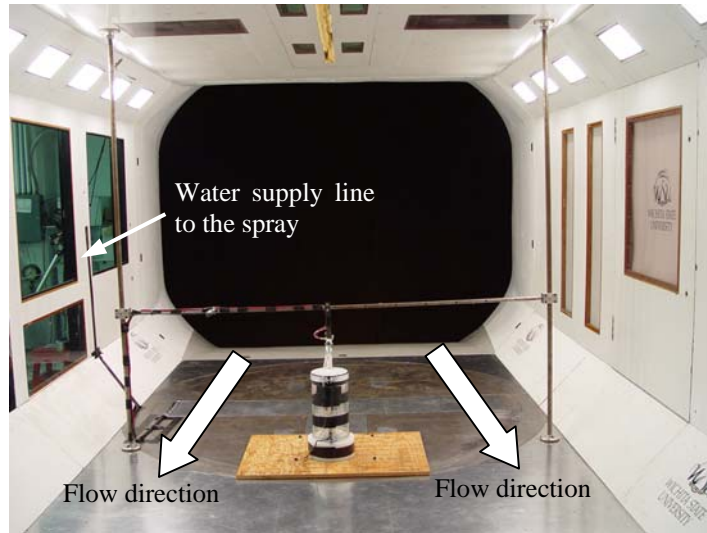


FIGURE 4-2. INSTALLATION OF THE REFERENCE PROBE IN THE WSU 7- BY 10-ft WIND TUNNEL—FRONT VIEW

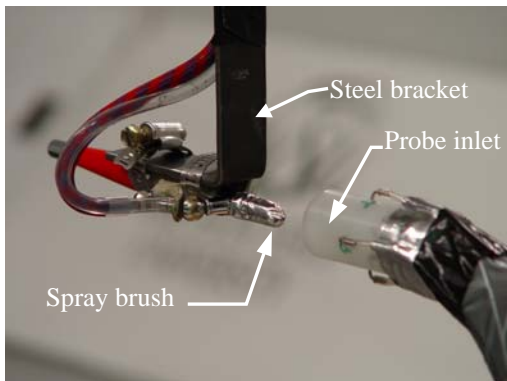


FIGURE 4-3. POSITION OF THE SPRAY BRUSH IN FRONT OF THE PROBE INLET



FIGURE 4-4. WATER SUPPLY FOR THE SPRAY BRUSH

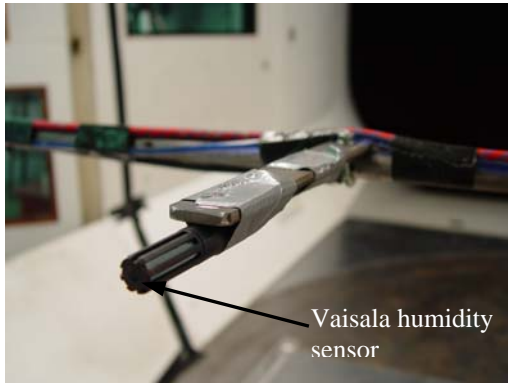


FIGURE 4-5. HUMIDITY SENSOR VAISALA

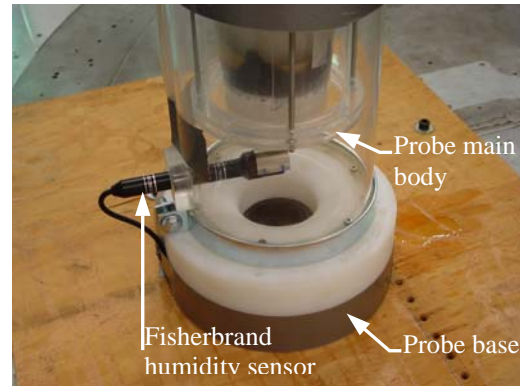


FIGURE 4-6. HUMIDITY SENSOR INSIDE THE REFERENCE PROBE

The room that housed the aerodynamic balance of the wind tunnel, which is located directly beneath the test section, was also used to house the suction fan, throttle valve, and data acquisition system (DAQ). The outlet of the reference probe was connected to the suction fan inlet with a long flexible hose via a hole in the tunnel floor, as shown in figures 4-7 and 4-8. Both the DAQ and throttle valve were parts of the ISFC system. Details of the ISFC system are described in section 4.3.

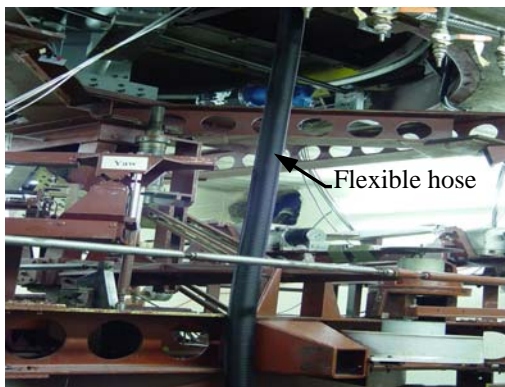


FIGURE 4-7. EXTENSION HOSE CONNECTS PROBE TO SUCTION FAN

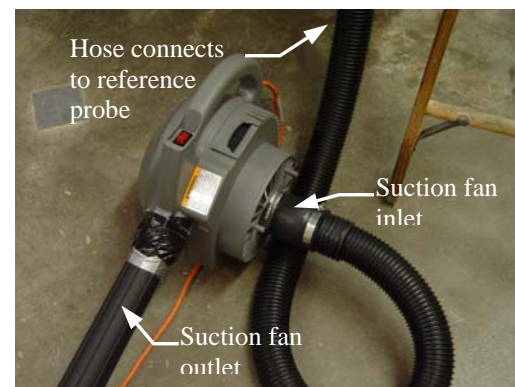


FIGURE 4-8. SUCTION FAN EXHAUST TO THROTTLE VALVE

### 4.3 ISO-KINETIC FLOW CONTROL SYSTEM.

The ISFC system consisted of a throttling valve, DAQ system, pressure transducers, and a computer program to control the closing and opening of the throttling valve. Iso-kinetic condition was attained when the flow velocity in the test section was equal to the probe inlet velocity. During this condition, the probe inlet static pressure was equal to the static pressure of the test section. Since the speed of the suction fan was fixed, it could not be adjusted to match the tunnel velocity. Thus, a throttling valve was used to change the volumetric airflow through the probe, hence adjusting the probe inlet velocity. The objective of the ISFC system, therefore, was to control the throttle valve opening area so that probe inlet velocity could be set equal to the free-stream velocity. Details of the ISFC system components follow.

### 4.3.1 Throttling Valve.

The throttling valve (BE3 PF150-513, RF Technologies Inc), figure 4-9, consisted of an internal elastomer shell enclosed by an outer body made from cast iron. The closing and opening of the shell is analogous to that of a pinch valve where a tube is being pressed by two metal plates to close or open the valve. A Posiflex electro-pneumatic positioner controlled the movements of these plates with a 4- to 20-mA control signal and a line air pressure of 100 psig. The inlet port diameter was 2 inches while the outlet port diameter was 3 inches. The inlet port was connected to the suction fan's exhaust (figure 4-8) via a flexible hose.

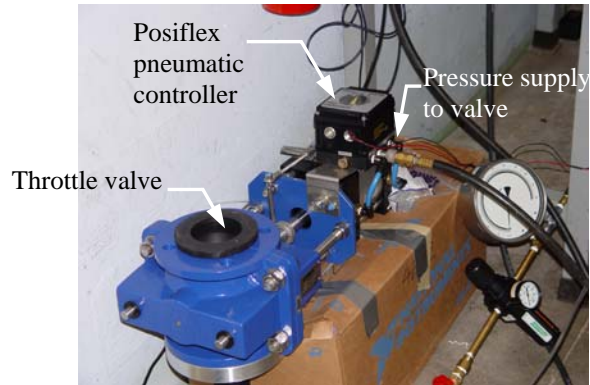


FIGURE 4-9. THROTTLE VALVE

The dynamic characteristics of the ISFC system were obtained by performing probe inlet pressure measurements at different valve openings. Figure 4-10 shows the characteristics of the valve with three different flow blockages. The blockage was created by installing a container (with a cutout hole) downstream of the suction fan exhaust, as shown in figures 3-17 and 3-18. The diameter of the hole in the container determined the range of achievable probe inlet pressures (or velocities), e.g., with 70% blockage. The possible probe inlet pressures were between 0.1 and 0.3 psig, corresponding to inlet speeds in the range of 75 to 130 mph. These characteristic curves were needed to accommodate a range of wind tunnel velocities.

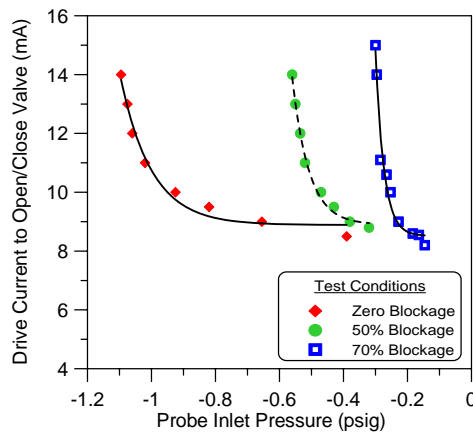


FIGURE 4-10. PROBE INLET PRESSURE VERSUS VALVE DRIVING CURRENT

### 4.3.2 The ISFC Software and Data Acquisition System.

A National Instrument DAQ system, the SCXI-1001 (figure 4-11), was used to record static pressures, RH and temperatures, and to generate a drive current to actuate the throttle valve. The DAQ system was housed in the room beneath the wind tunnel test section, whereas the desktop computer (figure 4-11(d)) was located adjacent to the tunnel control room. The DAQ system was remotely connected to the computer via a 16-ft cable. The SCXI-1001 system has 96 differential input channels, 6 analog channels, 32 digital input/output, and 6 strain-gauge channels. Static pressures were recorded with a pair of pressure transducers (DRUCK PTX7217, range 0-30 psig, 4-20 mA). The electric current output signals from these transmitters had to be converted into voltages by a signal-conditioning unit (SCC311, National Instrument Inc.) because the SCXI system was preconfigured to accept only voltage signal ( $\pm 5V$ ). The RH and temperature from the wind tunnel was recorded with the Vaisala HMP233 sensor (figure 4-5), whereas the Fisherbrand Traceable sensor (figure 4-6) was used inside the reference probe. The output signals from the Vaisala sensor were wired directly into the DAQ system, whereas the signals from the Fisherbrand sensor were connected via an RS323 port on the desktop computer due to the propriety nature of the output signals that prohibited direct connection to the DAQ system.

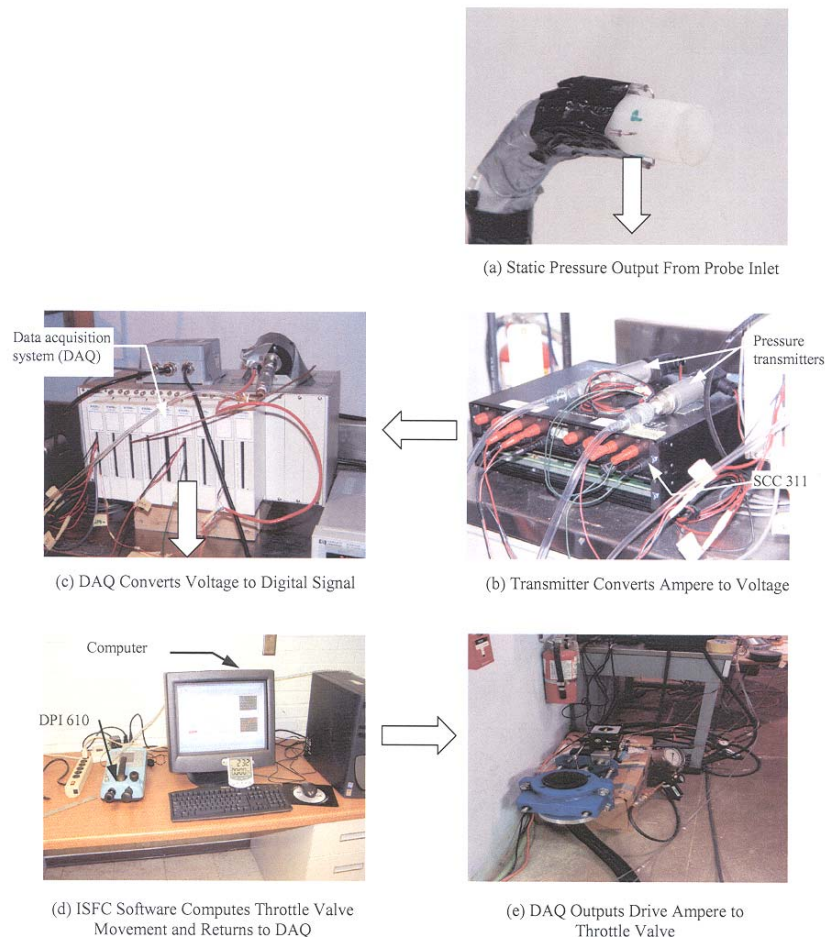


FIGURE 4-11. DATA ACQUISITION SYSTEM (SCXI-1001)

The ISFC software was developed using the LabView (V7.0) to record static pressures, RH, and temperatures. Figure 4-12 shows the front panel of the ISFC code. The software checked for iso-kinetic condition using the static pressures from the probe inlet and the wind tunnel in the following simple expressions:

$$P_{TOTAL}(probe) = P_{TOTAL} (test section) \quad (4-1)$$

hence

$$P_{STATIC}(probe) + P_{DYNAMIC}(probe) = P_{STATIC} (test section) + P_{DYNAMIC}(test section)$$

at iso-kinetic condition

$$P_{DYNAMIC}(probe) = P_{DYNAMIC} (test section) \quad (4-2)$$

therefore

$$P_{STATIC}(probe) = P_{STATIC} (test section) \quad (4-3)$$

where

$P_{TOTAL}$  = total (or stagnation) pressure

$P_{STATIC}$  = static pressure (recorded as gauge pressure by the DRUCK pressure transmitter)

$P_{DYNAMIC}$  = dynamic pressure

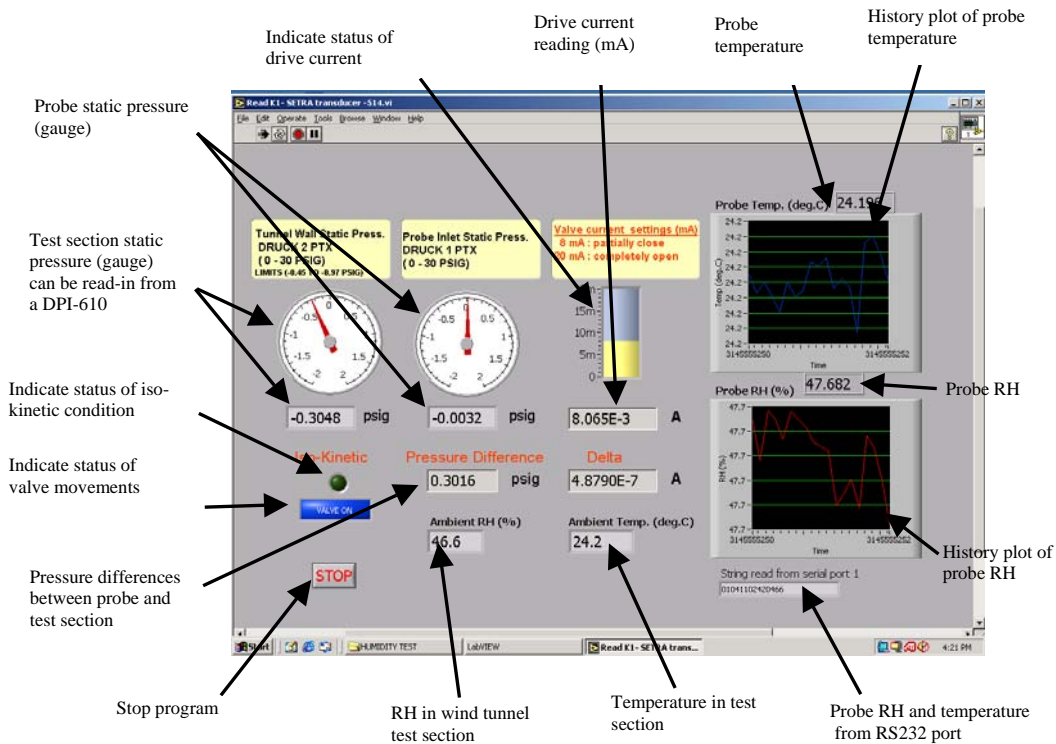


FIGURE 4-12. ISO-KINETIC FLOW CONTROL SOFTWARE

Iso-kinetic condition was attained when the static pressures and, therefore, the dynamic pressures in the probe and wind tunnel were equal. Note that iso-kinetic condition can also be established using the dynamic pressures alone. If the flow was not iso-kinetic, the valve characteristics in figure 4-10 were used to adjust the opening area of the throttle valve until the required iso-kinetic condition was accomplished. The ISFC software was tested prior to the wind tunnel tests in a laboratory to ensure proper integration between the hardware (e.g., pressure transmitters, humidity sensor, etc.) and software. The ISFC development tests involved using a digital pressure indicator (DRUCK DPI-610 in figure 4-11(d)) to simulate static pressures in a wind tunnel, according to equation 4-3. The following steps were used to test the software:

- Set simulated tunnel static pressure
- Start ISFC software
- Switched on suction fan, and run for a set duration
- Stop suction fan (after the set duration has been reached)
- Stop ISFC software and process data

The software recorded the data from the pressure transmitters and humidity sensors every 1.11 seconds and stored the data into a file in the following order (in free format):

- Column 1: Run time (s)
- Column 2: Ambient relative humidity (%RH)
- Column 3: Relative humidity inside probe (%RH)
- Column 4: Ambient temperature (°C)
- Column 5: Temperature inside probe (°C)
- Column 6: Static pressure of tunnel test section (psig)
- Column 7: Probe inlet static pressure (psig)
- Column 8: Integer value (1 indicates iso-kinetic, 0 indicates non-iso-kinetic)

Graphical plots were generated from this output file as shown in figures 4-13 to 4-15, which provide static pressures, RH, and total air temperatures versus run time. Figure 4-13 indicates that iso-kinetic condition was attained at the probe inlet within 3 seconds of engaging the suction fan, followed by a rapid recovery to the initial conditions after disengaging the fan. It also showed that during iso-kinetic condition, the probe inlet static pressure reading was almost equal to the simulated tunnel static pressure. The RH inside the probe is shown in figure 4-14. The results shown in this figure indicate that the humidity exhibited rapid changes during the process of engaging and disengaging the suction fan. The temperature distribution, shown in figure 4-15, did not exhibit the characteristic rapid changes since it was not expected to vary significantly in the laboratory.

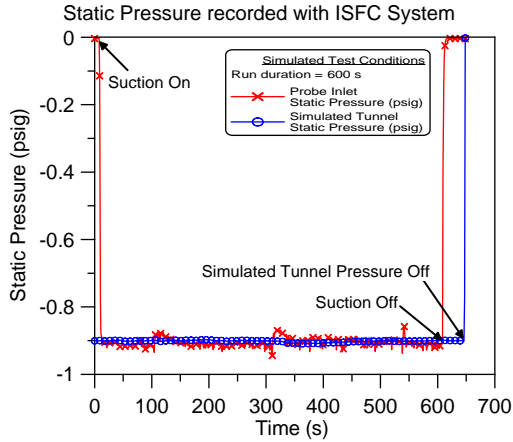


FIGURE 4-13. STATIC PRESSURE PLOTS—LABORATORY

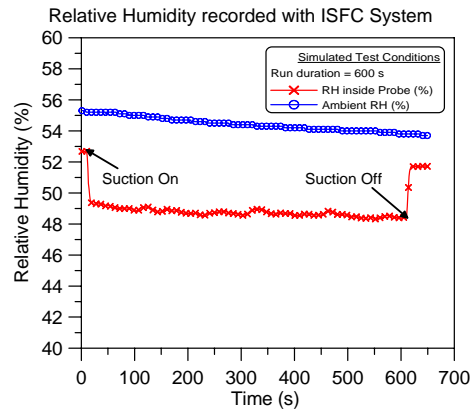


FIGURE 4-14. RELATIVE HUMIDITY PLOTS—LABORATORY

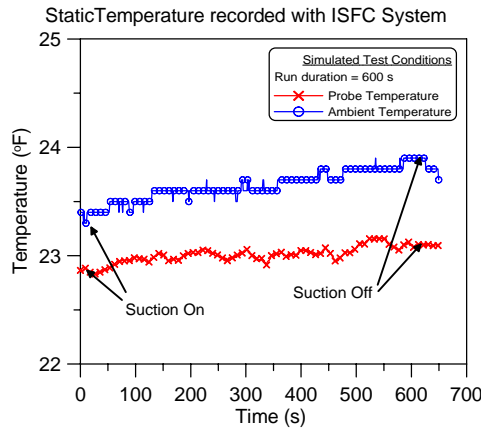


FIGURE 4-15. TEMPERATURE PLOTS—LABORATORY

When the ISFC software was initiated in the laboratory tests, a sequence of events occurred between the various sensors and the DAQ system. This sequence of events is illustrated in figure 4-11 and is described in the following steps:

- a. A pair of pressure transmitters records the static pressures from both the tunnel test section and probe inlet.
- b. The pressure transmitters convert these pressures into voltages ( $\pm 5$  V) for the DAQ system.
- c. The DAQ converts these voltages into digital signals, which were then routed to the computer and read by the ISFC software.
- d. The software computes the difference between the two pressure readings and checks with a set tolerance of  $\pm 0.035$  psig. If it is outside this tolerance, it calculates the amount of valve movement and converts this into the appropriate drive current (mA) via the DAQ system.

- e. This current (4 to 20 mA from the DAQ) operates the pneumatic controller that moves the valve.

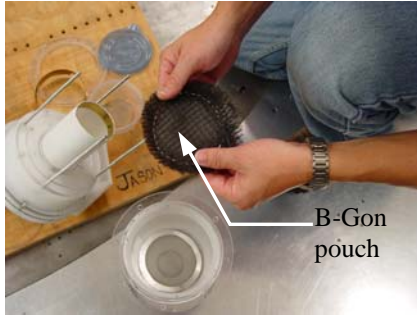
Steps a. to e. were repeated in a loop until iso-kinetic flow condition was achieved. Following the successful development of the ISFC system in the laboratory, the DAQ system and associated sensors were moved to the WSU 7- by 10-ft wind tunnel for iso-kinetic testing, as described in section 4.4.

#### 4.4 TEST PROCEDURE.

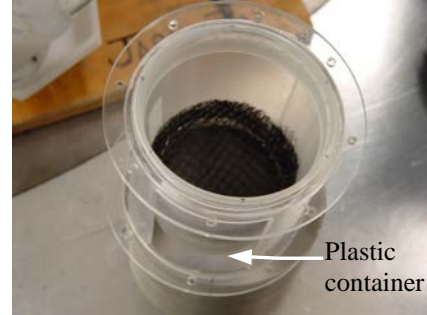
The test procedure previously developed for the laboratory tests (see appendix C, section C.1) was enhanced to include additional procedures required for testing in a wind tunnel. This is written in (appendix C, section C.2). The procedural changes implemented included special features to suit the atmospheric pressure in the test section of the WSU (7- by 10-ft) wind tunnel. The walls of the test section have a number of built-in louvers that were exposed to the outside environmental conditions; therefore, the tunnel velocity was deduced from the dynamic pressure calculated from the tunnel's own calibrated velocity chart. The tunnel crew denoted this dynamic pressure as the Q value, and the unit of measure in pounds per square foot (psf). Although there are static pressure measurements in the test section, they are combined with the static pressure in the plenum to obtain Q.

For iso-kinetic calculations, this (Q) value was converted into static pressures (equation 4-3, section 4.3) and simulated with the DPI-610 digital pressure indicator (figure 4-16(e)) using the methodology described earlier in the testing of the ISFC software in the laboratory (section 4.3.2). The tunnel operator read out the Q value to the ISFC system operator who then entered this value into the DPI-610. The ISFC software (figure 4-12) reads the value entered into the DPI-610 and treat this as the static pressure in the test section of the wind tunnel. The test procedures that were developed for the laboratory (section C.1, appendix C) had to be modified for the wind tunnel tests. The modified test procedure is shown in section C.2, appendix C (modifications are written in *italics*). The following summarizes the wind tunnel tests:

- Prepare water sample, silica gel, B-Gon, and blotter tube and install into reference probe
- Start ISFC software
- Tunnel operator starts wind tunnel and reads out the Q value (psf) to the ISFC operator
- ISFC operator enters the Q value into the DPI-610, thus setting the simulated tunnel static pressure
- Switch on suction fan
- Start water spray
- Stop suction fan (after the set duration has been reached)
- Stop wind tunnel and ISFC software, process data



(a) Preparation of B-Gon Pouch Filled With Silica Gel



(b) Installation of B-Gon Into Plastic Container



(c) Preparation of Blotter Tube



(d) ISFC Operation and Control



(e) Digital Pressure Indicator DPI-610

FIGURE 4-16. PREPARATION OF THE REFERENCE PROBE AND ISFC CONTROL

Figure 4-16 shows the preparation of the reference probe and ISFC control, figure 4-16(a) shows the B-Gon pouch being prepared for the plastic container, figure 4-16(b) shows the B-Gon pouch inside the plastic container, figure 4-16(c) shows the blotter tube and brass rings that were used to maintain the shape of the tube, figure 4-16(d) shows the operation and control of the ISFC software, and figure 4-16(e) shows the DPI-610 that was used to simulate the static pressure in the test section of a wind tunnel.

#### 4.5 TEST MEASUREMENTS.

The reference LWC probe test program in the WSU wind tunnel was carried out during a 4-day period between July 29 and August 1, 2003. The installation of the reference probe and ISFC system were completed in the first day of the test program. The second day involved the assessment of the water spray brush in the wind tunnel and the structural integrity of the reference probe at a range of tunnel velocities.

Two problems with the spray brush were discovered during the preliminary assessment: (1) water had entered the probe static pressure ports causing blockages to the pressure transmitters and (2) a continuous drip had developed in the spray brush. The first problem did not occur during laboratory tests (section 3) because the suction fan was always operating during these tests. However, it was discovered that if the suction fan was switched off while water was sprayed into the probe, blockage would occur. Water in the pressure lines was eventually cleared with compressed air. The second problem was solved by simply raising the height of the water bottle above the level of the floor.

During the integrity test of the reference probe, it was discovered that the main body (of the probe) had detached itself from the base that was bolted to the plywood platform (figure 4-6). This had occurred at a tunnel velocity of approximately 140 mph (63m/s) or  $Q \approx 50.4$  psf (0.35 psi). This problem was solved by permanently joining the probe main body to the base with a solvent-based adhesive. As an added precaution, it was also decided to limit the maximum tunnel velocity to 130 mph (58 m/s) or  $Q \approx 43.2$  psf (0.30 psi). Iso-kinetic and water collection efficiency tests were conducted in the last two days of the test program. Prior to these tests, the appropriate characteristics of the throttle valve in the wind tunnel had to be established because of the low tunnel velocities or ( $Q$  values). It was found that the suction fan with a 70% blockage (figure 4-10) was capable of providing the range of probe velocities required to match the tunnel velocities.

The results are shown in figures 4-17 and 4-18 and table 4-1. Tests 1 to 17 were conducted with the wind tunnel on, and tests 18 to 20 represent static spray tests that were also conducted in the wind tunnel but the wind tunnel was off (i.e., zero airspeed). Appendix D shows plots of static pressures, RH, and temperatures for tests 1 to 20. The following test conditions were used:

- Water used or sprayed 0.67 to 2.9 g
- Spray brush pressure setting 25 to 50 psig
- Spray duration 130 s
- Spray rate 0.0051 to 0.0224 g/s
- LWC 0.14 to 0.79 g/m<sup>3</sup>
- Test duration 130 s

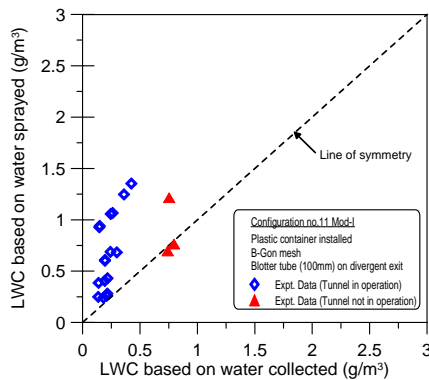


FIGURE 4-17. COMPARISON BETWEEN LWCs BASED ON WATER COLLECTED AND SPRAYED

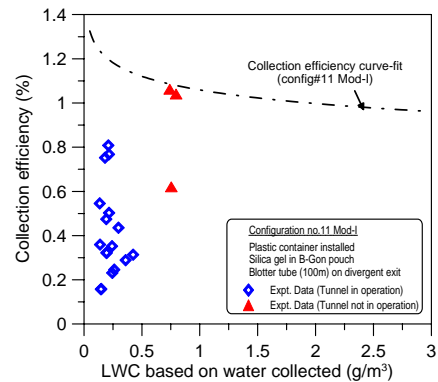


FIGURE 4-18. LIQUID WATER CONTENT VERSUS COLLECTION EFFICIENCY

TABLE 4-1. TEST RESULTS FOR CONFIGURATION 11 MOD-I (WIND TUNNEL)

Test No.	Weight of Blotter Paper		Amount of Water Collected (g)	Weight of Spray Water Used		Amount of Water Used (g)	Inlet Pressure (psig)	Spray Pressure (psig)
	Before	After		Before	After			
1	26.5380	26.7387	0.9924	139.7827	136.6169	3.1658	0.20	50
	26.7995	27.5912	0.7917					
2	26.4162	27.4820	0.8425	136.6139	133.6964	2.9175	0.20	50
	26.8897	26.6664	-0.2233					
3	26.3796	26.4871	0.6401	133.6949	130.9292	2.7657	0.25	50
	26.6339	27.1665	0.5326					
4	26.4268	26.5365	0.6856	130.9282	128.1402	2.7880	0.25	50
	26.8324	27.4083	0.5759					
5	26.5098	26.4621	0.4177	128.1390	125.4819	2.6571	0.30	50
	26.9385	27.4039	0.4654					
6	26.3865	26.3243	0.4266	125.4802	122.7861	2.6941	0.30	50
	26.7569	27.2457	0.4888					
7	26.5069	26.4530	0.6969	119.2784	117.6788	1.5996	0.20	50
	26.5893	27.3401	0.7508					
8	26.5527	26.4508	0.5670	117.7110	116.1017	1.6093	0.20	50
	26.7576	27.4265	0.6689					
9	26.6245	26.4878	0.5108	116.0941	114.5026	1.5915	0.25	50
	26.8820	27.5295	0.6475					
10	26.4907	26.3445	0.5084	114.4993	112.9259	1.5734	0.25	50
	26.4684	27.1230	0.6546					
11	26.6495	26.5003	0.5070	112.9178	111.9098	1.0080	0.20	35
	26.7335	27.3897	0.6562					
12	26.4151	26.2761	0.5030	111.9080	110.8483	1.0597	0.25	35
	26.7071	27.3491	0.6420					
13	26.3765	26.2180	0.3974	110.8455	109.7392	1.1063	0.30	35
	26.6949	27.2508	0.5559					
14	26.5009	26.3567	0.5059	109.7380	109.0791	0.6589	0.20	25
	26.6838	27.3339	0.6501					
15	26.4478	26.2983	0.5495	109.0580	108.3780	0.6800	0.25	25
	26.6458	27.3448	0.6990					
16	26.4315	26.2641	0.3895	108.3748	107.6608	0.7140	0.30	25
	26.7504	27.3073	0.5569					
17	26.4541	26.3278	0.5211	107.6581	106.9656	0.6925	0.30	25
	26.6889	27.3363	0.6474					
18	26.4160	26.8135	1.7639	122.6318	119.7889	2.8429	0.20	50
	26.9036	28.2700	1.3664					
19	26.5445	26.9524	1.8615	122.6224	120.8334	1.7890	0.20	50
	26.8788	28.3324	1.4536					
20	26.4325	26.6972	1.7332	120.9156	119.2840	1.6316	0.20	50
	26.8776	28.3461	1.4685					

TABLE 4-1. TEST RESULTS FOR CONFIGURATION 11 MOD-I  
(WIND TUNNEL) (Continued)

Spray Duration (s)	Rate of Spray (g/s)	Collection Efficiency (%)	Water Lost/Gain (g)	LWC Water Collected (g/m <sup>3</sup> )	LWC Water Sprayed (g/m <sup>3</sup> )	LWC Collected by Blotter (%)	LWC Collected by Silica (%)
130.0	0.024	31.35	(2.1734)	0.4241	1.3529	6.34	25.01
130.0	0.022	28.88	(2.0750)	0.3600	1.2468	36.53	-7.65
130.0	0.021	23.14	(2.1256)	0.2447	1.0571	3.89	19.26
130.0	0.021	24.59	(2.1024)	0.2621	1.0657	3.93	20.66
130.0	0.020	15.72	(2.2394)	0.1457	0.9271	-1.80	17.52
130.0	0.021	15.83	(2.2675)	0.1489	0.9401	-2.31	18.14
130.0	0.012	43.57	(0.9027)	0.2978	0.6836	-3.37	46.94
130.0	0.012	35.23	(1.0423)	0.2423	0.6877	-6.33	41.56
130.0	0.012	32.10	(1.0807)	0.1952	0.6083	-8.59	40.68
130.0	0.012	32.31	(1.0650)	0.1943	0.6014	-9.29	41.60
130.0	0.008	50.30	(0.5010)	0.2167	0.4308	-14.80	65.10
130.0	0.008	47.47	(0.5567)	0.1923	0.4051	-13.12	60.58
130.0	0.009	35.92	(0.7089)	0.1387	0.3860	-14.33	50.25
130.0	0.005	76.78	(0.1530)	0.2162	0.2816	-21.88	98.66
130.0	0.005	80.81	(0.1305)	0.2100	0.2599	-21.99	102.79
130.0	0.005	54.55	(0.3245)	0.1359	0.2491	-23.45	78.00
130.0	0.005	75.25	(0.1714)	0.1818	0.2416	-18.24	93.49
130.0	0.022	62.05	(1.0790)	0.7538	1.2149	13.98	48.06
130.0	0.014	104.05	0.0725	0.7955	0.7645	22.80	81.25
130.0	0.013	106.23	0.1016	0.7407	0.6973	16.22	90.00

## 4.6 RESULTS AND DISCUSSIONS.

The collection efficiencies obtained during the wind tunnel test varied from 15% to 81% for runs 1 to 17 and from 62% to 106% for test runs 18 to 20. The inlet static pressures recorded during these tests varied from 0.2 to 0.3 psi (5.5 to 8.3 in. of water). A limited range of LWC intensities were considered in the wind tunnel investigation. It was not possible to conduct tests over a wider range of LWC because of the limited resources allocated for wind tunnel tests.

Figure 4-17 shows that for tests 1 to 17, the amount of water collected was much lower than that sprayed into the reference probe. Therefore, the probe collection efficiencies were also well below the maximum value of 100%, as shown in figure 4-18. The main cause of these poor results was the significant amount of water lost through evaporation during the tests. Typical RH and temperatures that were recorded in the wind tunnel for all the experimental tests are shown in figures 4-19 and 4-20 respectively. In a normal test lasting only 130 seconds, the tunnel RH decreased from about 28% to 20% (indicated by the blue dots in figure 4-19), while tunnel total temperature increased from about 97° to 108°F (36° to 42°C, indicated by blue dots in figure 4-20). The RH recorded inside the probe decreased from 35% to 33% (indicated by the red dots in figure 4-19) and the temperature increased from 97° to 108°F (36° to 43°C, indicated by red dots in figure 4-20). These measurements were different from those recorded during the spray tests with the tunnel off, tests 18 to 20. Figure 4-21 shows that the RH recorded inside the probe increased from 43% to 46%, whereas figure 4-22 indicates that the temperature decreased from 86° to 82°F (30° to 28°C). The tunnel RH and temperature recorded during these tests remained fairly constant at 41% and 85°F (29.3°C), respectively. Therefore, collection efficiencies within 100% were obtained for these tests, except in test 18 where the probe water collection efficiency was 62%. However, these results were consistent with those conducted in the laboratory (section 3.5). The evaporation effects shown in table 4-1 where water evaporation from the dry blotter paper was observed (based on weight measurements of the blotter before and after the test) were recorded in tests 5 to 17, while water adsorption by the paper was observed during spray tests 18 to 20.

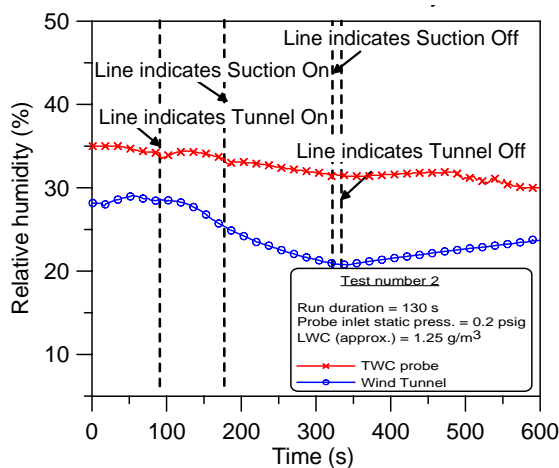


FIGURE 4-19. PROBE AND TUNNEL RH DISTRIBUTION—WIND TUNNEL IN OPERATION

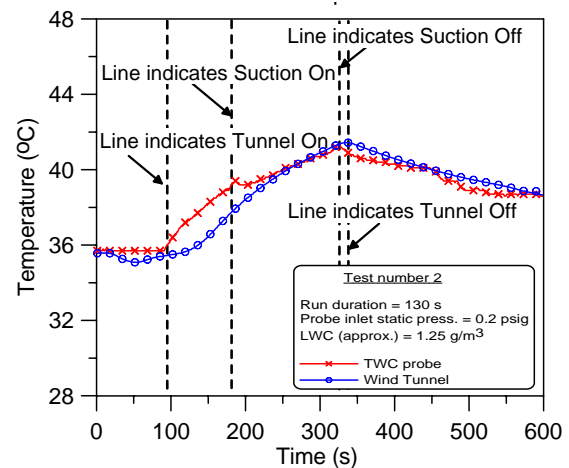


FIGURE 4-20. PROBE AND TUNNEL TEMPERATURE DISTRIBUTION—WIND TUNNEL IN OPERATION

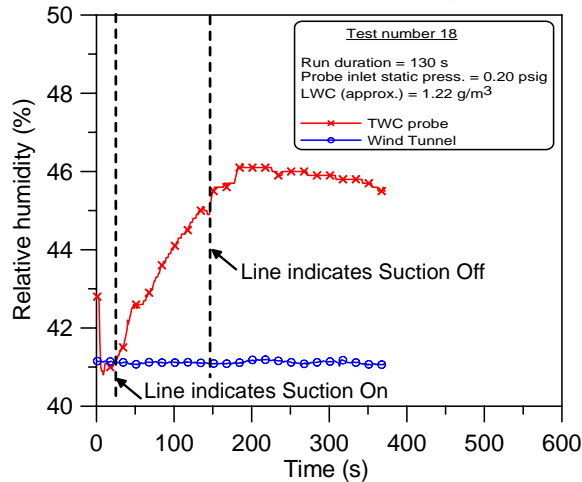


FIGURE 4-21. PROBE AND TUNNEL RH DISTRIBUTION—STATIC SPRAY TEST

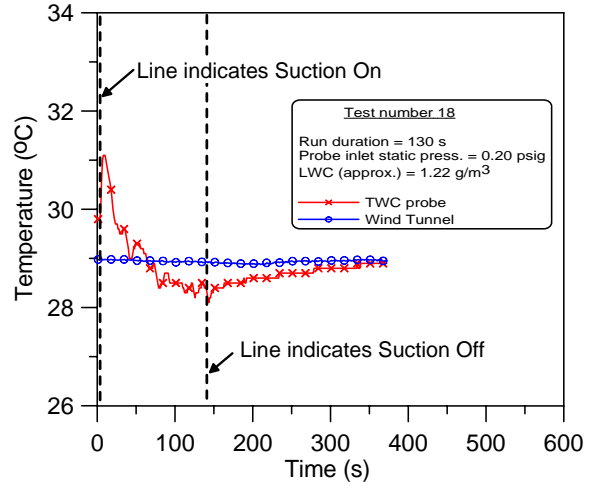


FIGURE 4-22. PROBE AND TUNNEL TEMPERATURE DISTRIBUTION—STATIC SPRAY TEST

Iso-kinetic conditions were accomplished in all the experimental tests for tunnel velocities between 105 and 130 mph (47 to 58 m/s, Q 28.8 to 43.2 psf). Typical static pressure measurements at the probe inlet are shown in figures 4-23 (test 2) and 4-24 (test 18). These two test points were selected because the test conditions and amount of water sprayed (or used) were similar, although test 2 was conducted while the wind tunnel was operating, whereas for test 18, the tunnel was off. Figure 4-23 shows that prior to switching on the suction fan, a ramp pressure had developed inside the reference probe. Upon switching the fan on the static pressure decreased rapidly and iso-kinetic flow was attained in less than 3 seconds. The drift in the probe inlet static pressure was due primarily to the unstable aerodynamic performance of the suction fan at low volumetric flows, which was created by blocking 70% of the fan exhaust flow (figure 4-10). However, the ISFC software was able to adjust the throttle valve and maintained iso-kinetic condition. The difference between the tunnel and probe inlet static pressures was  $\pm 0.035$  psi (preset in the software). When the suction fan was switched off, the probe inlet static pressure returned rapidly to the initial state where a ramp pressure had been present. These characteristic static pressure distributions recorded during the tunnel operation (figure 4-23) were similar to those recorded during the static spray tests presented in figure 4-24, except that the ramp pressure was no longer present (in the spray tests). Therefore, the iso-kinetic performance of the probe in a laboratory was similar to that in the wind tunnel.

In summary, although iso-kinetic flows were attained quite rapidly, water collection efficiencies were quite poor due to the extreme conditions in the WSU wind tunnel (RH  $\sim$  20% to 40%, temperatures  $\sim$  100°F). It was believed that had the tests been conducted at conditions similar to those found in icing wind tunnels (RH  $\sim$  90% to 100%, temperatures  $\sim$  32°F), significant improvements would have been obtained. However, the addition of the humidity sensor inside the reference probe revealed the effect of evaporation on collection water efficiency and provided a new way for accounting for these effects. The use of a humidity sensor to correct for the effects of water evaporation inside the probe is discussed in section 5.

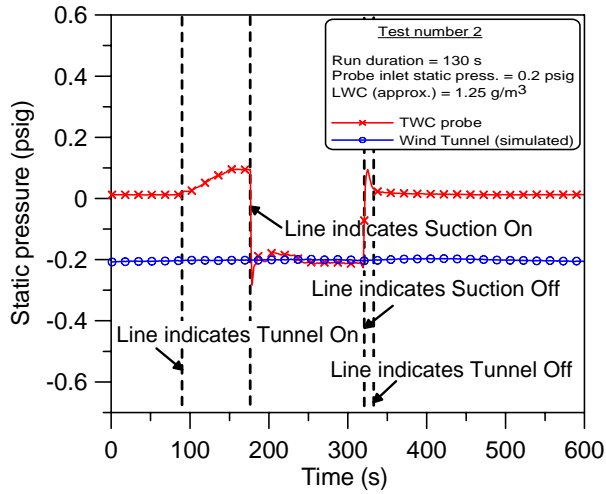


FIGURE 4-23. PROBE AND TUNNEL PRESSURE DISTRIBUTION—WIND TUNNEL IN OPERATION

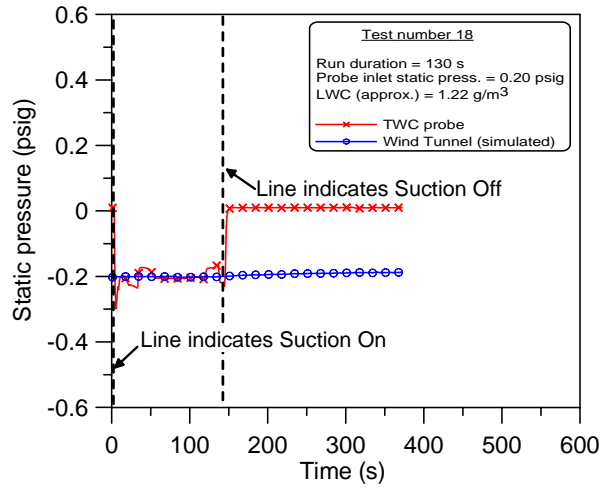


FIGURE 4-24. PROBE AND TUNNEL PRESSURE DISTRIBUTION—STATIC SPRAY TEST

## 5. EXPERIMENTAL INVESTIGATION WITH THE WATER COLLECTOR CONFIGURATION 11 MOD-II DESIGN.

The water collector configuration 11 Mod-I was successfully tested under laboratory conditions. This design used a combination of blotter paper, silica gel, and B-Gon fiber to adsorb and trap incoming water droplets. However, the tests (collection efficiencies) conducted in the wind tunnel were less successful due to the dry conditions in the test section that led to excessive evaporation. Humidity sensors that were installed inside the probe and wind tunnel had recorded temperatures of around 100°F and humidity below 35%. It must be recognized that the reference probe (final production version) is expected to perform at near-freezing conditions and humidity of about 100%; therefore, the test conditions in the WSU wind tunnel were far from ideal. In addition, silica gel desiccant (encased in the B-Gon mesh) also adsorbed moisture from the test environment as well as those evaporated by the water droplets from the spray cloud. Although they made significant contributions to the water collection efficiency measurements (as shown in figure 3-21), it was difficult to quantify their respective contributions due to the presence of the desiccant material, which affected the RH measurements. To overcome this problem, the desiccant was removed from the Mod-I design, and the hydrophobic B-Gon layer mesh was increased from two to six layers to prevent trapped water (in between the mesh) from escaping through the collector exit. The low-accuracy humidity sensor inside the reference probe was also replaced with a more accurate sensor, as shown in figure 5-1. This modified setup was renamed as configuration 11 Mod-II design since the only difference to the Mod-I design was the absence of the silica gel desiccant. A technique for computing the LWC values, water mass from the spray cloud, and environmental moisture was also devised using data recorded by the humidity sensor.

A limited number of tests were performed in a laboratory with the Mod-II design due to the time constraint. This section describes the method of computing the LWC, test measurement, data reduction technique, and the results obtained.

### 5.1 METHOD OF COMPUTING LWC WITH RELATIVE HUMIDITY MEASUREMENTS.

The proposed methodology relies on the measured data from the dry (spray-off) and wet (spray-on) tests, which would have been conducted consecutively under similar conditions, i.e., same probe inlet velocities and test conditions. The RH measurements recorded at the water collector exit (inside the probe) consisted of vapor from the test environment and evaporated moisture from the spray cloud. These measurements were converted to the absolute values by employing a set of humidity equations given in appendix F. In a dry (spray-off) test, the absolute vapor mass ( $M_{v|dry}$ ) from the test environment alone was computed as follows:

$$M_{v|dry} = RH_{sp|dry} \times M_h|dry \quad (5-1)$$

Similarly for a wet (spray-on) test, i.e., vapor attributed to the evaporated droplets and test environment

$$M_{v|wet} = RH_{sp|wet} \times M_h|wet \quad (5-2)$$

where

$RH_{sp}$  = specific humidity (ratio of the mass of water vapor (g) to the mass of humid air (g))  
 $M_h$  = mass of humid air (air from the test environmental air)

By performing the dry and wet tests consecutively, the errors due to changes in the environmental RH, temperature, and pressure as well as water lost due to evaporation inside the probe were minimized. (*The test conditions must be similar, i.e., same probe inlet static pressures and test durations*). The evaporated water droplets due only to the spray cloud ( $M_{evp}$ ) were obtained by subtracting the above water vapor masses in equations 5-1 and 5-2 as follow:

$$M_{evp} = M_{v|wet} - M_{v|dry} \quad (5-3)$$

The total mass of the evaporated water, water adsorbed by the blotter paper ( $M_{blotter}$ ) and B-Gon fiber ( $M_{B-Gon}$ ), must be equal to the amount of water that was sprayed into the reference probe, assuming no losses. Hence,

$$M_{sprayed} = M_{evp} + M_{blotter} + M_{B-Gon} \text{ (assumes no losses)}$$

Therefore, the LWC value was computed as follows:

$$LWC = \frac{(M_{evp} + M_{blotter} + M_{B-Gon})}{M_{h|dry} \text{ \{or } M_{h|wet} \}}$$

since  $M_{h|dry} = M_{h|wet}$ , assuming that the dry and wet tests were performed under the same conditions.

## 5.2 TEST MEASUREMENTS.

The ISFC system (section 4.3) was set up in the WSU laboratory where the initial tests to select an efficient water collector configuration was conducted (section 3). The Fisherbrand Traceable humidity probe that was installed in the reference probe was replaced with a Vaisala humidity sensor (figure 5-1), which is considerably more accurate. The Fisherbrand probe (figure 5-2) was used to record the environmental RH and temperature in the icing laboratory. To minimize the effects due to reingestion of the evaporated vapor, the exhaust air from the throttle valve was extracted from the laboratory by placing the throttle valve inside a fume cupboard, as shown figure 5-3. Figure 5-4 shows the instrumentations of the ISFC system including the DAQ system and DPI-601, which was used to provide a simulated tunnel static pressure.

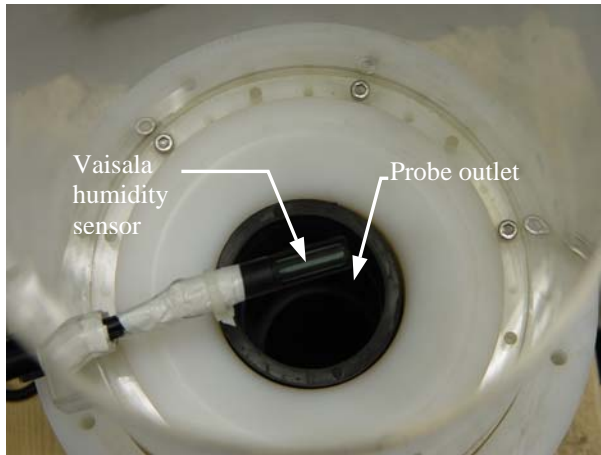


FIGURE 5-1. HUMIDITY SENSOR INSIDE THE REFERENCE PROBE



FIGURE 5-2. FISHERBRAND HUMIDITY SENSOR

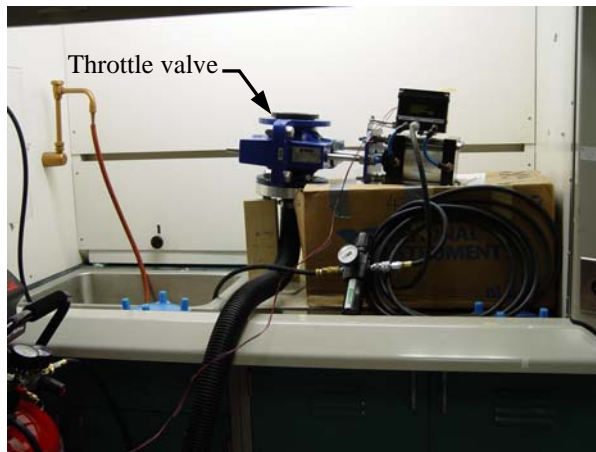


FIGURE 5-3. THROTTLE VALVE INSTALLED IN A FUME CUPBOARD



FIGURE 5-4. ISO-KINETIC FLOW CONTROL SYSTEM

The test procedures, described in appendix C, section C.1, were applied to the two consecutive tests (i.e., dry and wet tests). As mentioned earlier, probe inlet conditions for the wet and dry tests should be identical. However, in practice, inlet conditions can change to some extent when test durations are excessively long. To minimize this effect, the test (or run) durations were set to between 5 and 10 minutes. It was anticipated that the blotter paper would have to adsorb more water due to the longer test durations (compared to the test durations conducted previously in sections 3 and 4); therefore, a multilayered blotter paper tube was fabricated instead of the single-layered design used in previous tests. Figure 5-5 shows the method of fabricating a multilayered blotter tube design. The two-layered B-Gon fiber mesh was replaced with a six-layered mesh to prevent trapped water (in between the mesh) from escaping through the collector exit. It was found that the aerodynamic performance (inlet suction) of the probe with this thicker mesh was unaffected, which seems to suggest that the pressure loss in the fiber mesh was similar to that caused by the silica gel.



FIGURE 5-5. METHOD OF CREATING A MULTILAYERED BLOTTER TUBE

The results are shown in figures 5-6 to 5-9 and table 5-1; tests 1 to 4 were conducted with a probe inlet pressure of 0.9 psig, whereas tests 5 to 9 were conducted with 0.4 psig. The run duration in tests 8 and 9 were longer than the spray duration (i.e., the test run time was longer than the spray time). The graphical plots of the static pressure, relative humidity, and temperature for the tests, listed in table 5-1, are shown in appendix E. Due to time constraints, only a limited number of tests were performed. The following test conditions were used:

- Water used or sprayed 3.05 to 19.8 g
- Spray brush pressure setting 30 psig
- Spray duration 300 to 600 s
- Spray rate 0.009 to 0.066 g/s
- LWC 0.24 to 2.56 g/m<sup>3</sup>
- Run duration 300 to 420 s

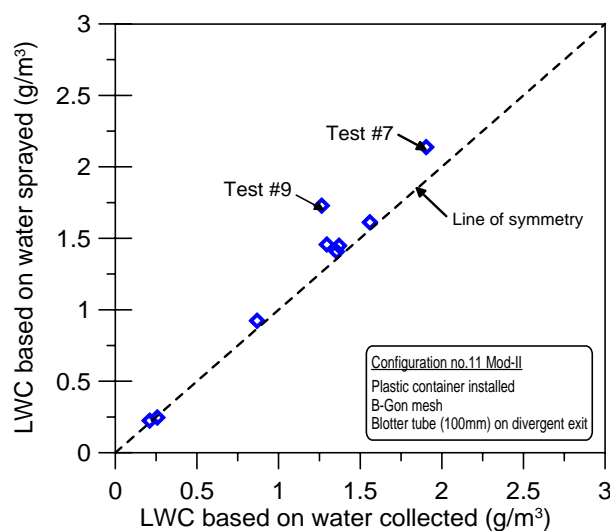


FIGURE 5-6. COMPARISON BETWEEN LWCs BASED ON WATER COLLECTED AND WATER SPRAYED

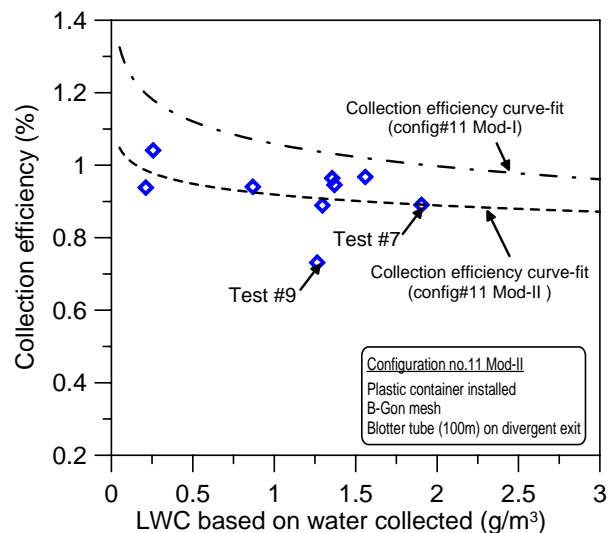


FIGURE 5-7. LIQUID WATER CONTENT BASED ON WATER COLLECTED VERSUS COLLECTION EFFICIENCY

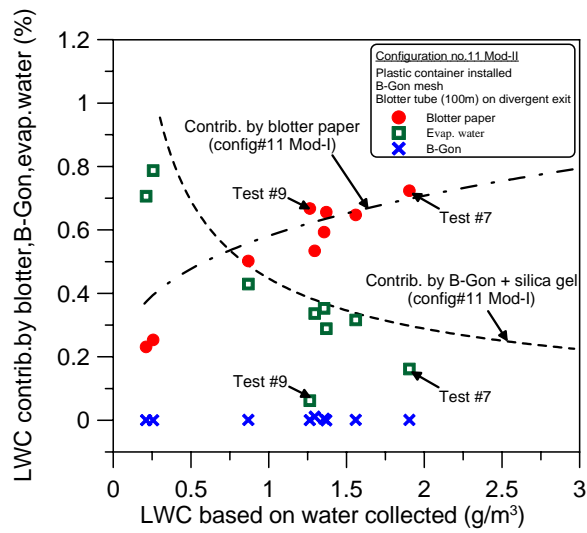


FIGURE 5-8. CONTRIBUTION TO THE LWC BY BLOTTER, B-GON, AND EVAPORATED WATER

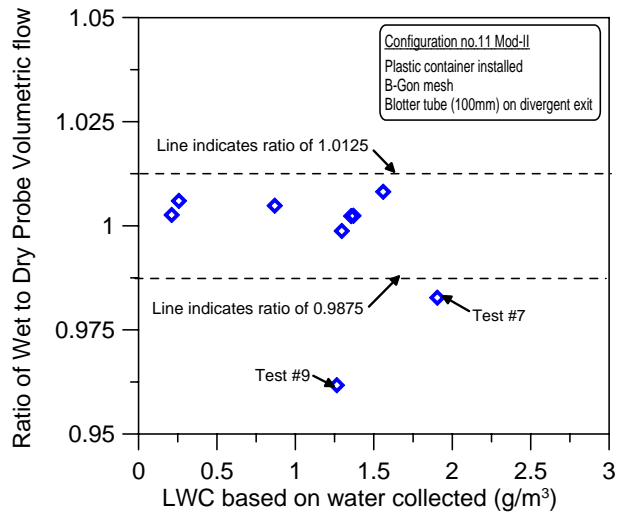


FIGURE 5-9. DISTRIBUTION OF PROBE VOLUMETRIC MASS FLOW RATIO

TABLE 5-1. TEST RESULTS FOR CONFIGURATION 11 MOD-II (LABORATORY)

Test No.	Row 1: Weight of Blotter Paper		Row 2: Weight of B-Gon		Total Amount of Water Collected (g)	Weight of Spray Water Used		Total amount of Water Used (g)	Probe Inlet Pres. (psig)	Spray Pres. (psig)	Water Spray Duration (s)	Run Duration (s)	Rate of Spray (g/s)	Collection Efficiency (B-Gon) (%)	Collection Efficiency (Blotter) (%)	Loss Due to Evap. (g)	LWC (Based on Water Used) (g/m <sup>3</sup> )	LWC (Based on Water Collected) (g/m <sup>3</sup> )
	Before	After	Before	After														
1	28.7339	30.0283	108.5984	103.0045	5.5939	0.9	30	600.0	0.009	0.05	23.1	(4.2968)	0.2442	0.0566				
	22.6448	22.6475																
2	28.6090	29.3813	111.6938	108.6464	3.0474	0.9	30	300.0	0.010	0.01	25.3	(2.2747)	0.2661	0.0675				
	22.6475	22.6479																
3	28.6767	34.4202	107.7081	96.2707	11.4374	0.9	30	300.0	0.038	0.12	50.2	(5.5937)	0.9986	0.5102				
	22.6443	22.6577																
4	42.208	53.8775	115.4514	97.6659	17.7855	0.9	30	300.0	0.059	-0.01	65.6	(6.0988)	1.5528	1.0204				
	22.609	22.6072																
5	28.6567	35.5926	126.6400	114.9471	11.6929	0.4	30	300.0	0.039	0.51	59.3	(4.5456)	1.5313	0.9360				
	22.6370	22.6972																
6	28.6554	35.1798	96.2394	84.0242	12.2152	0.4	30	300.0	0.041	1.15	53.4	(5.4638)	1.5997	0.8842				
	22.6403	22.7805																
7	42.2233	54.9578	96.2190	78.6219	17.5971	0.4	30	300.0	0.059	0.12	72.4	(4.7699)	2.3046	1.6799				
	22.6356	22.6561																
8	41.4475	51.8481	94.9912	78.9244	16.0668	0.4	30	300.0	0.054	0.13	64.7	(5.6027)	2.1042	1.3704				
	22.6331	22.6546																
9	42.3359	55.5723	111.6247	91.7976	19.8271	0.4	30	300.0	0.066	0.05	66.8	(6.5536)	2.5648	1.7170				
	20.9647	20.9755																

TABLE 5-1. TEST RESULTS FOR CONFIGURATION 11 MOD-II (LABORATORY) (Continued)

Test No.	Dry Test					Wetted Test				
	Integrated Run Duration (s)	Integrated Air Mass Flow (kg)	Integrated Vapor Mass (g)	Actual Amount of Water Used (g)	Total Vapor and Water Used (g)	Integrated Run Duration (s)	Integrated Air Mass Flow (kg)	Integrated Vapor Mass (g)	Amount of Water Collected by Blotter (g)	Total Vapor and Water Collected (g)
1	598.4	24.826	233.876	5.5939	239.470	599.0	24.891	237.828	1.2971	239.125
2	298.7	12.297	114.327	3.0474	117.374	298.6	12.371	116.726	0.7727	117.499
3	297.7	12.325	114.840	11.4374	126.278	297.5	12.385	119.751	5.8437	125.595
4	297.71	12.24698	114.22327	17.7855	132.009	297.70	12.276	119.356	11.6867	131.043
5	299.0	8.294	80.389	11.6929	92.082	299.3	8.313	84.515	7.1473	91.662
6	300.0	8.396	80.974	12.2152	93.190	300.0	8.385	85.085	6.7514	91.836
7	300.0	8.376	81.116	17.5971	98.713	300.2	8.231	83.965	12.8272	96.792
8	358.3	9.888	96.730	16.0668	112.797	358.7	9.969	101.811	10.4641	112.275
9	419.9	11.927	115.477	19.8271	135.304	419.4	11.471	116.703	13.2735	129.976

TABLE 5-1. TEST RESULTS FOR CONFIGURATION 11 MOD-II (LABORATORY) (Continued)

Computed Amount of Water Collected (g)	Ratio Between Wetted and Dry Air Mass Flow	Ratio Between Wetted and Dry Total Vapor and Water Mass	(Collection Efficiency) Ratio Between Water Collected and Sprayed (%)	LWC (Based on Computed Amount of Water Collected) (g/m <sup>3</sup> )	LWC (Based on Actual Amount of Water Sprayed) (g/m <sup>3</sup> )	Percent Difference LWC	LWC Collection Contributed by B-Gon (%)	LWC Collection Contributed by Blotter (%)	LWC Collection Contributed by Humidity (%)
5.248	1.003	0.999	93.82%	0.211	0.225	-6.18	23	0	71
3.172	1.006	1.001	104.07%	0.256	0.246	4.07	25	0	79
10.755	1.005	0.995	94.03%	0.868	0.924	-5.97	51	0	43
16.820	1.002	0.993	94.57%	1.370	1.449	-5.43	66	0	29
11.273	1.002	0.995	96.41%	1.356	1.407	-3.59	61	1	35
10.862	0.999	0.985	88.92%	1.295	1.457	-11.08	55	1	34
15.676	0.983	0.981	89.08%	1.904	2.138	-10.92	73	0	16
15.545	1.008	0.995	96.75%	1.559	1.612	-3.25	65	0	32
14.499	0.962	0.961	73.13%	1.264	1.728	-26.87	67	0	6

### 5.3 DATA REDUCTION.

The water vapor mass (from the dry and wet tests) was computed from the data recorded by the ISFC software (section 4.3). Typical measurements are shown in figures 5-10 to 5-12. These measurements contained time traces of the probe inlet static pressure, RH, and temperature measurements. The specific humidity ( $RH_{sp}$ ) in equations 5-1 and 5-2, section 5.1, was computed by integrating the probe's humidity distribution over the test duration for the dry and wet tests, respectively, as shown in figure 5-10. The start and end points of the integral represents the duration in which iso-kinetic condition was established in the probe (indicated by the overlap of the static pressure curves shown in figure 5-13). In a wet test, water would have been injected into the probe during this time, hence, RH inside the probe would also increase accordingly. The humid air mass ( $M_h$ ) in equations 5-1 and 5-2, section 5.1, was computed using the method described in section 3.5, in conjunction with the static pressure and temperature traces shown in figures 5-11 and 5-12, respectively. An equal amount of humid air should enter into the probe during the dry and wet tests if the probe operation and test conditions (in both tests) had been identical, i.e., equal suction pressures, temperature, and RH. However, in practice, there will always be a small difference due to local variations in the laboratory. The data reduction technique for computing LWC was based on the humidity formulations (equations F-1 to F-6) given in appendix F, hence, for a dry test, the steps involved are defined as follow:

1. Compute the saturated vapor pressure ( $E_{sat}$ ) using the temperature traces (figure 5-12).
2. Compute the vapor pressure ( $E_v$ ) in equation F-1, appendix F, using the relative humidity traces (figure 5-10).
3. Compute the mixing ratio (W) in equation F-2, appendix F, using the ambient pressure (assumed as 100 kPa) and vapor pressure from step 2.
4. Compute the specific humidity ( $RH_{sp}$ ) in equation F-3, appendix F, using the mixing ratio from step 3.
5. Compute the probe inlet velocity and air density (assumed ideal state) using the pressure (figure 5-6) and temperature (figure 5-11) trace curves, and then compute the mass of humid air ( $M_h$ ) using equation F-4.
6. Compute the mass of water vapor ( $M_v$ ) in equation F-8, appendix F, i.e., multiply the mass of humid air (step 5) by the specific humidity value (step 4).
7. Repeat steps 1 to 6 for each time step of the integration period (figure 5-10). This will generate a distribution curve of the water vapor mass versus time.
8. Compute the total water vapor mass ( $M_v|_{dry}$ , equation 5-1, section 5.1) by integrating the distribution curve generated in step 7 for the test duration, i.e., between the start and end points of the integration period.
9. Repeat steps 1 to 8 to obtain the total vapor mass ( $M_v|_{wets}$ , equation 5-2 in section 5.1) for the wet test.

10. Compute the mass of the evaporated water droplets from the spray cloud ( $M_{evp}$ ) only, i.e.,  $M_{evp} = M_{v|wet} - M_{v|dry}$ .
11. Compute the LWC using the mass of water collected by the blotter paper ( $M_{blotter}$ ) and B-Gon mesh ( $M_{B-Gon}$ ), i.e.,

$$LWC = \frac{(M_{evp} + M_{blotter} + M_{B-Gon})}{M_{h|dry} \text{ \{or\} } M_{h|wet}}$$

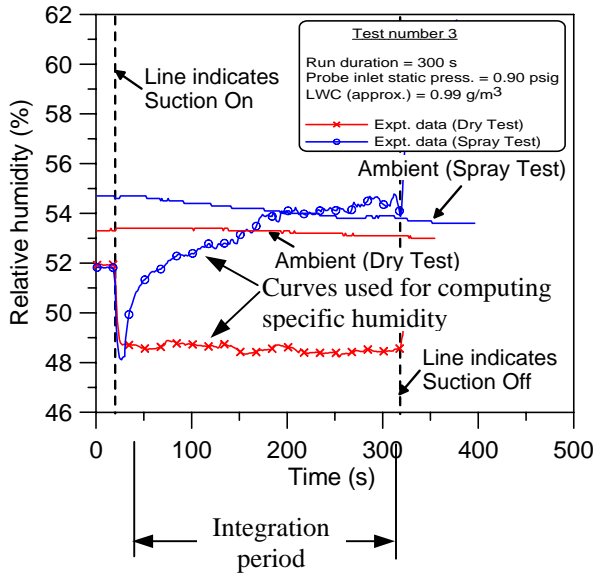


FIGURE 5-10. PROBE RH DISTRIBUTION

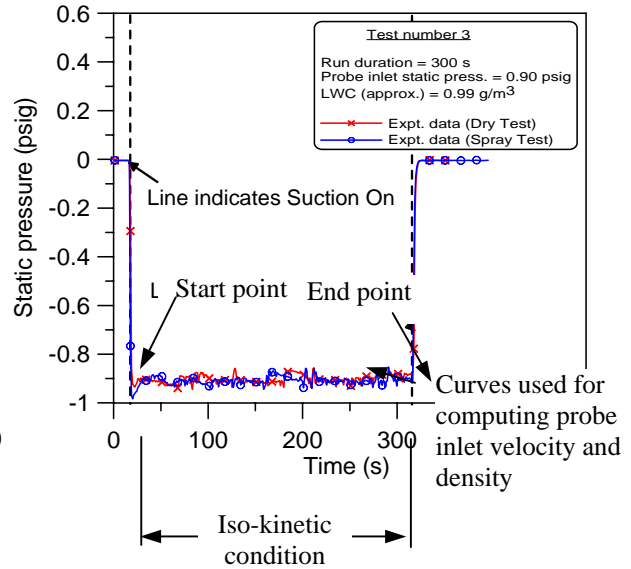


FIGURE 5-11. PROBE STATIC PRESSURE DISTRIBUTION

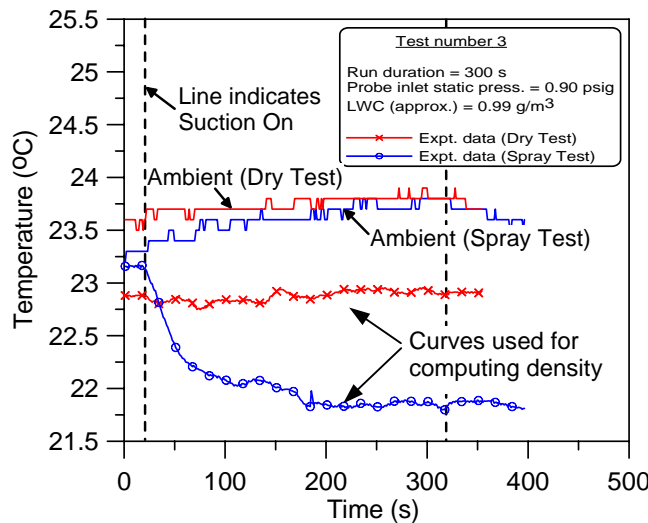


FIGURE 5-12. PROBE TEMPERATURE DISTRIBUTION

## 5.4 RESULTS AND DISCUSSION.

Figure 5-9 shows that the amount of water collected for all the test data, except for tests 7 and 9, was almost equal to the amount sprayed into the reference probe and their collection efficiencies were within 95%, as shown in figure 5-7. The collection efficiencies for all the data varied from 73% to 104%. The amount of water collected in tests 7 and 9 was less than the amount sprayed. (The cause of the poor measurements is the unequal volumetric mass flow in tests 7 and 9, which will be explained later in this section.) The curve fitted to the collection efficiency obtained from configuration 11 Mod-I (section 3) is included in figure 5-10 for comparison. The results show that both curves exhibited similar trends, but the overall collection efficiency obtained with the Mod-II collector was slightly lower than the Mod-I results. The mean collection efficiency and standard deviation (table 5-1) for the Mod-II collector were 92.1% and 8.28%, respectively, compared to 100.8% and 7.89%, respectively, for the Mod-I design. It must be noted that the statistical calculation used in the Mod-I analysis involved 65 data points, whereas only 9 data points were used here.

The contributions to the LWC (based on water collected) by the blotter paper, B-Gon fiber mesh, and evaporated water calculated from the humidity data are shown in figure 5-8. The fitted curves from the Mod-I collector were also included in this figure for comparison. The results (figure 5-8) show that the contributions by the blotter paper remained unchanged, whereas negligible contributions by the B-Gon mesh were found. The results also show that the contributions by the evaporated water seem to have replaced the contributions made by the silica gel desiccants in the Mod-I design. The effect of using a three-layered blotter paper instead of a single layer was negligible. The effect of extending the test duration after water spray was stopped (in tests 8 and 9 shown in figures D-8 and D-9 in appendix D) was difficult to characterize due to insufficient test data. It was clear that the computed evaporated water mass from test 9 was quite low.

Figure 5-9 shows the distribution of the volumetric mass flow ratio (between the wet and dry tests) plotted against the LWC (based on water collected). The volumetric mass flow represents the total amount of environmental air that entered the reference probe within a certain duration, e.g., a ratio of unity implied that equal volumetric mass flow for the wet and dry tests. The results show that in all cases except for tests 7 and 9, the ratio of volumetric flow for the dry and wet tests was between 0.9875 and 1.0125 (indicated by the dotted lines). The ratios obtained for tests 7 and 9 were less than 0.9875, and the corresponding probe collection efficiencies were 89.1% and 73.1%, respectively. It was noticed that when the ratios of the volumetric mass flow laid between the limiting values 0.9875 and 1.0125, the collection efficiencies would lie near the maximum value of 100%. This characteristic trend could be used in the future to determine the quality of the measurements. The reasons for the low volumetric mass ratios in tests 7 and 9 can be explained by studying the distributions of probe inlet static pressure in appendix E. Two test cases were selected: test 2 in figure 5-13 and test 7 in figure 5-14. For the cases where the ratios were between the limits of 0.9875 and 1.0125, the pressure distributions measured in the spray and dry tests were similar and characterized by coincident curves, as shown in figure 5-13. However, in tests 7 and 9, where the ratios laid below 0.9875, the pressure distribution curves were not coincident. This implied unequal volumetric mass flows in the spray and dry tests for tests 7 and 9, hence, did not satisfy the required conditions for calculating the evaporated water droplets, as described in section 5.1 (highlighted in italics). The probe inlet static pressure

distributions for all other tests presented in appendix E exhibited coincidence curves, hence, higher collection efficiencies.

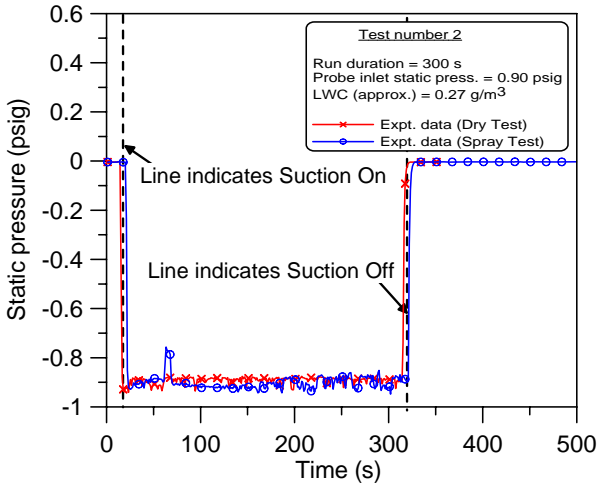


FIGURE 5-13. STATIC PRESSURE DISTRIBUTION—TEST 2

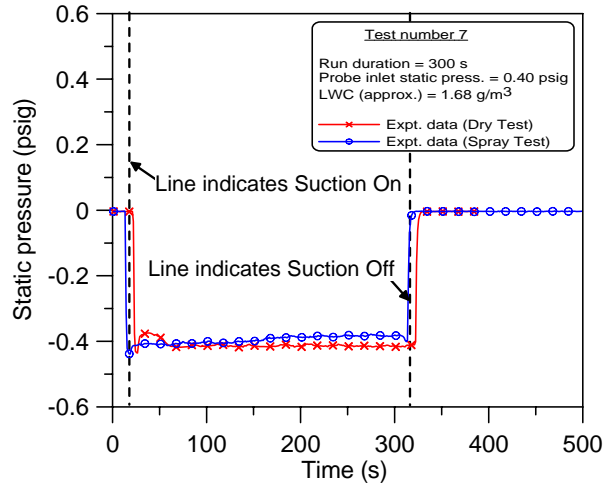


FIGURE 5-14. STATIC PRESSURE DISTRIBUTION—TEST 7

In conclusion, a new technique of calculating the LWC with humidity measurements has been developed. This technique could be implemented to develop an accurate LWC instrument for warm cloud conditions.

## 6. SUMMARY.

This section gives a summary of the work tasks that led to the successful development of the conceptual probe, and they are described as follows.

- A conceptual probe was designed and fabricated by the Icing Group in the Department of Aerospace Engineering at Wichita State University. This probe was used to demonstrate the concept of applying iso-kinetic flow to the measurement of the LWC for spray clouds with small and large water droplets.
- The probe consisted of a 90 degree elbow tube and a water collector assembly that was attached to an enclosed chamber with a single exit nozzle that was connected to a suction fan. The material used in the construction included Ultra-High-Molecular Weight Polyethylene, Perspex, and stainless steel wire mesh.
- Computer fluid dynamics analyses simulating the probe internal flow and the external flow about the probe installed in a wind tunnel were performed to support the initial design process.
- Significant effort was directed at the development of an efficient water collector and calibration of the collector water catch efficiency in a laboratory and wind tunnel. A total of 11 different configurations of the water collector, involving a range of different water-adsorbent materials, were tested in a laboratory.
- The collector design with the highest collection efficiency was selected for further testing. This design, which was named configuration 11 Mod-I (C11 Mod-I), consisted of an enclosed chamber with a central exit hole and contained silica gel desiccant, blotter paper, and B-Gon fiber mesh.
- Calibration tests were conducted in a laboratory to ascertain the measurement accuracy of the C11 Mod-I collector. This involved injecting a known amount of water droplets into the probe and comparing this to the amount adsorbed by the water collector. The LWC was determined from the amount of water used (or collected) and the volumetric air drawn by the probe.
- Limited tests were conducted at the WSU 7- by 10-ft tunnel to check the iso-kinetic performance of the probe. Prior to the wind tunnel tests, a LabView computer program that could maintain iso-kinetic flow condition at the probe inlet was developed and tested in a laboratory.
- During the wind tunnel experiments, humidity sensors were installed inside the probe and in the wind tunnel to monitor the humidity level inside the probe and in the free stream. Extremely high temperatures and low relative humidity levels were recorded.
- The installation of a humidity sensor inside the probe led to an improved technique of measuring the LWC. Limited tests were conducted in a laboratory to determine the

amount of water evaporated inside the probe and this measurement was used to correct the calculation of the LWC. With the inclusion of the humidity sensor in the probe and water collector, C11 Mod-I was renamed C11 Mod-II.

- The preliminary experimental tests used to develop an efficient water collector configuration resulted in two successful designs.
  - Configuration 11 Mod-I consists of an enclosed chamber with a central exit nozzle, cylindrical tube fabricated from blotter paper, B-Gon hydrophobic fiber mesh, and silica gel desiccant.
  - Configuration 11 Mod-II consists of an enclosed chamber with a central exit nozzle, cylindrical tube fabricated from blotter paper, B-Gon hydrophobic fiber mesh, and relative humidity sensor.

## 7. CONCLUSIONS.

The following conclusions were drawn from the work conducted.

- The water collector configuration (C11 Mod-I) consisting of an enclosed chamber with a central exit tube, blotter paper, and hydrophobic fiber mesh exhibited the highest water collection efficiencies. The mean and standard deviation of the collection efficiency were 100.8% and  $\pm 7.89\%$ , respectively. These were determined in a laboratory for liquid water content (LWC) values in the range of 0.54 and 8.5 g/m<sup>3</sup>.
- The mass of water collected by the blotter paper increased with increasing LWC, whereas water collected by the silica gel and B-Gon material decreased. The water collected by the silica gel, B-Gon, and blotter paper materials was almost equal to the water sprayed into the probe. The amount of water sprayed (or used) in the laboratory tests varied from 2.26 to 10.5 g, and the spray durations were between 30 and 130 seconds.
- The collection efficiencies obtained with the C11 Mod-I design in the Wichita State University (WSU) wind tunnel were quite low because of the high temperature and very low humidity conditions in the tunnel air stream, which led to excessive evaporation of the water droplets from the spray cloud.
- The probe was tested in the WSU wind tunnel at velocities between 105 and 130 mph (or 47 and 58 m/s). Although the probe inlet velocity was capable of operating at velocities up to 220 mph (~100 m/s), the selected airspeeds for the tests were lower to reduce the loads on the probe and mounting system. It was thought that the probe, which was fabricated from Ultra-High-Molecular Weight Polyethylene and Perspex materials, might not have adequate structural integrity to withstand the forces at higher tunnel velocities.
- The iso-kinetic flow control system was able to maintain iso-kinetic conditions at the probe inlet during the experimental tests in the WSU wind tunnel. Iso-kinetic condition at the probe inlet was attained within 3 seconds of operating the probe suction system.
- The removal of silica gel desiccant and the addition of an accurate humidity sensor to configuration 11 led to the development of an improved LWC reference probe design. This modified configuration was named configuration 11 Mod-II (C11 Mod-II). The mean and standard deviation of the water collection efficiency (based on limited test data) were 92.1% and  $\pm 8.28\%$ , respectively. These were determined in a laboratory with water sprays having LWC in the range of 0.24 and 2.56/m<sup>3</sup>. The amount of water used during the test sprays varied from 3.05 to 19.8 g, and the spray durations were in the range of 5 to 10 minutes. The C11 Mod-II design was not tested in the wind tunnel due to time and cost constraints.

## 8. RECOMMENDATIONS.

The end of the development phase produced two methods of water collection that could potentially be turned into an accurate instrument for measuring LWC under supercooled droplets conditions. Both the C11 Mod-I and C11 Mod-II collector designs were successfully demonstrated under laboratory conditions. The iso-kinetic performance of the probe was also successfully demonstrated in a wind tunnel at velocities up to 130 mph. There is a need for further experimentations to fully develop the iso-kinetic probe for an icing wind tunnel. This can be carried out in three phases: Phase 2 compares the LWC measured by the reference probe and an existing LWC instrument in a wind tunnel, Phase 3 involves fabricating a new airfoil-shaped reference probe suitable for a wind tunnel, and Phase 4 assesses the probe's performance in an icing wind tunnel.

## 9. REFERENCES.

1. Ide, R.F., "Comparison of Liquid Water Content Measurement Techniques in an Icing Wind Tunnel," NASA TM-1999-209643, 1999.
2. Rudoff, R.C., Bachalo, E.J., and Bachalo, W.D., "Liquid Water Content Measurement Using the Phase Doppler Particle Analyzer in the NASA Lewis Icing Research Tunnel," AIAA 93-0298, Reno, NV, 1993.
3. Tan, S.C. and Bartlett, P.G., "An Experimental Study of Droplet Break-Up Using a Wind Tunnel," AIAA-2003-391, 2003.
4. Mundo, Chr, Sommerfeld, M., and Tropea, C., "Droplet-Wall Collisions: Experimental Studies of the Deformation and Breakup Process," *Int. J. Multiphase Flow*, Vol. 21, No. 2, 1995, pp. 151-173.
5. Cohen, J.M. and Rosfjord, T.J., " Spray Patterning at High Pressure," AIAA-89-2323, Monterey, CA, 1989.
6. Papadakis, M., Hung, K.E, and Yeong, H.W., "Experimental Investigation of Water Impingement on Single and Multi-Element Airfoils," AIAA-2000-0100, 2000.
7. Von Glahn, U., Gelder, T.F., and Symers, W.H. Jr., " A Dye Tracer Technique for Experimentally Obtaining Impingement Characteristics of Arbitrary Bodies and a Method for Determining Droplet Size Distribution," NACA TN3338, March 1955.

APPENDIX A—CHARACTERISTICS OF SILICA GEL AND MOLECULAR SIEVE DESICCANTS

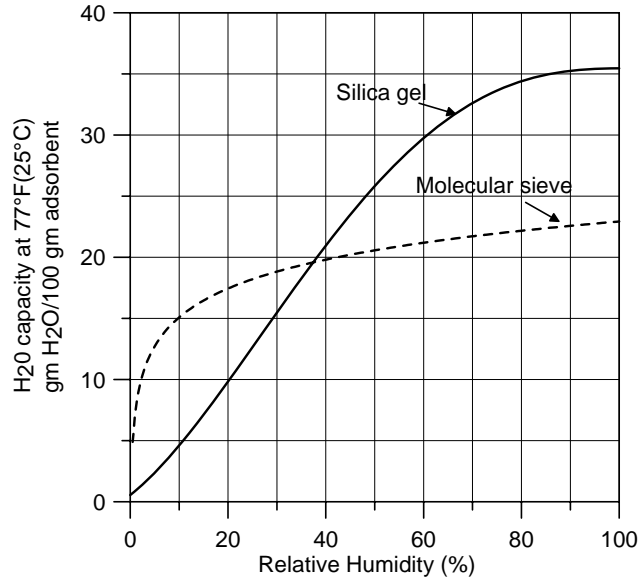


FIGURE A-1. VARIATION OF DESICCANT ADSORPTIVE CAPACITY WITH RELATIVE HUMIDITY

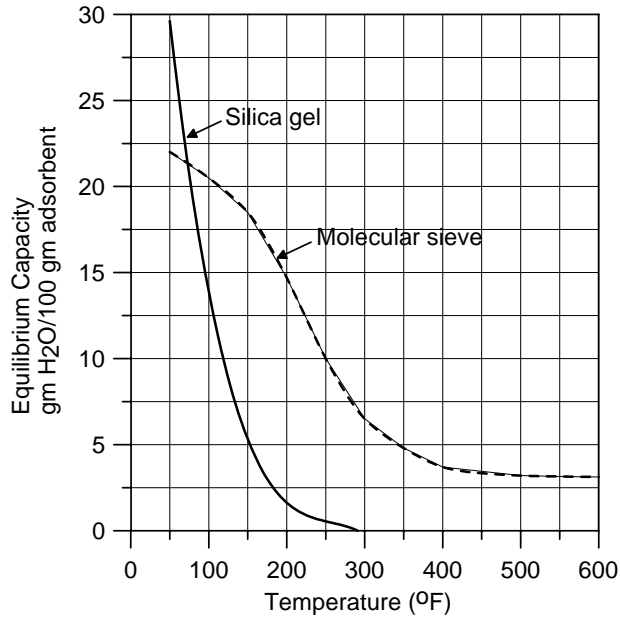


FIGURE A-2. VARIATION OF DESICCANT ADSORPTIVE CAPACITY WITH TEMPERATURE

## APPENDIX B—WATER COLLECTOR CONFIGURATION TESTS

The following describes the configurations of the water collector including their results and findings using the definitions for the collection efficiency and rate of spray given in section 3.3.

### B.1 CONFIGURATION 1.

#### B.1.1 Description.

B-Gon fiber was wrapped around the sidewalls of the container, whereas the base (of the container) was wrapped with water-adsorbent paper over the B-Gon fiber. Both the B-Gon fiber and adsorbent paper were secured with elastic bands. A centrifuge was also installed at the base of the divergent nozzle of the probe top section. It was anticipated that water would be trapped in the fiber while the (adsorbent) paper would adsorb water. Figures B-1a and B-1b show the components of the water collector before and after assembly. The test conditions and configuration of the water collector are defined as follows:

- Water collection medium            B-Gon fiber mesh, water-adsorbent paper
- Weighed components                Inner container, B-Gon, water-adsorbent paper
- Features                                Centrifuge installed
- Water used or sprayed                2.5 to 14.0 g
- Spray brush pressure setting        20, 30 psig
- Spray duration                        15 to 60 s
- Spray rate                              0.083 to 0.530 g/s
- Run duration                          20 to 60 s

#### B.1.2 Findings.

The results are shown in figure B-1c and table 3-1. Tests 1 to 4 were conducted at a spray pressure of 20 psig with a number of different spray and run durations. Tests 5 to 16 were conducted at a spray pressure of 30 psig with equal spray and run durations.

Visual examination of the collector showed that the wetted regions were found on the B-Gon fiber but a small amount was also found on the base of the container. The collection efficiencies varied from 30% to 70%. Figure B-1c shows that collection efficiency increased with the rate of water sprayed. The total amount of water sprayed into the probe has minimal effect on the final collection efficiency. Extending the run durations (tests 1 to 4) after the water spray was stopped also has minimal effect. Tests conducted at lower spray pressures (tests 1 to 4) have higher collection than those conducted at higher pressures (tests 5 to 16). The droplet size generated by the spray brush depends on the spray rate and pressure; high water flow rates or low spray pressures usually produce large droplets, and vice-versa. Therefore, water collection efficiency tends to increase with droplet size.

In summary, this configuration did not exhibit high collection efficiency, although measurements were repeatable.

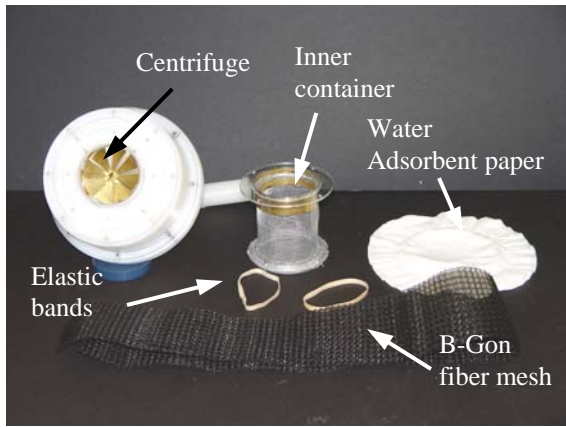


FIGURE B-1a. CONFIGURATION 1  
(BEFORE ASSEMBLY)



FIGURE B-1b. CONFIGURATION 1  
(AFTER ASSEMBLY)

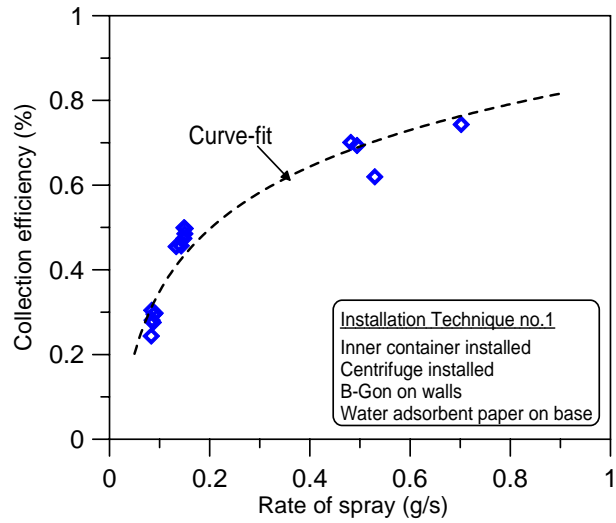


FIGURE B-1c. CONFIGURATION 1

## B.2 CONFIGURATION 2.

### B.2.1 Description.

Water-adsorbent paper was wrapped around the sidewalls of the container and around the base of the container. The adsorbent papers were secured with elastic bands. A centrifuge was also installed at the base of the divergent nozzle of the top probe section. It was anticipated that (adsorbent) paper alone would collect all the water. Figures B-2a and B-2b show the components of the water collector before and after assembly. The test conditions and configuration of the water collector are defined as follows:

- Water collection medium            Water-adsorbent paper
- Weighed components            Inner container, water-adsorbent paper
- Feature                              Centrifuge installed
- Water used or sprayed            2.5 to 5.2 g
- Spray brush pressure setting    30 psig
- Spray duration                    20 to 60 s
- Spray rates                        0.085 to 0.175 g/s
- Run duration                       20 to 60 s

### B.2.2 Findings.

The results are shown in figure B-2c and table 3-2. Tests 1 to 14 were conducted with decreasing spray rates (i.e., decreasing volume mass), whereas tests 15 and 16 have two layers of water-adsorbent papers (all other tests had only one layer) but the spray duration in test 15 was twice as long as test 6.

Visual examination of the collector showed that the wetted regions were found on the sidewalls and base of the container but a small amount was also found on the base. The collection efficiencies varied from 28% to 53%. Similar characteristics to the previous configuration were found for this configuration, i.e., collection efficiency increases with spray rate (figure B-2c), the total amount of water sprayed has minimal effect on the collection efficiency. In addition, adding an extra layer of water adsorbent or doubling the test durations did not improve upon the collection efficiency.

In summary, this configuration performed slightly worse than the previous configuration. It also did not exhibit high collection efficiency although measurements were repeatable.

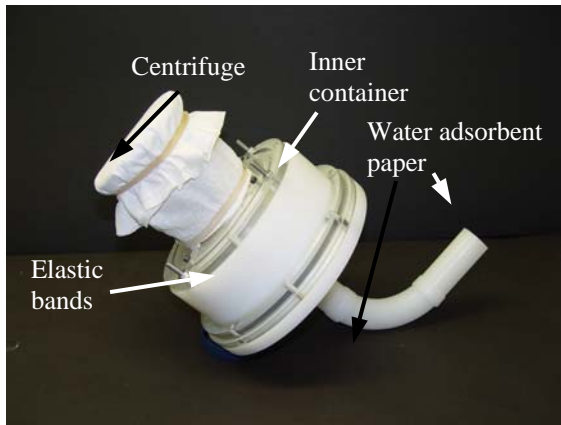


FIGURE B-2a. CONFIGURATION 2  
(BEFORE ASSEMBLY)



FIGURE B-2b. CONFIGURATION 2  
(AFTER ASSEMBLY)

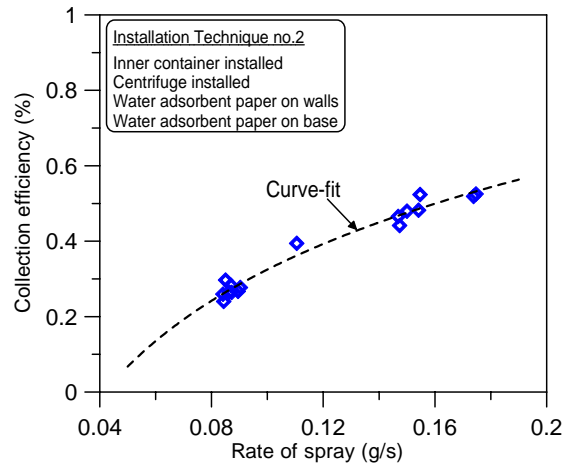


FIGURE B-2c. CONFIGURATION 2

### B.3 CONFIGURATION 3.

#### B.3.1 Description.

This is a variant of configuration 2, except the centrifuge has been removed. Water-adsorbent papers were used to wrap the sidewalls and base of the inner container. The adsorbent papers were secured with elastic bands. Figures B-3a and B-3b show the components of the water collector before and after assembly. The test conditions and configuration of the water collector are defined as follows:

- Water collection medium            Water-adsorbent paper
- Weighed components                Inner container, water-adsorbent paper
- Water used or sprayed               1.2 to 5.0 g
- Spray brush pressure setting        30 psig
- Spray duration                        20 to 40 s
- Spray rate                             0.039 to 0.156 g/s
- Run duration                          20 to 40 s

#### B.3.2 Findings.

The results are shown in B3c and table 3-3. Tests 1 to 7 were conducted with a decreasing water spray rates (or decreasing volume mass).

Visual examination of the collector showed that the wetted regions were found on the base of the container but a small amount was also found on the sidewalls. This (wetted) region was biased towards one corner of the base, which was similar to the computational fluid dynamics predictions in section 2.3.2. The collection efficiencies varied from 40% to 63%. The removal of the centrifuge enhanced the efficiencies slightly compared to configuration 2 without the centrifuge. However, they were similar to those measured with configuration 1 (for the same water spray rates). Similar characteristics to the previous configuration were found for this configuration, i.e., collection efficiency increases with spray rate (figure B-3c), the total amount of water sprayed has minimal effect on the collection efficiency.

In summary, this configuration did not exhibit high collection efficiency, although measurements were repeatable.

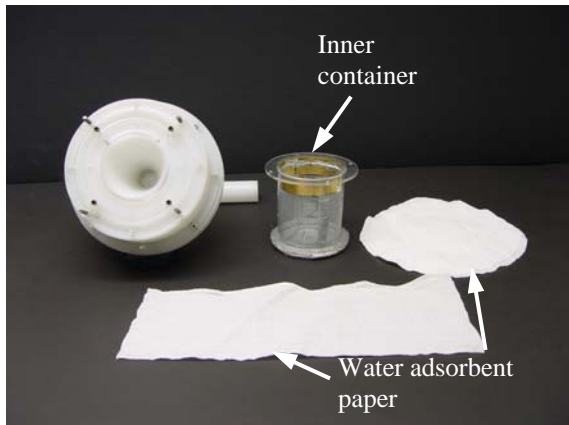


FIGURE B-3a. CONFIGURATION 3  
(BEFORE ASSEMBLY)



FIGURE B-3b. CONFIGURATION 3  
(AFTER ASSEMBLY)

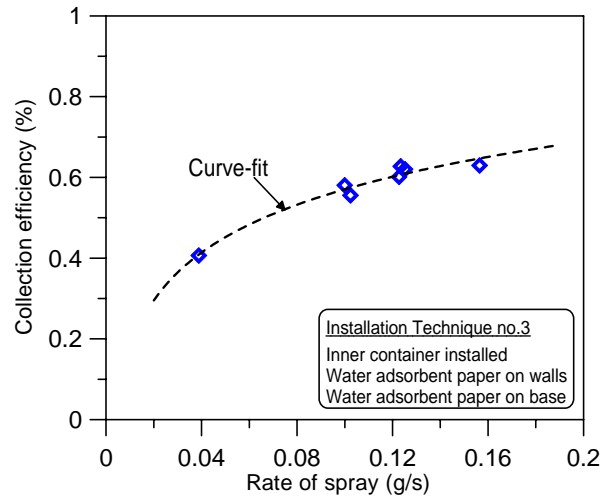


FIGURE B-3c. CONFIGURATION 3

## B.4 CONFIGURATION 4.

### B.4.1 Description.

This is a variant of configuration 3 where an additional outer layer of water adsorbent paper was added in the form of an enclosed bag. This layer was attached using the outer container supports by removing the wire mesh. The bag was secured against the edge of the probe top section by the outer container supports and four elongated screws. Figures B-4a and B-4b show the components of the water collector before and after assembly. The test conditions and configuration of the water collector are defined as follows:

- Water collection medium            Water-adsorbent paper
- Weighed components                Inner container, water-adsorbent paper
- Water used or sprayed                2.7 g
- Spray brush pressure setting        30 psig
- Spray duration                        30 s
- Spray rate                              0.090 g/s
- Run duration                            30 s

### B.4.2 Findings.

The results are shown in figure B-4c and table 3-4. Test 1 has one layer of adsorbent paper wrapped around the sidewalls of the inner container, whereas test 2 has three layers (wrapped around the inner container).

Visual examination of the collector showed that the wetted regions were concentrated on the base of the container but a small amount was also found on the sidewalls. The (wetted) region was also biased towards one corner of the base. The collection efficiencies for tests 1 and 2 were 55% and 49%, respectively. The addition of the extra adsorbent layer did not show significant improvement to the collection efficiency.

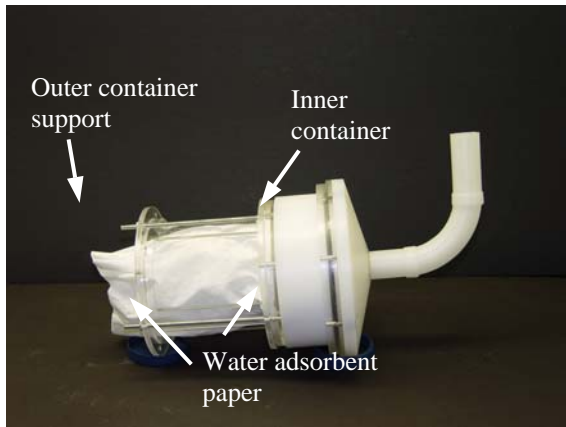


FIGURE B-4a. CONFIGURATION 4  
(BEFORE ASSEMBLY)

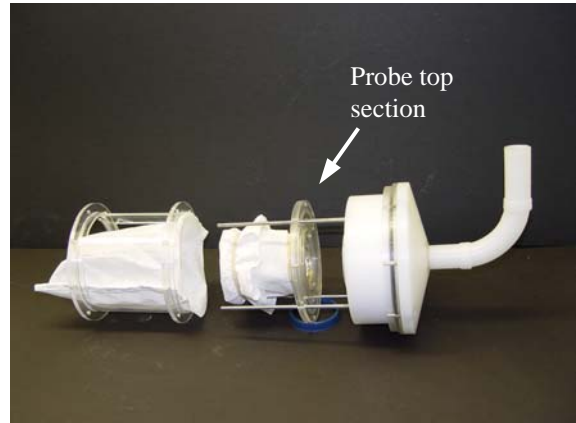


FIGURE B-4b. CONFIGURATION 4  
(AFTER ASSEMBLY)

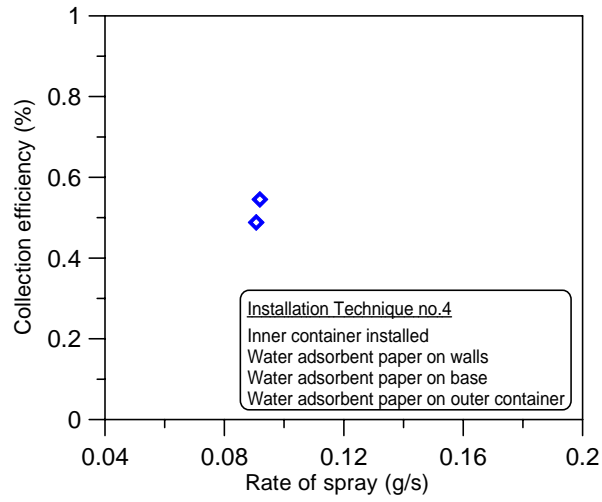


FIGURE B-4c. CONFIGURATION 4

## B.5 CONFIGURATION 5.

### B.5.1 Description.

B-Gon fiber was wrapped around the sidewalls and base of the inner container. The fiber mesh was secured with elastic bands and held-in place by the outer container supports. It was anticipated that the B-Gon fiber would trap water between layers of the mesh. Figures B-5a and B-5b show the components of the water collector before and after assembly. The test conditions and configuration of the water collector are defined as follows:

- Water collection medium            B-Gon fiber mesh
- Weighed components                Inner container and B-Gon fiber mesh
- Water used or sprayed                1.8 to 5.4 g
- Spray brush pressure setting        30 psig
- Spray duration                        30 to 60 s
- Spray rate                              0.061 to 0.094 g/s
- Run duration                          30 to 60 s

### B.5.2 Findings.

The results are shown in figure B-5c and table 3-5. Tests 1 to 14 were conducted at a spray pressure of 30 psig at similar water spray rates.

Visual examination of the collector showed that the wetted regions were concentrated on the base of the container but a small amount was also found on the sidewalls. The collection efficiencies varied from 21% to 62%. Figure B-5c showed a scattered distribution of collection efficiencies that did not vary with either the spray rates or the amount of water sprayed.

In summary, the collection efficiencies were random, nonrepeatable, and did not exhibit high collection efficiency.

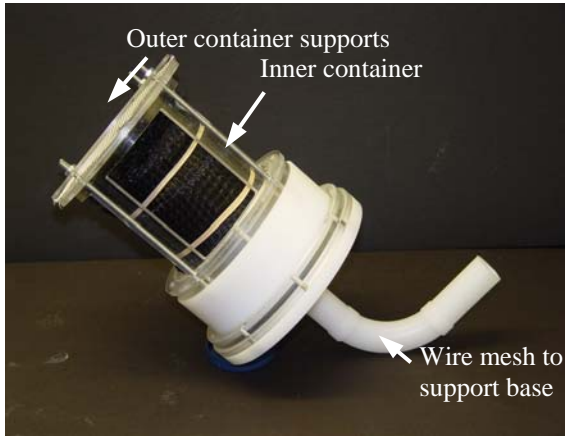


FIGURE B-5a. CONFIGURATION 5  
(BEFORE ASSEMBLY)



FIGURE B-5b. CONFIGURATION 5  
(AFTER ASSEMBLY)

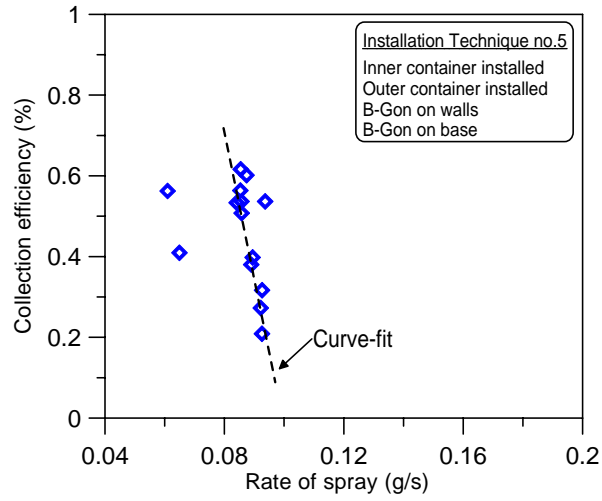


FIGURE B-5c. CONFIGURATION 5

## B.6 CONFIGURATION 6.

### B.6.1 Description.

A single Perspex tube (1-inch diameter) was fitted directly onto the 90 degree elbow tube and bypasses the divergent nozzle of the probe top section. The exit end of the Perspex tube was connected to a plastic container (diameter 4.8 inches, length 5.5 inches), which has a perforated top cover. It was anticipated that water droplets exiting from the tube would be adsorbed with a multilayered water-adsorbent material before being exhausted through the perforated cover of the plastic container. The adsorbent materials used were molecular sieve pellets that had been packed into 1-inch-square pouches fabricated from highly porous paper. Figures B-6a and B-6b show the components of the water collector before and after assembly. The test conditions and configuration of the water collector are defined as follows:

- Water collection medium            B-Gon fiber mesh, molecular sieve desiccant
- Weighed components                Plastic container, B-Gon, molecular sieve
- Water used or sprayed               2.2 to 3.2 g
- Spray brush pressure setting        30 psig
- Spray duration                        30 s
- Spray rate                              0.072 to 0.108 g/s
- Run duration                            30 s

### B.6.2 Findings.

The results are shown in figure B-6c and table 3-6. Tests 1 to 4 were conducted at a spray pressure of 30 psig.

Visual examination of the collector showed that some water had leaked through the top cover of the plastic container. The collection efficiencies varied from 54% to 68%. The collection efficiencies obtained from this configuration were slightly higher than previous configurations at similar spray rates. It was believed that this was probably due to the water adsorbed by the molecular sieve pellets (rather than the B-Gon fiber). There were insufficient data to ascertain the repeatability in the measurements but overall collection efficiencies were well below 100%.

In summary, this configuration was not considered as an efficient water collector.

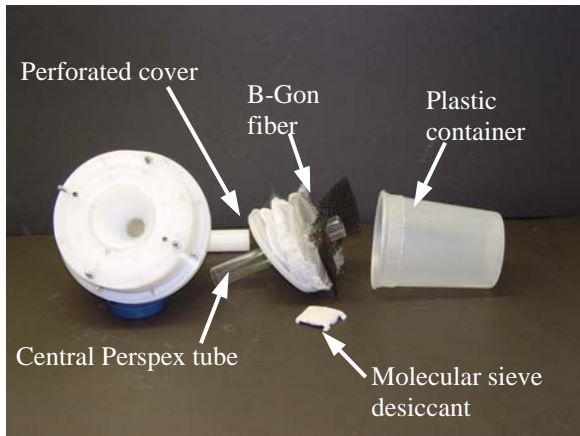


FIGURE B-6a. CONFIGURATION 6 (BEFORE ASSEMBLY)

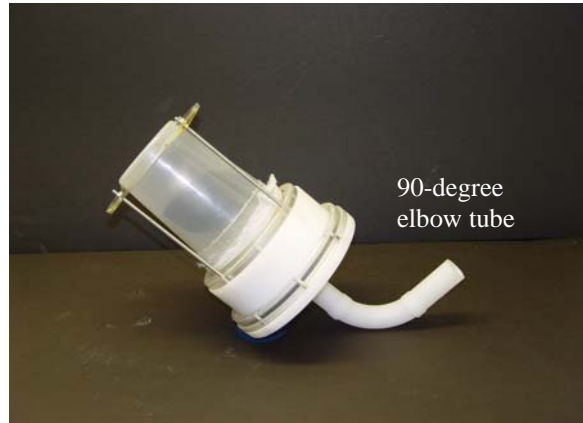


FIGURE B-6b. CONFIGURATION 6 (AFTER ASSEMBLY)

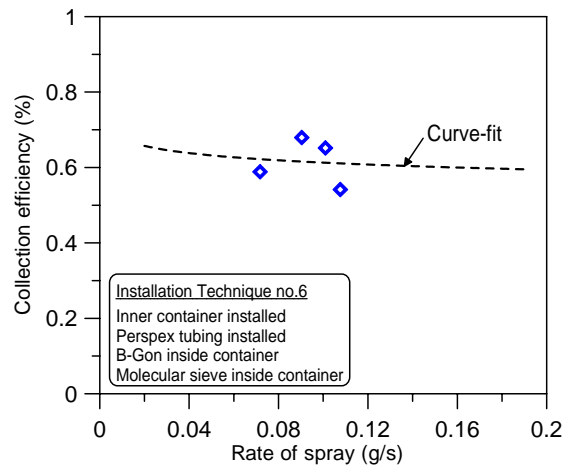


FIGURE B-6c. CONFIGURATION 6

## B.7 CONFIGURATION 7.

### B.7.1 Description.

This is a variant of configuration 2, except the centrifuge has been replaced with special holder assembly that contained DRIMOP and molecular sieve pellets (packed into 1-inch-square pouches). The holder was installed at the base of the divergent nozzle of the probe top section. Water-adsorbent paper was wrapped around the sidewalls and base of the inner container. The adsorbent papers were secured with elastic bands. Based on the results from configuration 6, it was hoped that desiccants would improve collection efficiency. Figures B-7a and B-7b show the components of the water collector before and after assembly. The test conditions and configuration of the water collector are defined as follows:

- Water collection medium            DRIMOP, molecular sieve, water-adsorbent paper
- Weighed components                Inner container, water-adsorbent paper, DRIMOP, molecular sieve desiccant and holder assembly
- Water used or sprayed                2.2 to 3.0 g
- Spray brush pressure setting        30 psig
- Spray duration                        30 s
- Spray rate                             0.073 to 0.099 g/s
- Run duration                          30 s

### B.7.2 Findings.

The results are shown in figure B-7c and table 3-7. Test 1 used both DRIMOP and molecular sieve, test 2 used molecular sieve, and tests 3 to 5 used DRIMOP as the main water-adsorbent material.

Visual examination of the collector showed that the sidewalls and base of the inner container were quite dry. The collection efficiencies varied from 51% to 63%. These results were similar to that obtained from configuration 6.

In summary, this configuration did not exhibit significant improvement in the collection efficiencies.

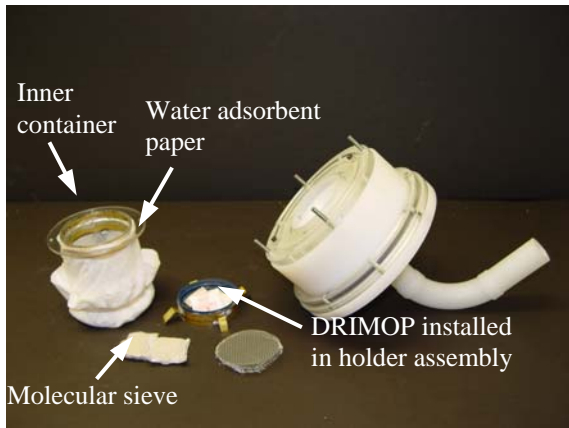


FIGURE B-7a. CONFIGURATION 7  
(BEFORE ASSEMBLY)

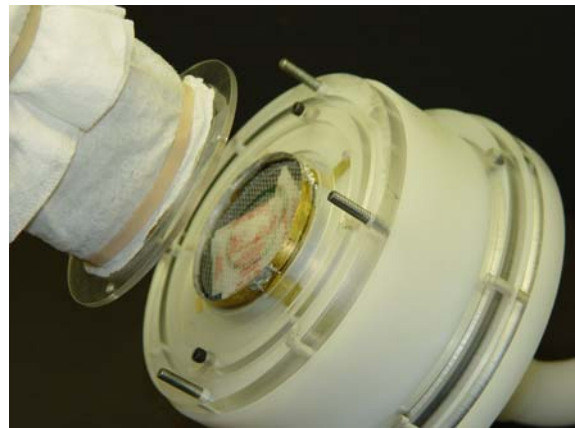


FIGURE B-7b. CONFIGURATION 7  
(AFTER ASSEMBLY)

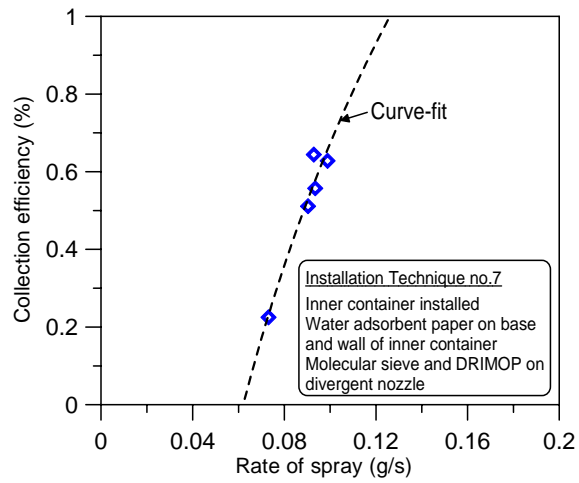


FIGURE B-7c. CONFIGURATION 7

## B.8 CONFIGURATION 8.

### B.8.1 Description.

This is a variant of configuration 3, except for the addition of blotter paper, which was installed inside the hollow well of the inner container. The blotter paper was arranged in a gridlock formation with 1/2 inch spacing. It was anticipated that both the blotter and water-adsorbent papers would adsorb the water. The gridlock arrangement increases the surface area of the blotter paper. Water-adsorbent paper was wrapped around the sidewalls and base of the container. The adsorbent papers were secured with elastic bands. Figures B-8a and B-8b show the components of the water collector before and after assembly. The test conditions and configuration of the water collector are defined as follows:

- Water collection medium                      Water-adsorbent paper, blotter paper
- Weighed components                         Inner container, water-adsorbent paper, blotter paper
- Water used or sprayed                        2.6 to 3.6 g
- Spray brush pressure setting                30 psig
- Spray duration                                 30 s
- Spray rate                                      0.087 to 0.120 g/s
- Run duration                                    30 s

### B.8.2 Findings.

The results are shown in figure B-8c and table 3-8. Tests 1 to 4 were conducted at a spray pressure of 30 psig.

Visual examination of the collector showed significant water deposition on the blotter paper and on the base of the container. Certain regions of the sidewall were also wetted. The collection efficiencies varied from 50% to 68%. The results indicated that the collection efficiency were similar to those obtained from configuration 3 but no significant improvement was found.

In summary, the addition of the blotter paper did not improve the collection efficiency.

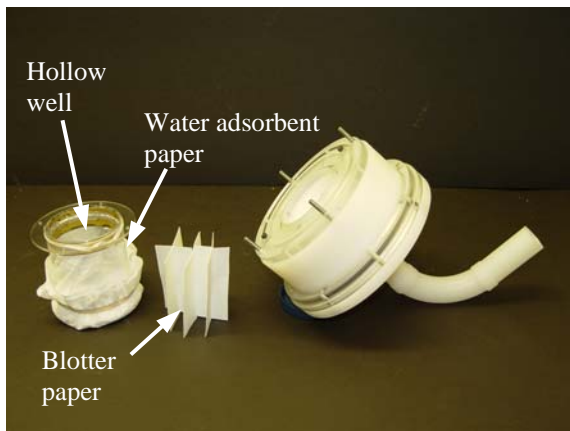


FIGURE B-8a. CONFIGURATION 8 (BEFORE ASSEMBLY)

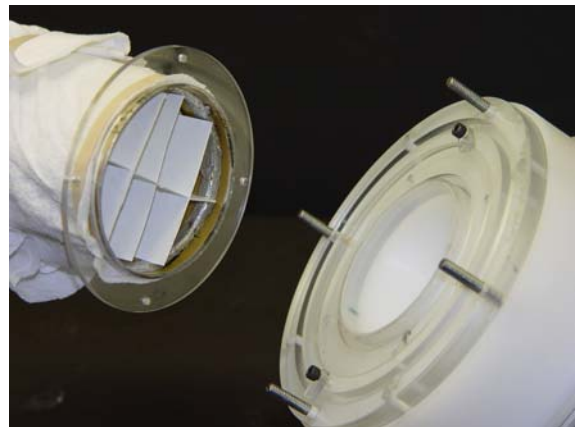


FIGURE B-8b. CONFIGURATION 8 (AFTER ASSEMBLY)

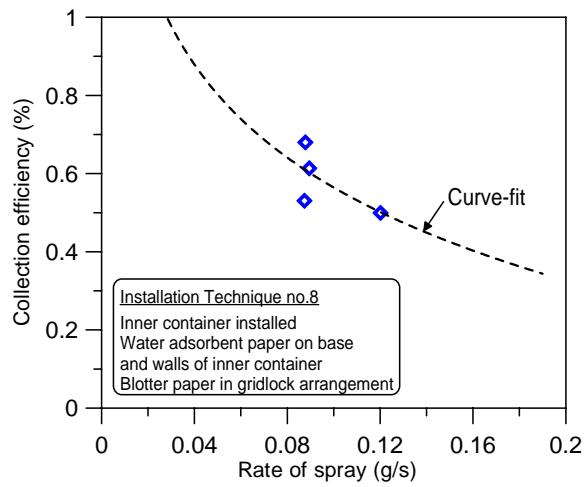


FIGURE B-8c. CONFIGURATION 8

## B.9 CONFIGURATION 9.

### B.9.1 Description.

This is a variant of configuration 8, except the blotter paper gridlock was replaced with a cylindrical tube that was also fabricated from blotter paper. This (tube) was attached to the base of the divergent nozzle (of the probe top section) and secured with a brass ring. The diameter of the cylindrical blotter tube was 3.0 inches, and the length was 3.94 inches (100 mm). An inverted plastic cup (2.5 inches diameter by 2 inches high) was also installed at the base of inner container. It was anticipated that the inverted cup would create partial blockage of the main airstream, thus diverting them towards the blotter tube where water droplets would be deposited. The base of the inverted cup was also installed with blotter paper. Water-adsorbent papers were used to wrap the sidewalls and base of the inner container. Figures B-9a and B-9b show the components of the water collector before and after assembly. The test conditions and configuration of the water collector are defined as follows:

- Water collection medium            Water-adsorbent paper, blotter paper
- Weighed components                Inner container, inverted cup, water-adsorbent paper, blotter paper
- Water used or sprayed                1.6 to 2.7 g
- Spray brush pressure setting        30 psig
- Spray duration                        30 s
- Spray rate                              0.053 to 0.091 g/s
- Run duration                          30 s

### B.9.2 Findings.

The results are shown in figure B-9c and table 3-9. Tests 1 to 18 were conducted at a spray pressure of 30 psig.

Visual examinations showed significant water deposition on the blotter tube but none was found in the cup or on the inner container. The collection efficiencies varied from 62% to 77%. A significant improvement in the collection efficiencies was obtained with this configuration. It was believed that this (improvement) was attributed to the water adsorbed by the cylindrical blotter tube from the divergent nozzle section of the probe.

In summary, the blotter tube design merited further investigations in the next configuration.

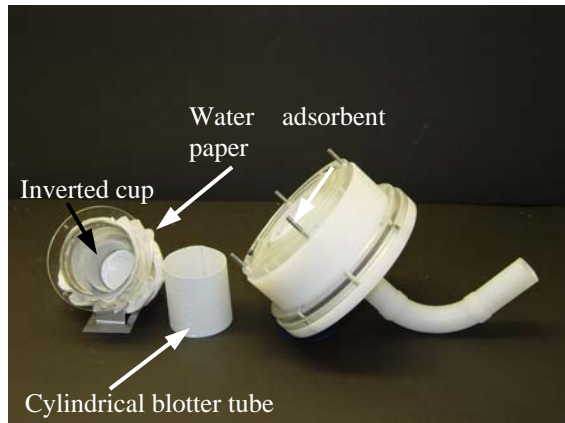


FIGURE B-9a. CONFIGURATION 9  
(BEFORE ASSEMBLY)



FIGURE B-9b. CONFIGURATION 9  
(AFTER ASSEMBLY)

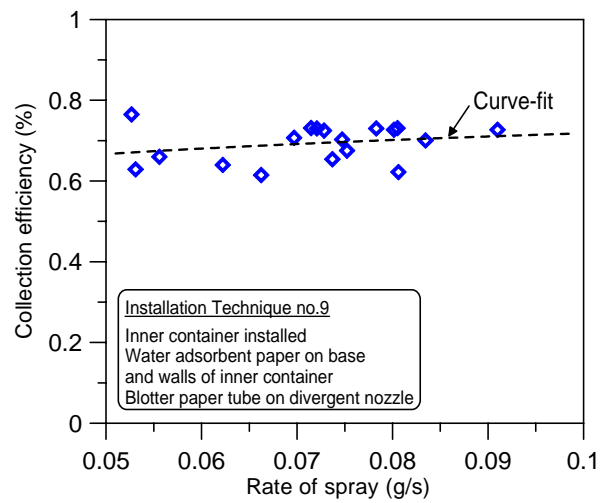


FIGURE B-9c. CONFIGURATION 9

## B.10 CONFIGURATION 10.

### B.10.1 Description.

This is a variant of configuration 9, except the inner container was replaced with a plastic container (diameter 4.8 inches by length 5.5 inches) with a bent central exit tube. It was anticipated that the plastic container would reduce evaporation of the cylindrical blotter tube. The central exit tube (of the plastic container) was bent because it was cut from a clear PVC elbow tube (diameter 1.5 inches, length 2 inches). A new 90 degree probe tube with four static pressure ports (figure 3-4) was installed into the probe top section to record the inlet pressure with a U-tube water manometer for the first time. Since the static pressures difference between the four ports were less than 0.036 psig (1"H<sub>2</sub>O), it was decided to use only the bottom port for measurement. Figures B-10a and B-10b show the components of the water collector before and after assembly. The test conditions and configuration of the water collector are defined as follows:

- Water collection medium           Blotter paper
- Weighed components            Cylindrical tube made from blotter paper
- Water used or sprayed           3.3 to 3.4 g
- Spray brush pressure setting     30 psig
- Spray duration                    30 s
- Spray rate                         0.109 to 0.115 g/s
- Run duration                      30 s

### B.10.2 Finding.

The results are shown in figure B-10c and table 3-10. Tests 1 to 4 used a 3.94-inch (100-mm) -long blotter tube, whereas tests 5 to 7 used a 3.54-inch (90-mm) blotter tube.

Visual examination of the collector showed significant water deposition on the cylindrical blotter tube but none was found on the plastic container. The collection efficiencies varied from 68% to 75%. The length of the blotter tube has negligible effects on the collection efficiencies.

These results were similar to those obtained from configuration 9. The probe inlet pressures were approximately 0.8 psig (22"H<sub>2</sub>O). Although collection efficiency data were quite repeatable over a small range of water spray rates, they were still well below the maximum value of 100%. It was thought that some of the water droplets might have escaped through the central exit tube (in plastic container) or simply due to evaporative loss. Therefore, it was decided to install a layer of desiccant materials into the plastic container to reduce these losses since desiccants were known to improve on the collection efficiency, e.g., configuration 6. These changes are described in section B.11.

In summary, this simpler design had dispensed with the inner container and water-adsorbent paper from the previous configuration without incurring any loss in collection performance. And together with the proposed idea of installing a layer of desiccant, the design merited further investigations.

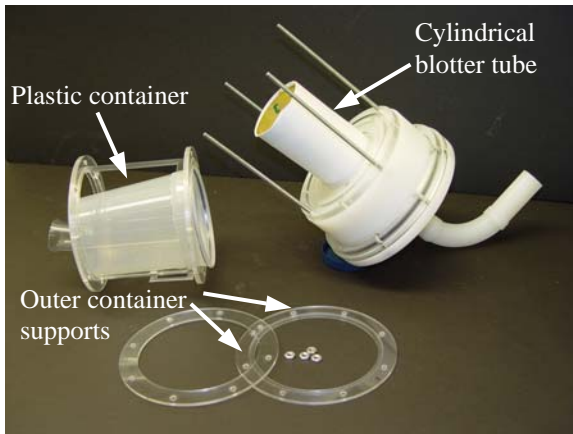


FIGURE B-10a. CONFIGURATION 10  
(BEFORE ASSEMBLY)

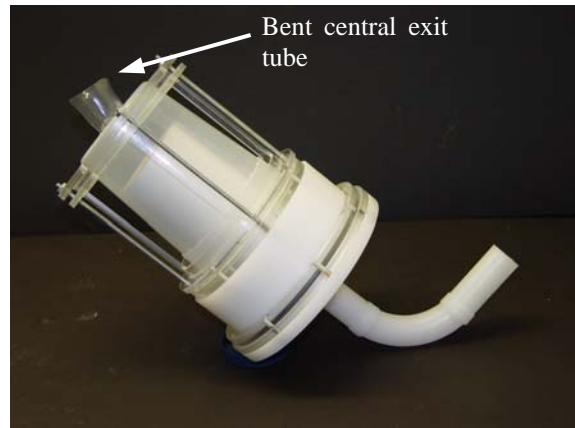


FIGURE B-10b. CONFIGURATION 10  
(AFTER ASSEMBLY)

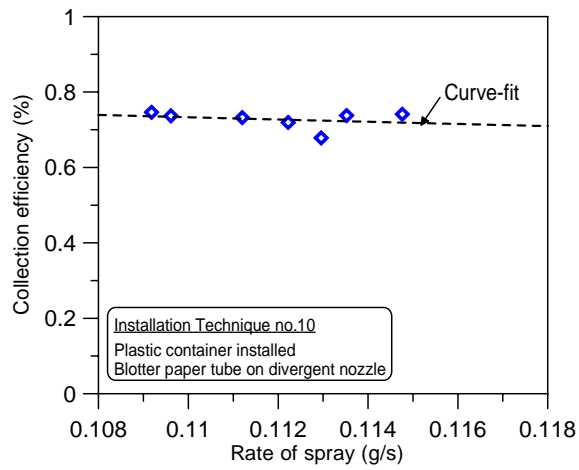


FIGURE B-10c. CONFIGURATION 10

## B.11 CONFIGURATION 11.

### B.11.1 Description.

This is a variant of configuration 10, except for the addition of a single porous layer containing silica gel desiccant. The layer was fabricated by sewing two circular-shaped B-Gon fiber meshes together to form a pouch. Silica gel or molecular sieve pellets were poured into the pouch through a small opening and sealed with wire ties. This (pouch) was installed into the plastic container and supported by a wire mesh (diameter 0.020 inch, opening 0.030 inch, 36% porosity), which was placed at about 2 inches from the base of the container. A retainer ring was used to secure the pouch during the test. Figures B-11a and B-11b show the components of the water collector before and after assembly. The test conditions and configuration of the water collector are defined as follows:

- |                                |   |
|--------------------------------|---|
| • Water collection medium      | Blotter paper, silica gel, molecular sieve, B-Gon |
| • Weighed components           | Blotter paper, silica gel, molecular sieve, B-Gon |
| • Water used or sprayed        | 2.8 to 3.9 g                                      |
| • Spray brush pressure setting | 30 psig   |
| • Spray duration               | 30 s  |
| • Spray rate                   | 0.093 to 0.131 g/s                                |
| • Run duration                 | 30 s  |

### B.11.2 Findings.

The results are shown in figure B-11c and table 3-11. Tests 1 to 6 were conducted to assess the effects on the collection efficiency due to silica gel and repeated usage of the desiccants, tests 7 to 12 assessed the effects due to different amounts of silica gel, tests 13 and 14 used molecular sieve, tests 15 and 16 assessed the effects on the collection efficiency due to the centrifuge, and test 17 used a different plastic container where the base had a number of drilled holes (figure B-11d).

Visual examination of the collector showed significant water deposition on the cylindrical blotter tube and none was found on the plastic container. There were also some traces of water droplets on the B-Gon pouch. The collection efficiencies obtained varied from 72% to 116%. Figure B-11c shows that collection efficiencies of 100% were obtained at certain test conditions. It was thought that this was attributed to the desiccant materials. The following summarized findings were found (based on limited test data in figure B-11c):

- Tests 1 to 6 showed that the adsorptive capability of silica gel desiccants degraded with repetitive usage, hence decreasing collection efficiencies. The most likely cause is the saturation of silica gel pellets over time.
- Tests 7 to 12 showed that the amount of desiccant required to obtain efficiency close to 100% must be equal to or greater than 7 g.

- Tests 13 and 14 showed that the adsorptive capability of molecular sieve desiccants was slightly lower than silica gel desiccant.
- Tests 15 and 16 showed that the addition of the centrifuge (at the divergent nozzle of the probe top section) degrades collection efficiency. The cause of this effect was unknown. Test 17 showed that using the plastic container with predrilled holes (figure B-11d) also degrades collection efficiency.

The inlet static pressures recorded during tests 1 to 12 (silica gel, no centrifuge) were about 0.65 psig (18" H<sub>2</sub>O) compared to the pressures recorded for tests 13 and 14 (molecular sieve, no centrifuge) and tests 15 and 16 (silica gel and centrifuge), which were only 0.54 psig (15" H<sub>2</sub>O). The inlet static pressures without the porous B-Gon layer was approximately 1.08 psig (30" H<sub>2</sub>O). The large drop in the pressure was attributed to the desiccant in the porous layer and the bent exit tube of the plastic container used in the tests.

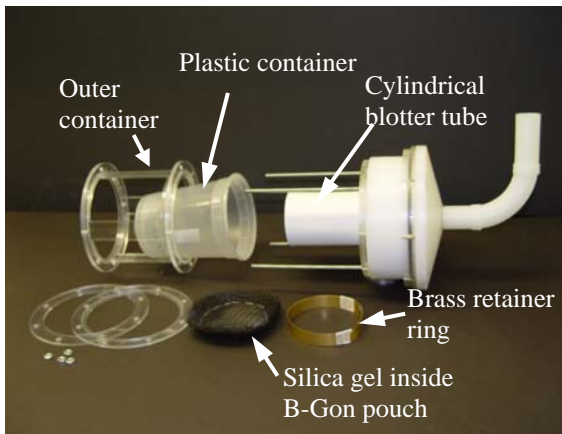


FIGURE B-11a. CONFIGURATION 11 (BEFORE ASSEMBLY)



FIGURE B-11b. CONFIGURATION 11 (AFTER ASSEMBLY)

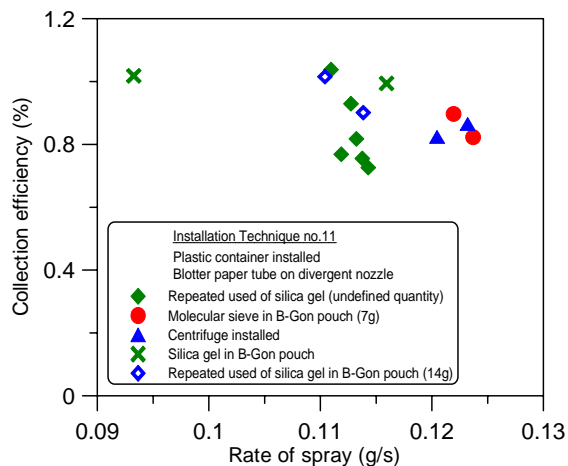


FIGURE B-11c. CONFIGURATION 11

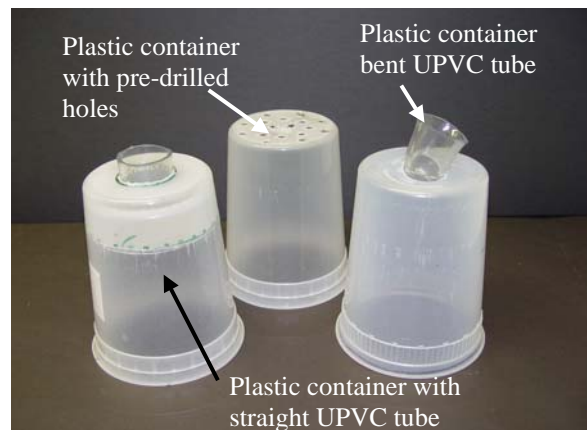


FIGURE B-11d. PLASTIC CONTAINERS WITH DIFFERENT EXIT DESIGNS

### B.11.3 Configuration 11 Mod-I.

The bent exit tube of the plastic container was replaced with a straight tube, as shown in figure B-11d. This modification was designated as configuration 11 Mod-I. Further tests were conducted with this modified design but only with (approximately) 7 g of silica gel desiccants, which were filled the B-Gon pouch.

The results are shown in figure B-11e and table 3-12.

Figure B-11e shows that significant improvement in the collection efficiencies and inlet static pressures were obtained with the Mod-I design. The collection efficiencies vary from 96% to 108%. The inlet static pressures were approximately 0.94 psig (26" H<sub>2</sub>O), which represented an improvement of nearly 40%. The collection efficiency was also unaffected by the variation in the spray rates.

In summary, based on limited data, configuration 11 Mod-I showed the highest collection efficiencies, which were within 100%. To quantify the measurement errors and repeatability, an extensive calibration test program was carried out for a wider range of flow conditions. The results are found in section 3.5.

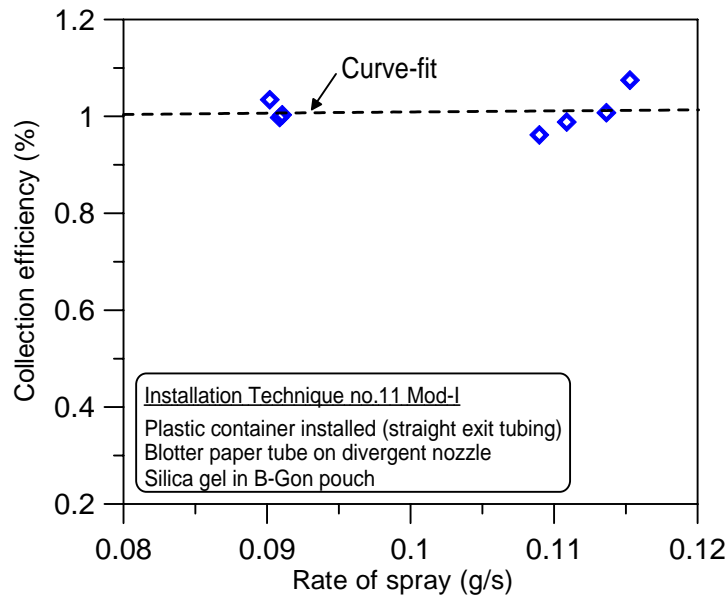


FIGURE B-11e. CONFIGURATION 11 MOD-I

## APPENDIX C—TEST PROCEDURE FOR CONFIGURATION 11 MOD-I

### C.1 LABORATORY TEST PROCEDURE.

1. Preparation of plastic container
  - Install container, brass ring retainer, gauze mesh, and secure to external cage support.
  - Place assembly inside main probe body.
  - Run for at least 1 minute to ensure the assembly is completely dry.
2. Preparation of silica gel and B-Gon
  - Dry B-Gon filter (without any silica) using the exhaust air from the vacuum device.
  - Weigh the B-Gon filter and container with a lid (without silica gel).
  - Cut two (7 g) packets and sieved silica pellets with a coarse and fine gauged wire meshes.
  - Seal silica pellets in a container with a lid to prevent the adsorption of vapor from surrounding air.
  - Weigh approximately 8 g of silica gel and pour into B-Gon pouch. Seal B-Gon with plastic ties.
  - Place B-Gon and silica in a sealed container.
3. Preparation of blotter paper
  - Using a new blotter paper (209 mm wide by 100 mm high), form a rolled tube (with a pencil) and fit onto a brass ring.
  - Place blotter over the two support brass rings (the one identified with arrow markings is to fit into the probe).
  - Secure both ends with elastic bands initially. Then join ends with a strong tape.
  - Blotter paper is ready for weighing.
  - Wrap blotter with a plastic bag and weigh.

4. Preparation of water sample (for spraying)

- Weigh and record a sample of water on electronic balance.
- Place a lid over water holder. This is to reduce evaporation.

5. Preparation of the test assembly

- After weighing the blotter paper, attach to the divergent nozzle of the probe top section.
- Insert blotter with the split line (i.e., the joint between two ends of the paper) aligned with the probe inlet.
- At this point, the weight of the water and blotter paper have already been recorded.
- Now weigh the B-Gon that contains the silica gel pellets. Ensure that the readings do not fluctuate. If so, leave it on the balance for a short period of time. It should stabilize after a while.
- Just before placing B-Gon inside plastic container, use fingers to spread the silica pellet to ensure uniform distribution. Ensure pellets are also near the edges of the B-Gon filter. (This step must be performed with haste as vapor is being adsorb during this phase.)
- Place B-Gon inside container carefully, ensuring that the B-Gon is kept level.
- Push onto B-Gon firmly until it fits snugly onto the wire gauze.
- Attach the brass retainer ring onto B-Gon.
- Attach the plastic container to the probe top section (with the blotter).
- Check to ensure the blotter paper is not pushing against the B-Gon filter (if so, check the height of the blotter paper to ensure it is 100 mm long).
- Place the assembly onto the probe main body.

6. Test procedure

- Clean out any remaining water from the spray nozzle.
- Check the pressure setting.
- Using a spare water bottle, fill spray nozzle (by pressing on the spray lever).

- Check to ensure bubbles are not caught in the water feed line. If bubbles are present, clean out water and refill from a spare water sample.
- Replace the water bottle with the one to be used for testing, taking care to ensure that no water was lost during the changeover.
- Start suction fan.
- Record probe inlet static pressure readings.
- Note start time and start spraying.
- When set duration has been reached, stop spray and stop suction fan.
- Remove the assembly from the main body.
- Remove plastic container.
- Remove B-Gon immediately and place in sealed container.
- Remove blotter paper and place inside plastic bag to reduce evaporation.
- Weigh and record blotter paper followed by the B-Gon.
- Check the probe for water droplets. If present, weigh a small piece of filter paper, wipe the droplets with the filter paper and weigh.
- Weigh and record a sample of water on electronic balance.

7. Calculation of probe collection efficiency

- Calculate the amount of water sprayed,  $m_s$ .
- Calculate the amount of water collected by blotter paper and B-Gon,  $m_c$ .
- Calculate collection efficiency,  $x = (m_c) / m_s$ .

C.2 WIND TUNNEL TEST PROCEDURE.

Steps 1 to 4 are similar to the preparation procedures described in section C.1.

1. Preparation of plastic container

- Install container, brass ring retainer, gauze mesh, and secure to external cage support.
- Place assembly inside main probe body.
- Run for at least 1 minute to ensure the assembly is completely dry.

## 2. Preparation of silica gel and B-Gon

- Dry B-Gon filter (without any silica) using the exhaust air from the vacuum device.
- Weigh the B-Gon filter and container with a lid (without silica gel).
- Cut two (7 g) packets and sieved silica pellets with a coarse and fine gauged wire meshes.
- Seal silica pellets in a container with a lid to prevent the adsorption of vapor from surrounding air.
- Weigh approximately 8 g of silica gel and pour into B-Gon pouch. Seal B-Gon with plastic ties.
- Place B-Gon and silica in a sealed container.

## 3. Preparation of blotter paper

- Using a new blotter paper (209 mm wide by 100 mm high), form a rolled tube (with a pencil) and fit onto a brass ring.
- Place blotter over the two support brass rings (the one identified with arrow markings is to fit into the probe).
- Secure both ends with elastic bands initially. Then join ends with a strong tape.
- Blotter paper is ready for weighing.
- Wrap blotter with a plastic bag and weigh.

## 4. Preparation of water sample (for spraying)

- Weigh and record a sample of water on electronic balance.
- Place a lid over water holder. This is to reduce evaporation.

## 5. Test procedure

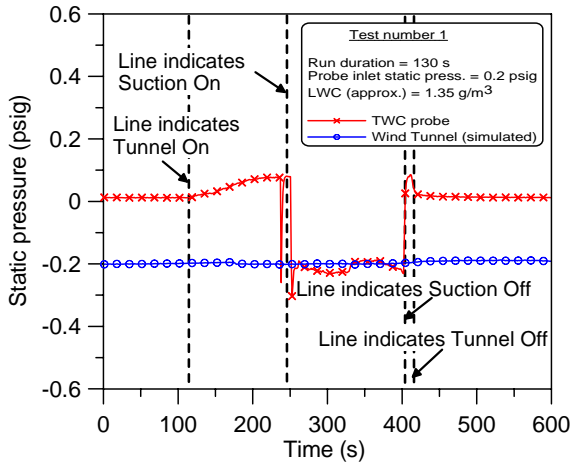
- Clean out any remaining water from the spray nozzle.
- Check the pressure setting.
- Using a spare water bottle, fill spray nozzle (by pressing on the spray lever).
- Check to ensure bubbles are not caught in the water feed line. If bubbles are present, clean out water and refill from a spare water sample.

- Replace the water bottle with the one to be used for testing, taking care to ensure that no water was lost during the changeover.
- *Start ISFC software.*
- *Tunnel operator startup wind tunnel.*
- *Tunnel operator reads out tunnel velocity in the form of a Q value (psf).*
- *ISFC operator enters Q value into the DPI-610.*
- Start suction fan.
- Record probe inlet static pressure readings.
- Note start time and start spraying.
- When set duration has been reached, stop spray and stop suction fan.
- *Tunnel operator stops wind tunnel.*
- Remove the assembly from the main body.
- Remove plastic container.
- Remove B-Gon immediately and place in the sealeable container.
- Remove blotter paper and place inside plastic sack to reduce evaporation.
- Weigh and record blotter paper followed by the B-Gon.
- Check the probe for water droplets. If present, weigh a small piece of filter paper, wipe the droplets with the filter paper and weigh.
- Weigh and record a sample of water on electronic balance.

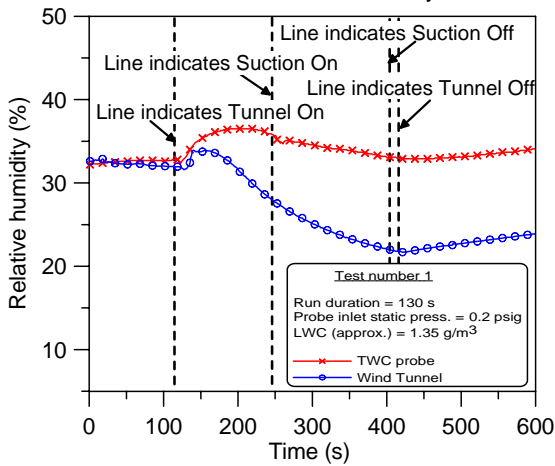
6. Calculation of probe collection efficiency

- Calculate the amount of water sprayed,  $m_s$ .
- Calculate the amount of water collected by blotter paper and B-Gon,  $m_c$ .
- Calculate collection efficiency,  $x = (m_c)/ m_s$ .

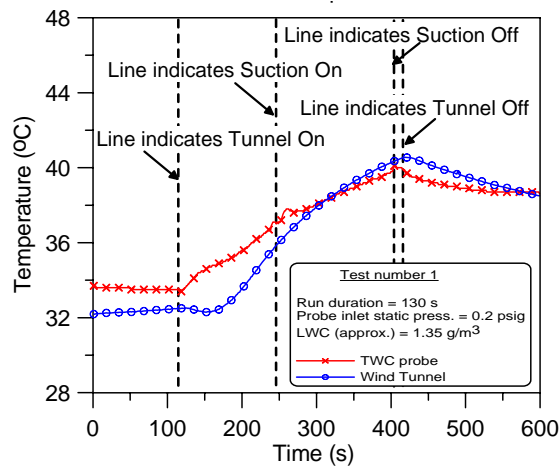
APPENDIX D—MOD-I TEST DATA—WIND TUNNEL



(a) Static Pressure Distribution

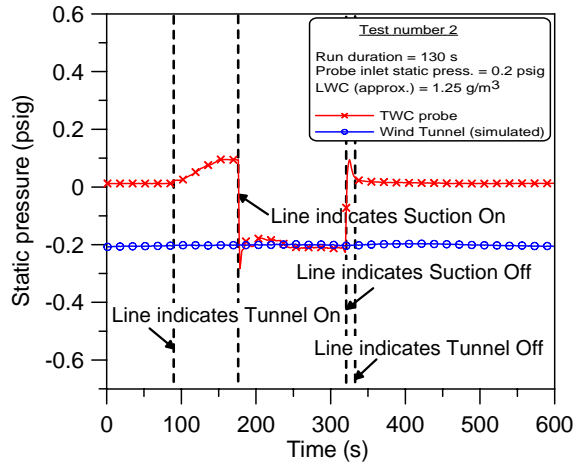


(b) Relative Humidity Distribution

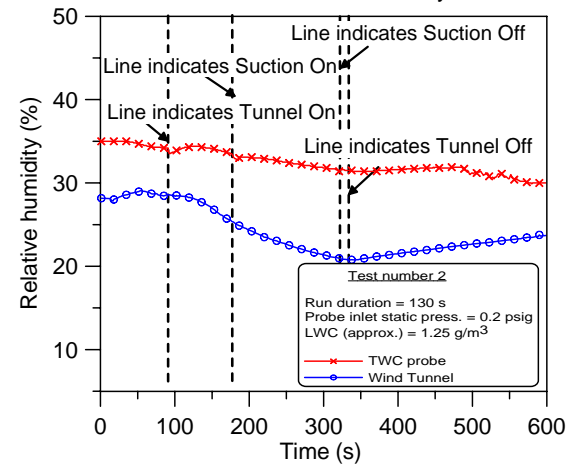


(c) Temperature Distribution

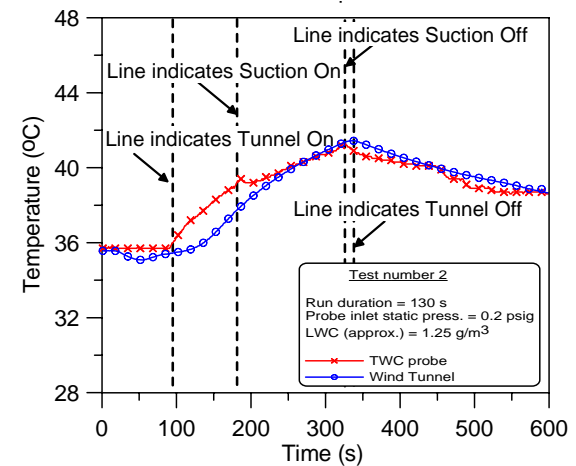
FIGURE D-1. RESULTS FOR TEST 1



(a) Static Pressure Distribution

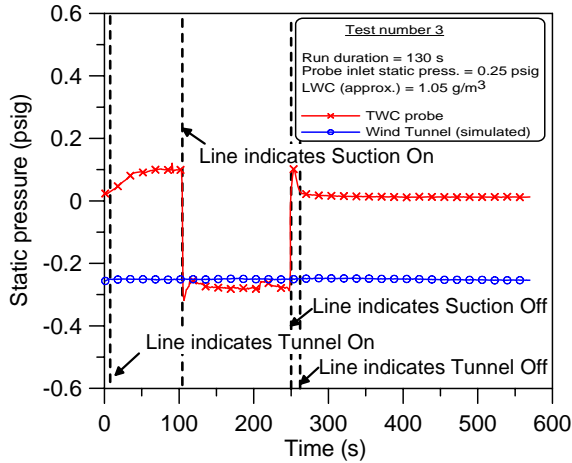


(b) Relative Humidity Distribution

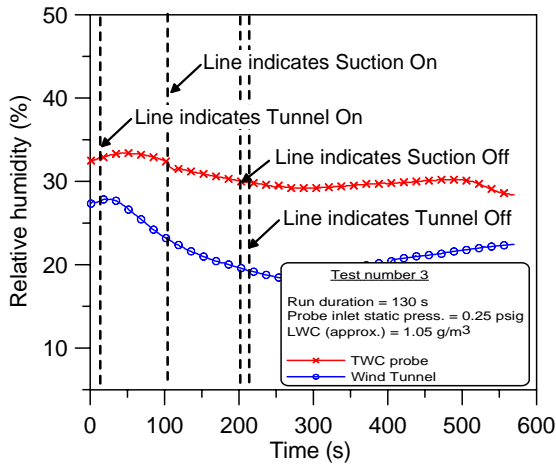


(c) Temperature Distribution

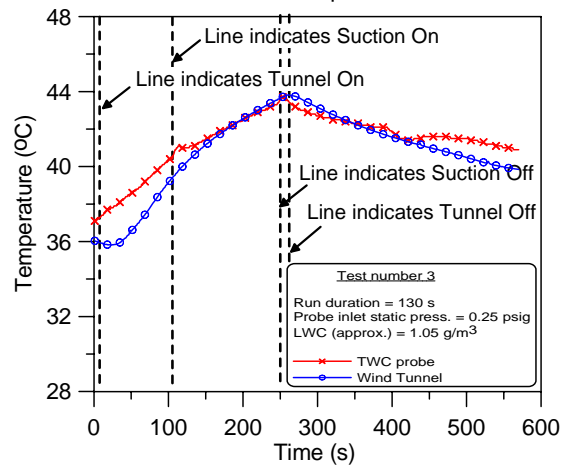
FIGURE D-2. RESULTS FOR TEST 2



(a) Static Pressure Distribution

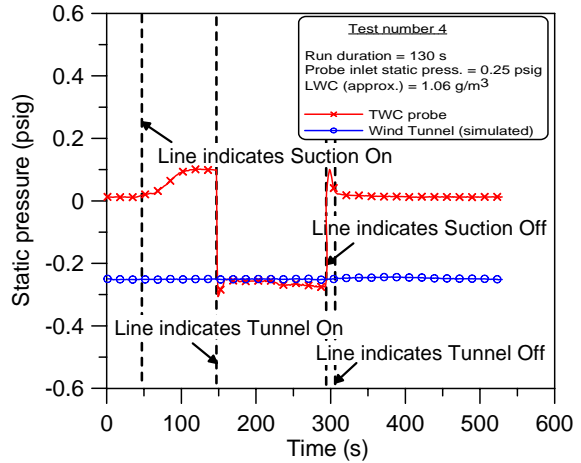


(b) Relative Humidity Distribution

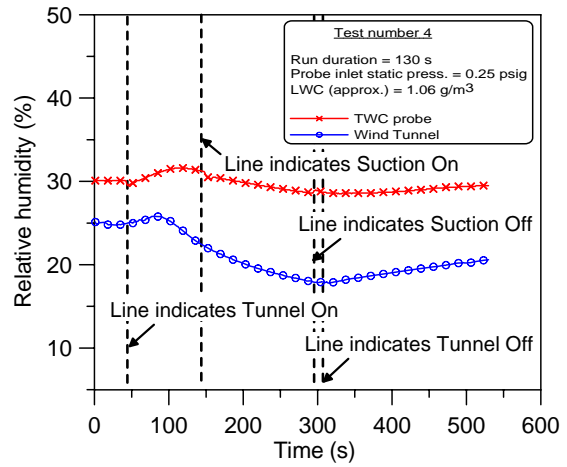


(c) Temperature Distribution

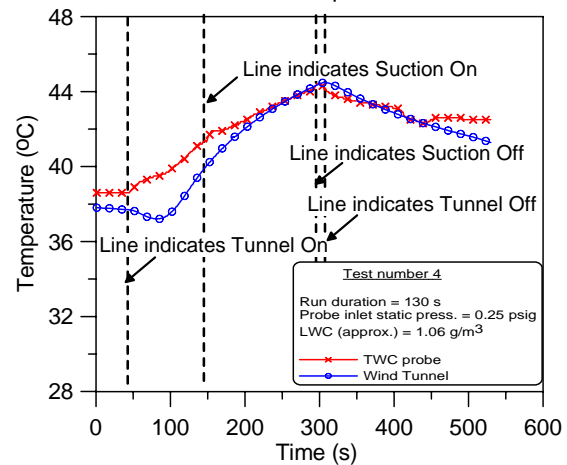
FIGURE D-3. RESULTS FOR TEST 3



(a) Static Pressure Distribution

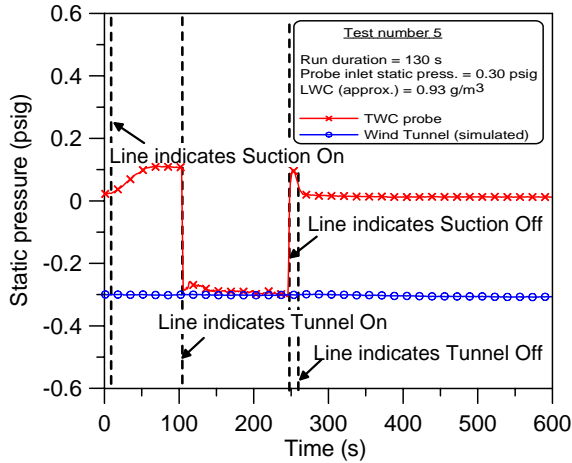


(b) Relative Humidity Distribution

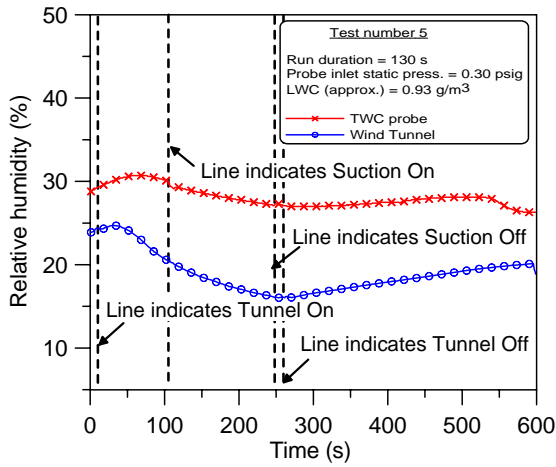


(c) Temperature Distribution

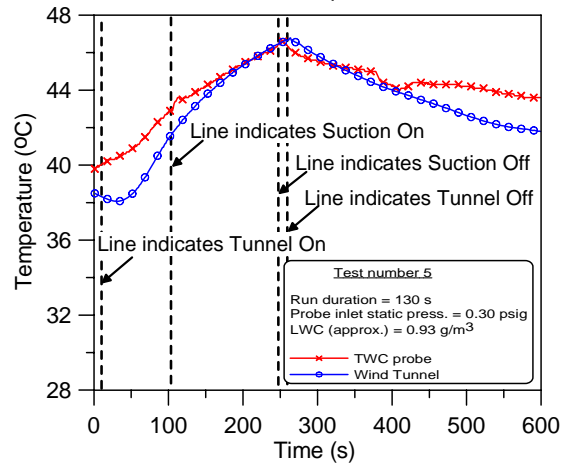
FIGURE D-4. RESULTS FOR TEST 4



(a) Static Pressure Distribution

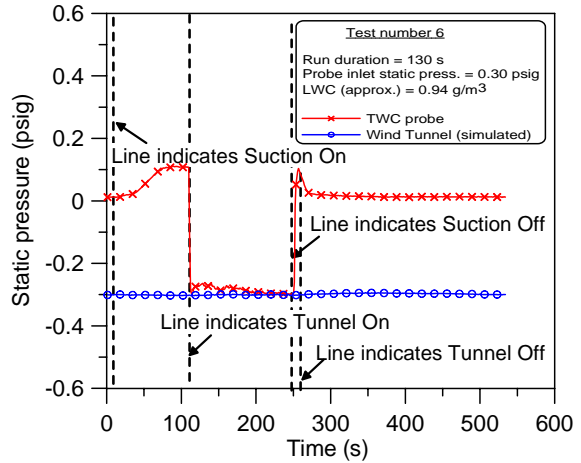


(b) Relative Humidity Distribution

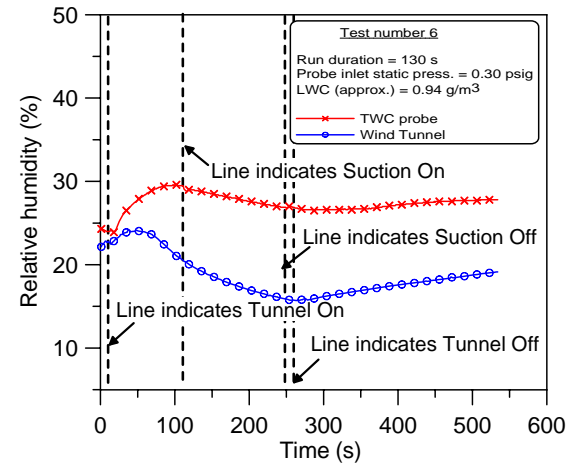


(c) Temperature Distribution

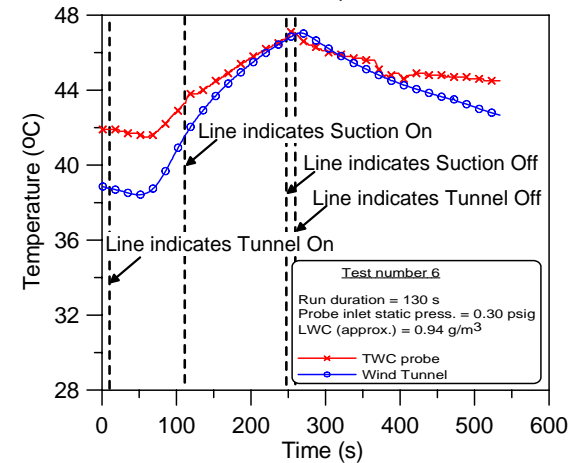
FIGURE D-5. RESULTS FOR TEST 5



(a) Static Pressure Distribution

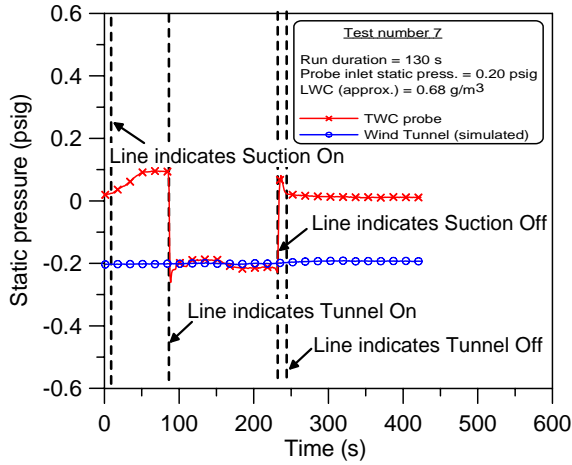


(b) Relative Humidity Distribution

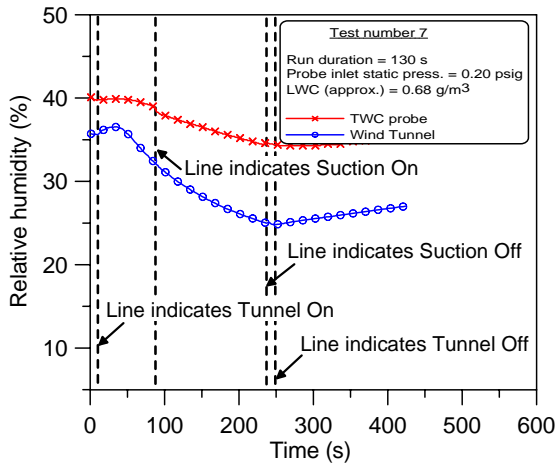


(c) Temperature Distribution

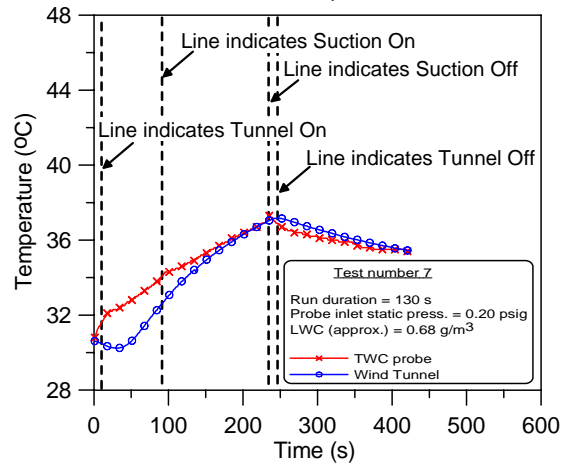
FIGURE D-6. RESULTS FOR TEST 6



(a) Static Pressure Distribution

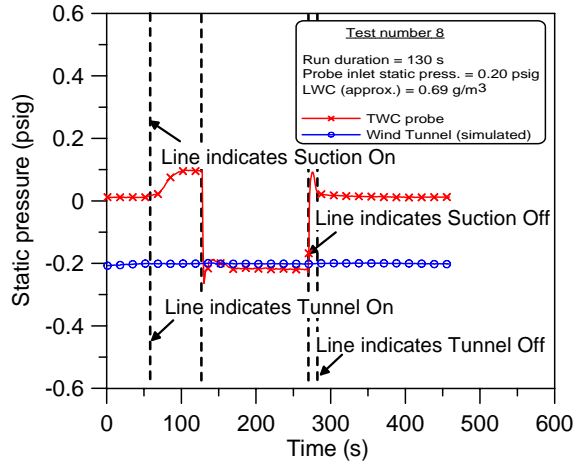


(b) Relative Humidity Distribution

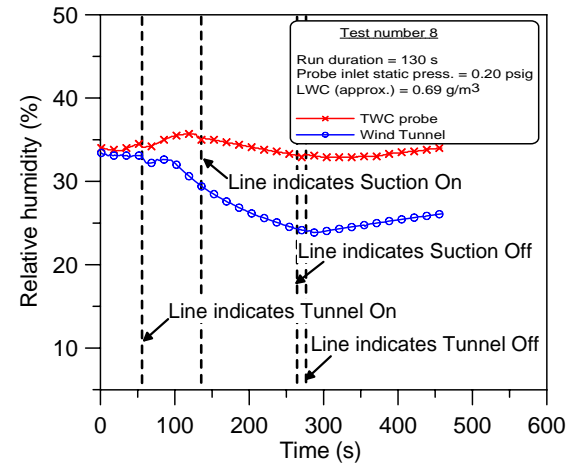


(c) Temperature Distribution

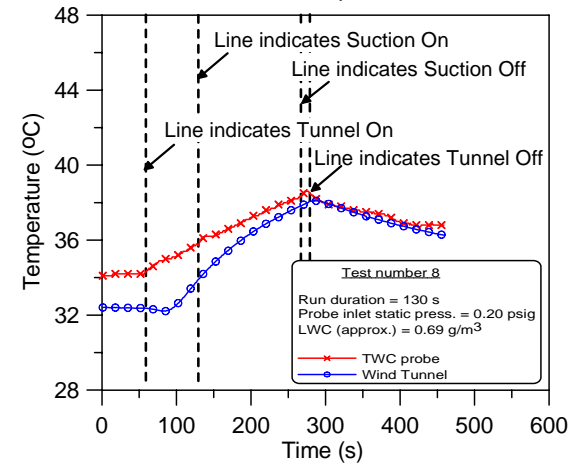
FIGURE D-7. RESULTS FOR TEST 7



(a) Static Pressure Distribution

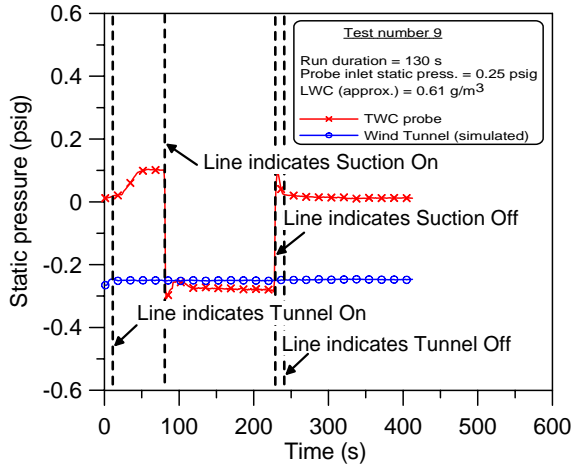


(b) Relative Humidity Distribution

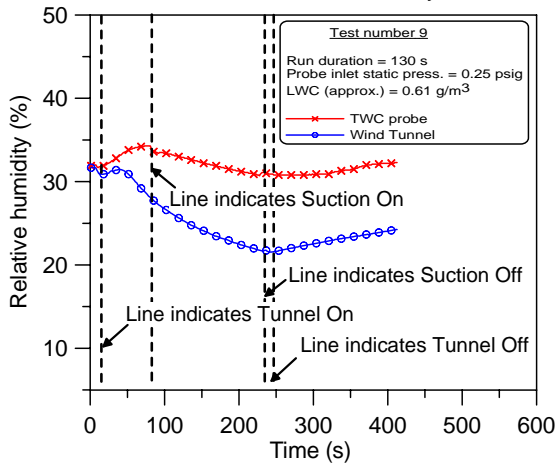


(c) Temperature Distribution

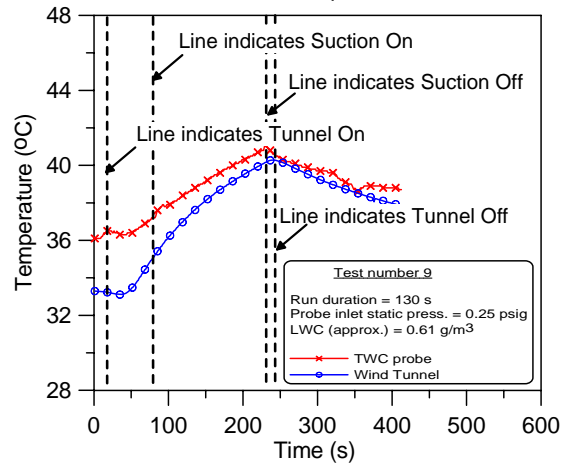
FIGURE D-8. RESULTS FOR TEST 8



(a) Static Pressure Distribution

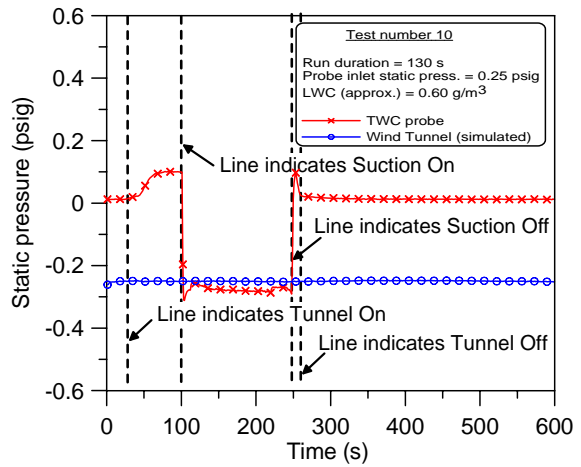


(b) Relative Humidity Distribution

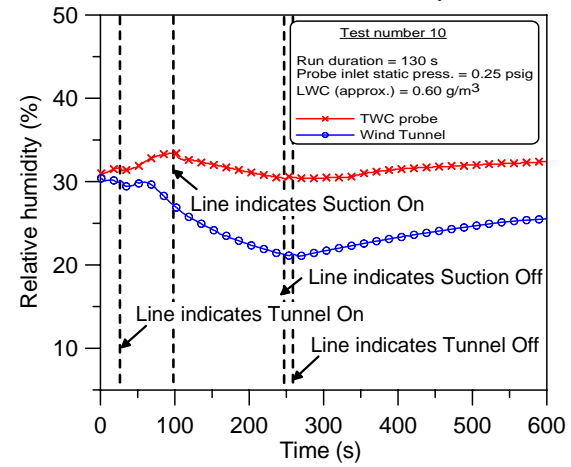


(c) Temperature Distribution

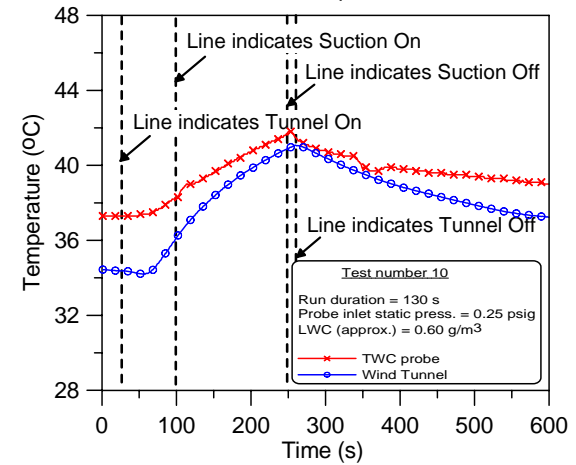
FIGURE D-9. RESULTS FOR TEST 9



(a) Static Pressure Distribution

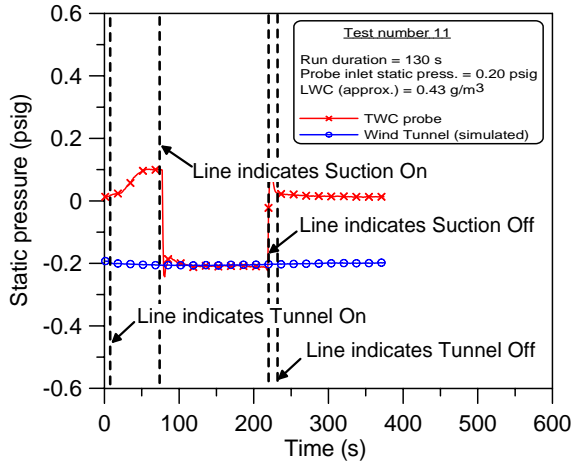


(b) Relative Humidity Distribution

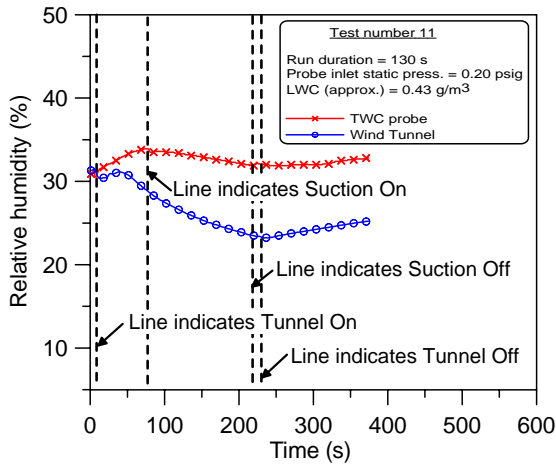


(c) Temperature Distribution

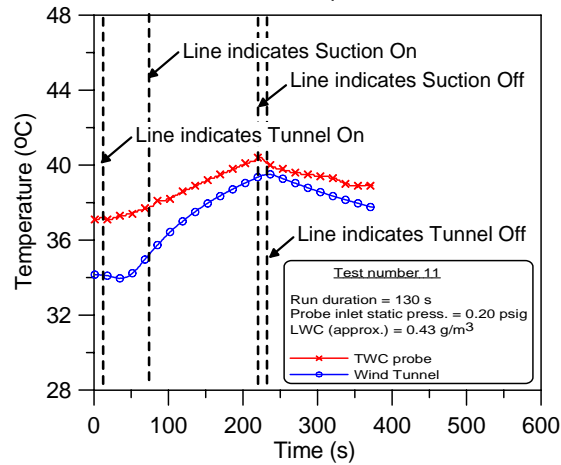
FIGURE D-10. RESULTS FOR TEST 10



(a) Static Pressure Distribution

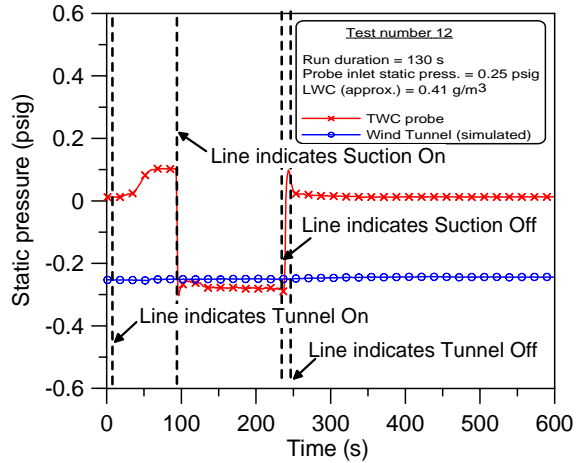


(b) Relative Humidity Distribution

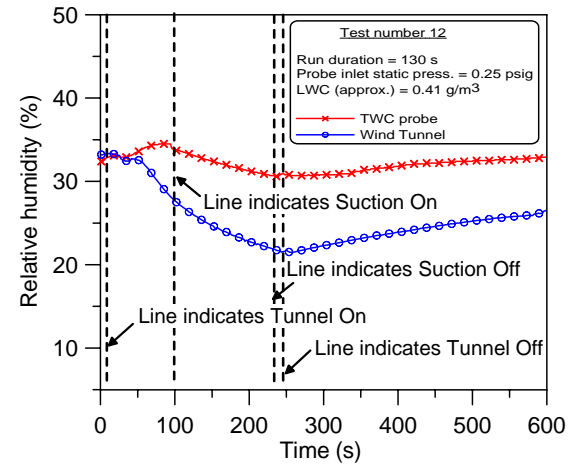


(c) Temperature Distribution

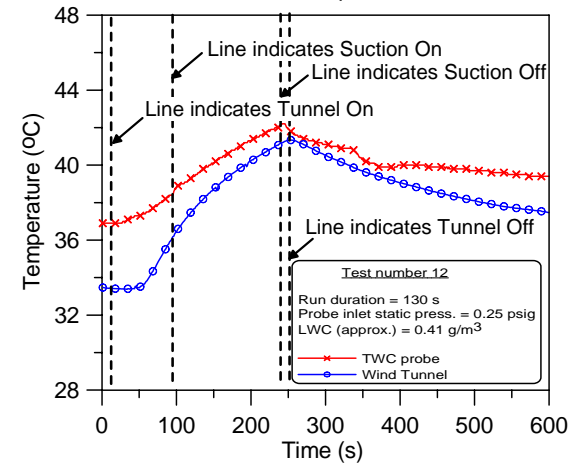
FIGURE D-11. RESULTS FOR TEST 11



(a) Static Pressure Distribution

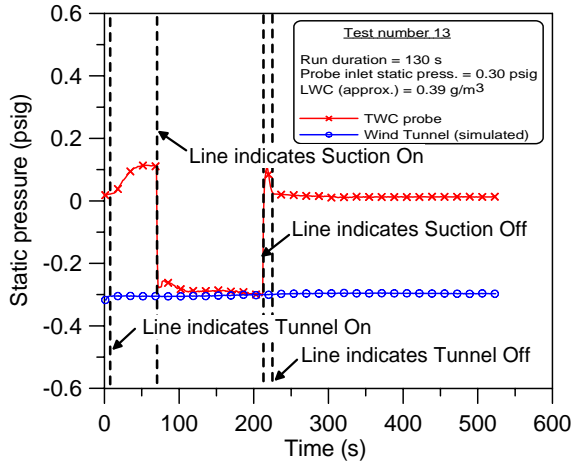


(b) Relative Humidity Distribution

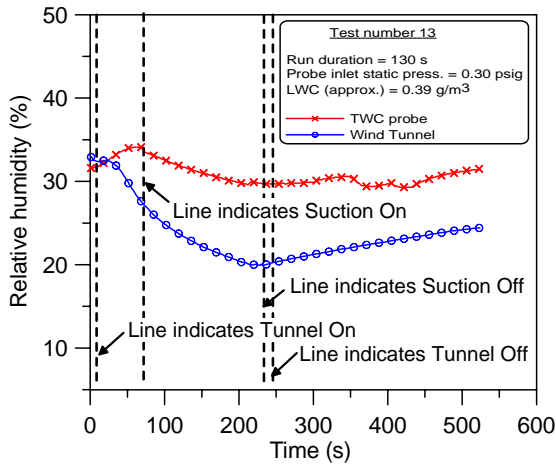


(c) Temperature Distribution

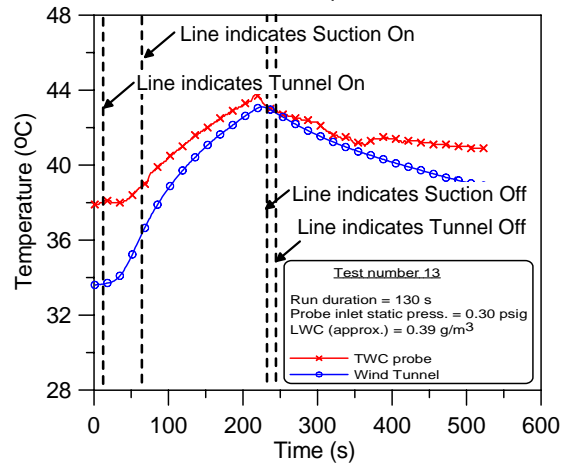
FIGURE D-12. RESULTS FOR TEST 12



(a) Static Pressure Distribution

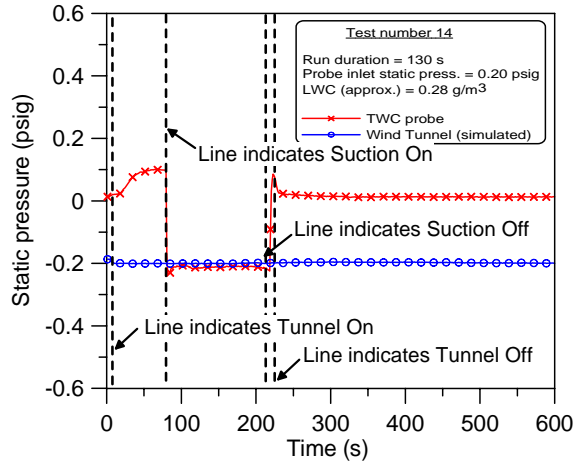


(b) Relative Humidity Distribution

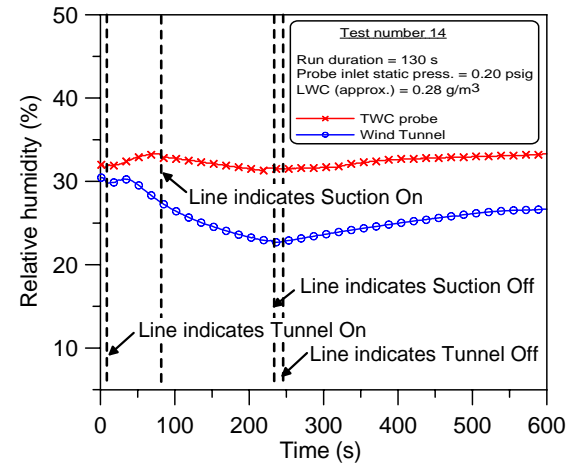


(c) Temperature Distribution

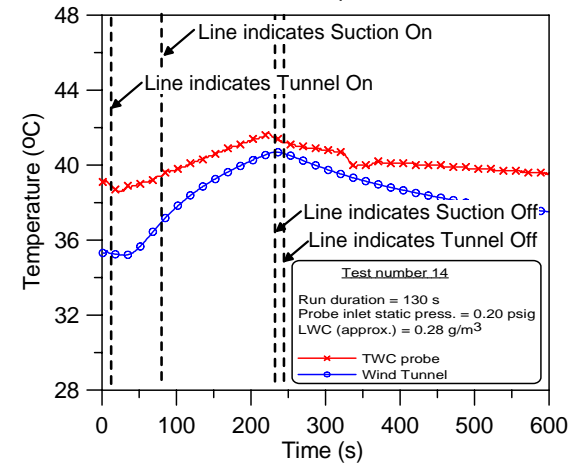
FIGURE D-13. RESULTS FOR TEST 13



(a) Static Pressure Distribution

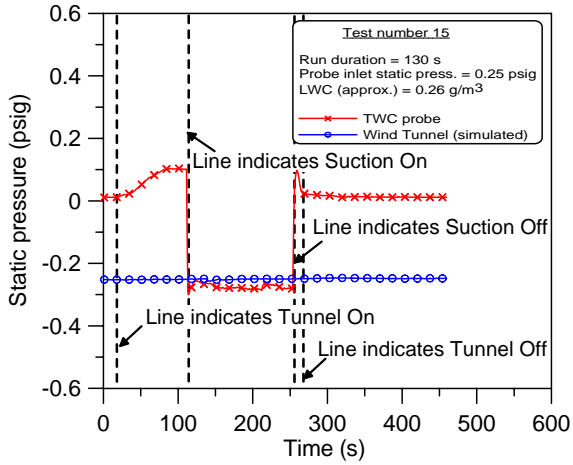


(b) Relative Humidity Distribution

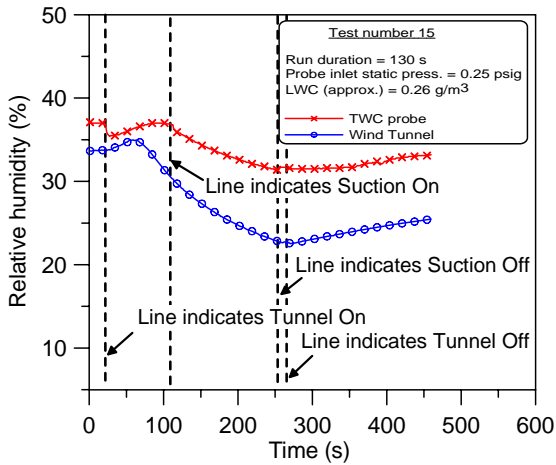


(c) Temperature Distribution

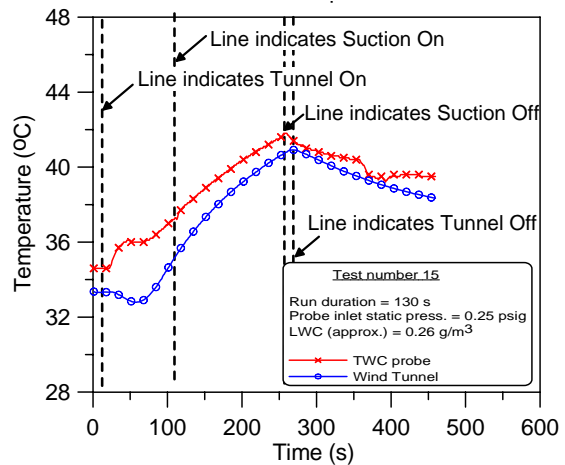
FIGURE D-14. RESULTS FOR TEST 14



(a) Static Pressure Distribution

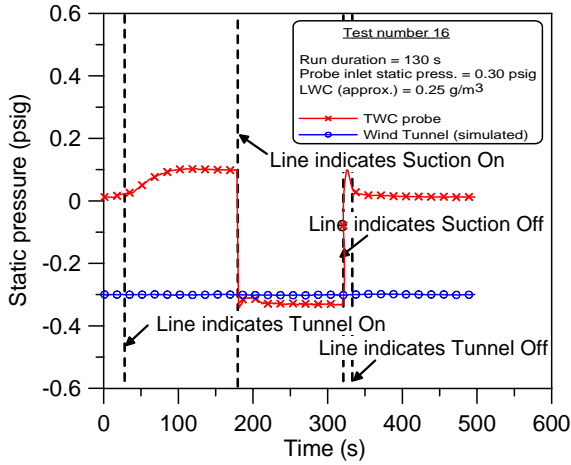


(b) Relative Humidity Distribution

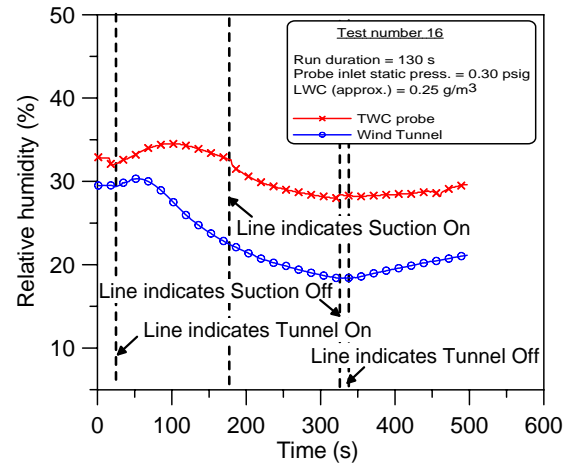


(c) Temperature Distribution

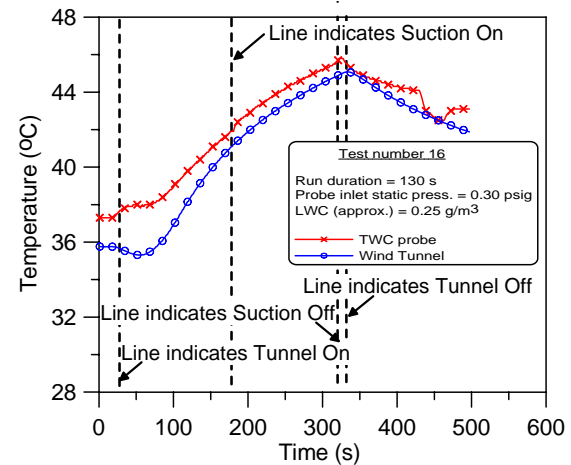
FIGURE D-15. RESULTS FOR TEST 15



(a) Static Pressure Distribution

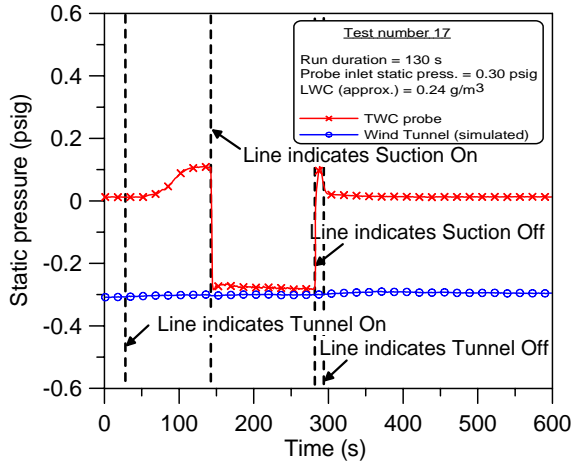


(b) Relative Humidity Distribution

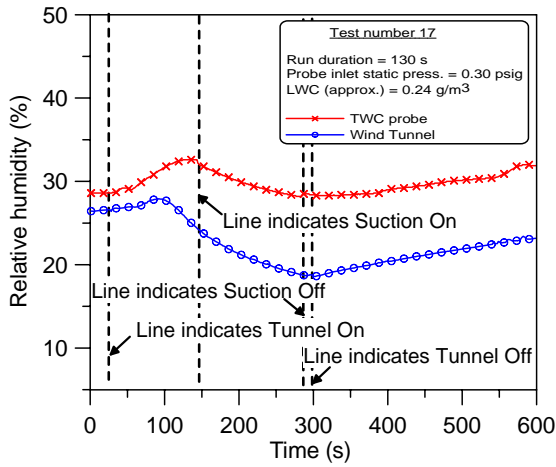


(c) Temperature Distribution

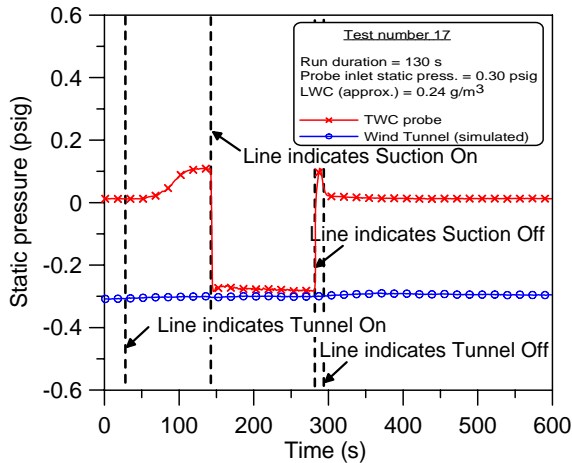
FIGURE D-16. RESULTS FOR TEST 16



(a) Static Pressure Distribution

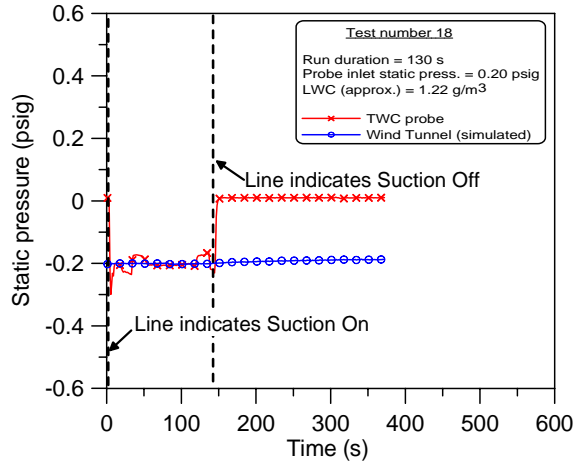


(b) Relative Humidity Distribution

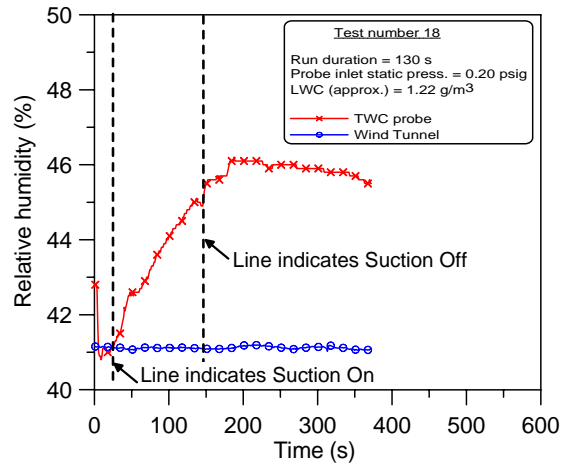


(c) Temperature Distribution

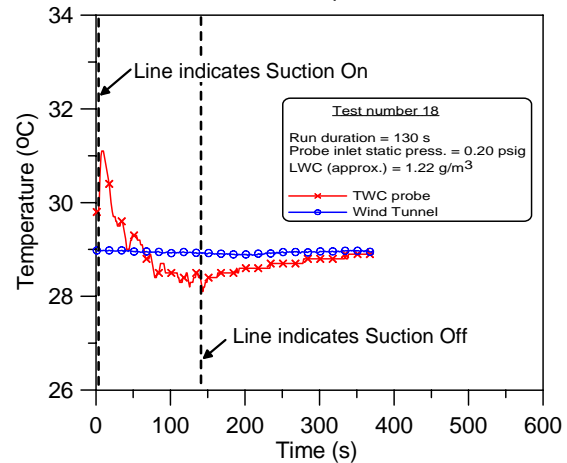
FIGURE D-17. RESULTS FOR TEST 17



(a) Static Pressure Distribution

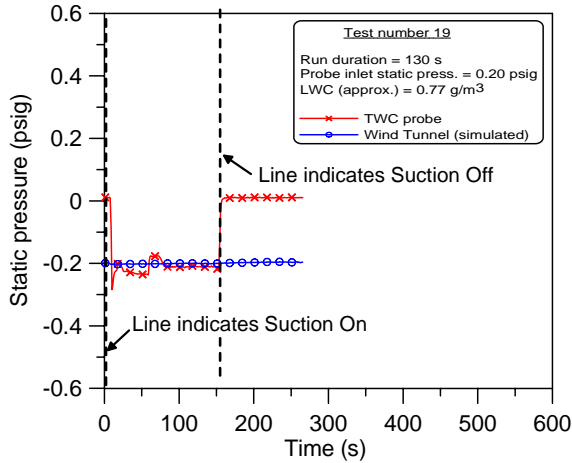


(b) Relative Humidity Distribution

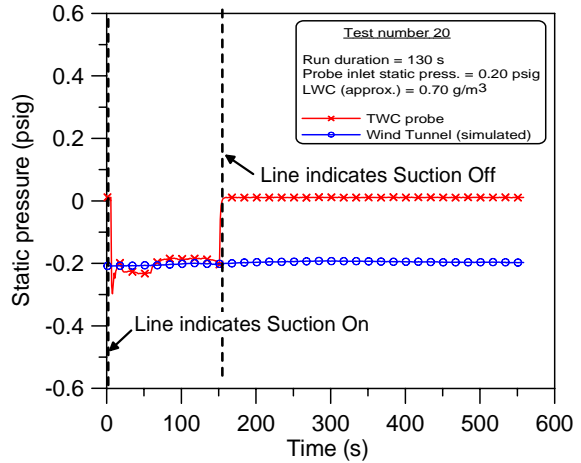


(c) Temperature Distribution

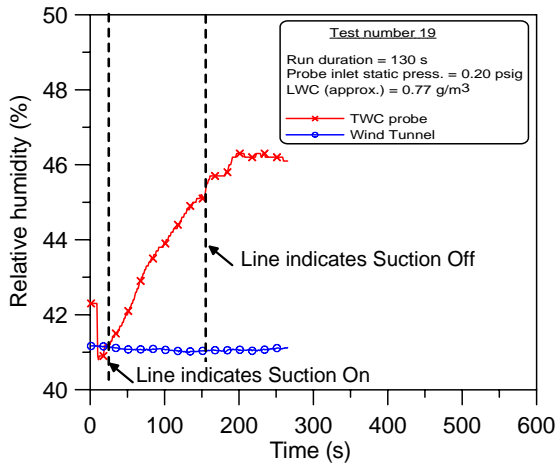
FIGURE D-18. RESULTS FOR TEST 18



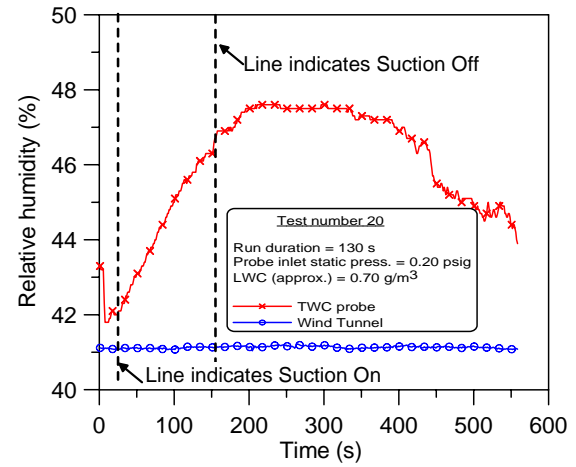
(a) Static Pressure Distribution



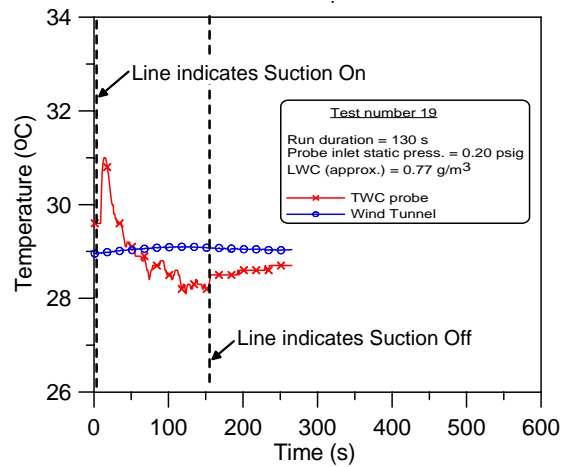
(a) Static Pressure Distribution



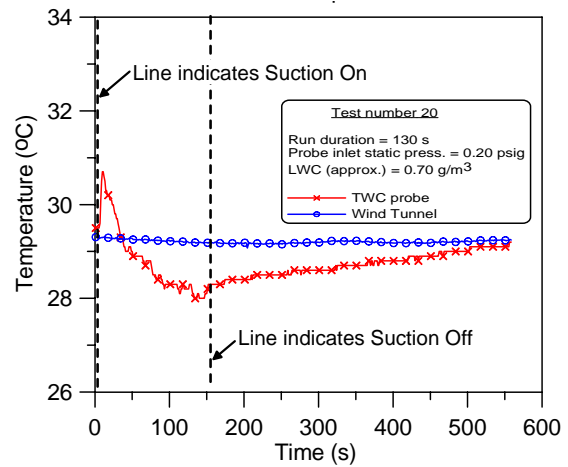
(b) Relative Humidity Distribution



(b) Relative Humidity Distribution



(c) Temperature Distribution

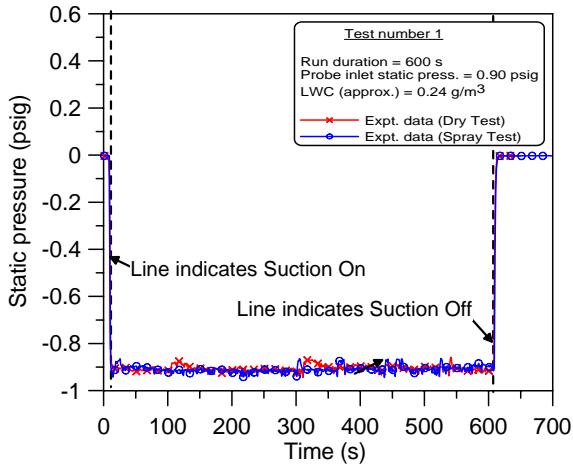


(c) Temperature Distribution

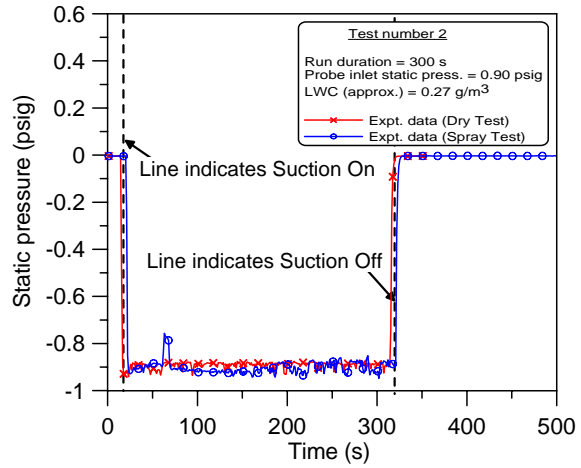
FIGURE D-19. RESULTS FOR TEST 19

FIGURE D-20. RESULTS FOR TEST 20

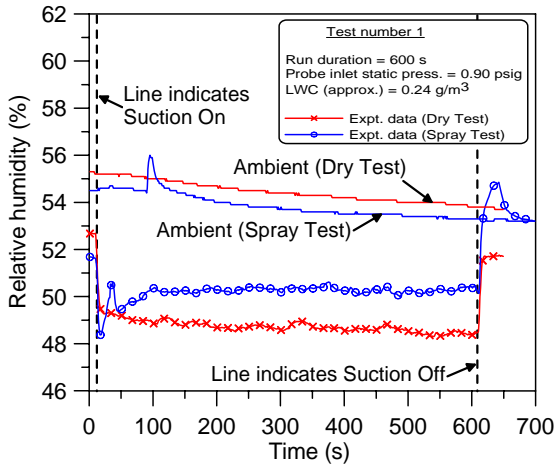
APPENDIX E—MOD-II TEST DATA—LABORATORY



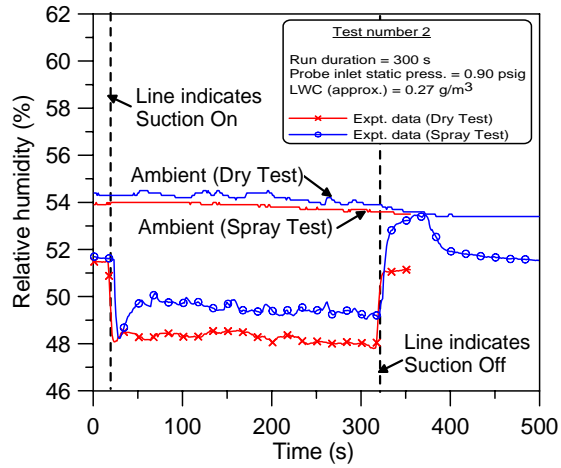
(a) Static Pressure Distribution



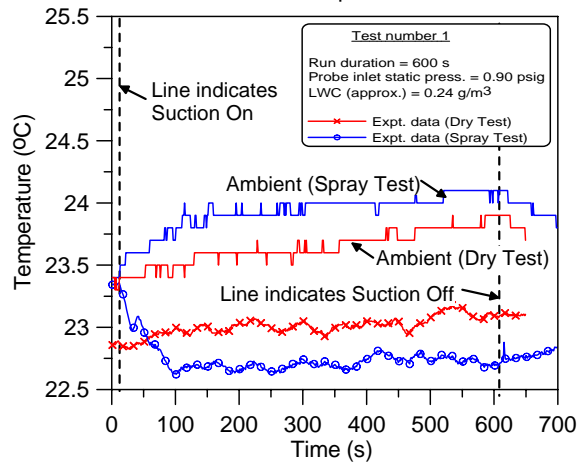
(a) Static Pressure Distribution



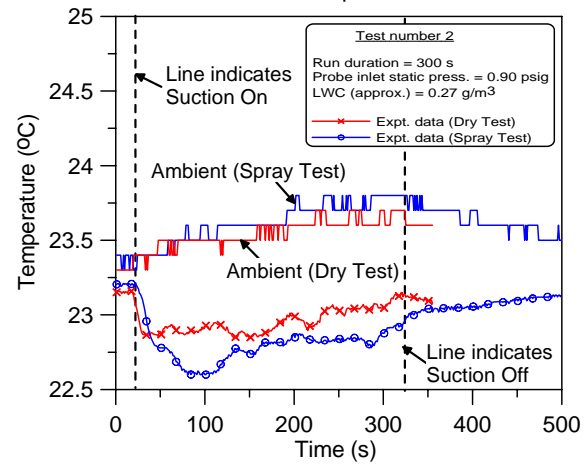
(b) Relative Humidity Distribution



(b) Relative Humidity Distribution



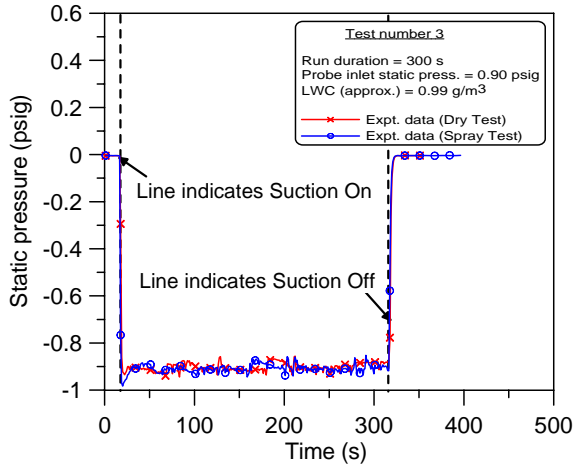
(c) Temperature Distribution



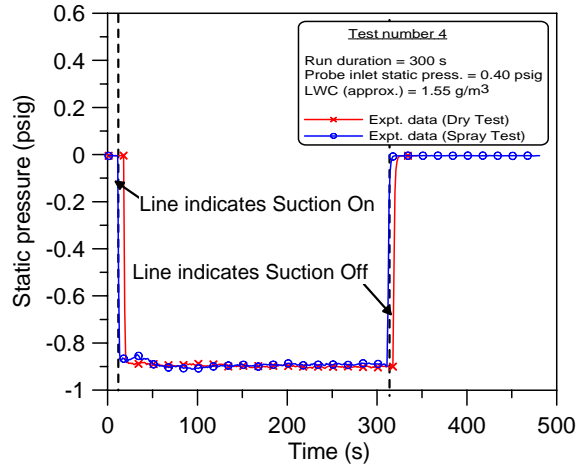
(c) Temperature Distribution

FIGURE E-1. RESULTS FOR TEST 1

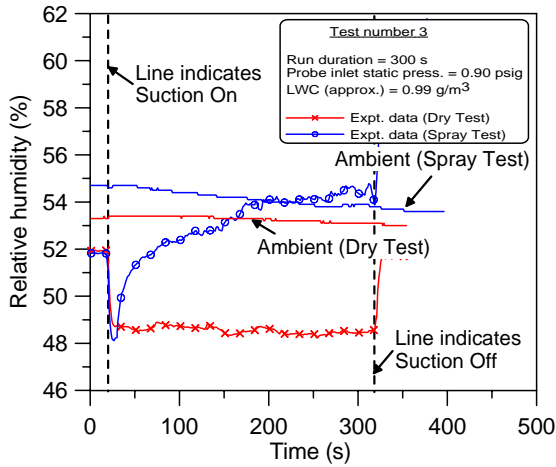
FIGURE E-2. RESULTS FOR TEST 2



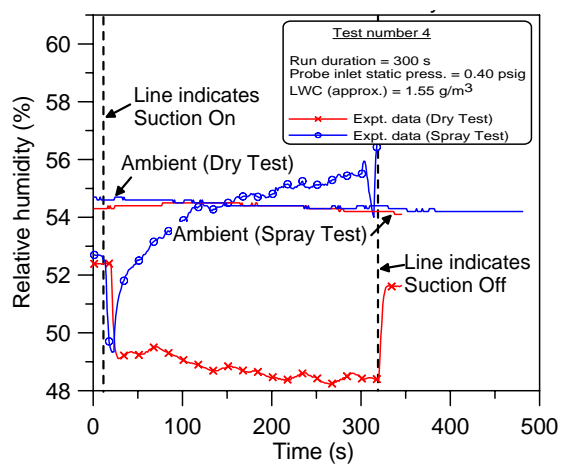
(a) Static Pressure Distribution



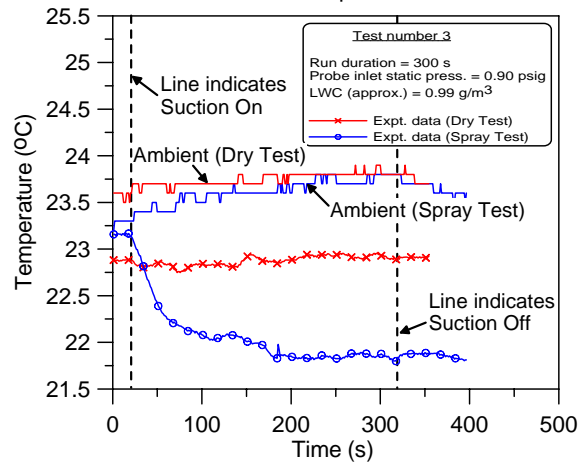
(a) Static Pressure Distribution



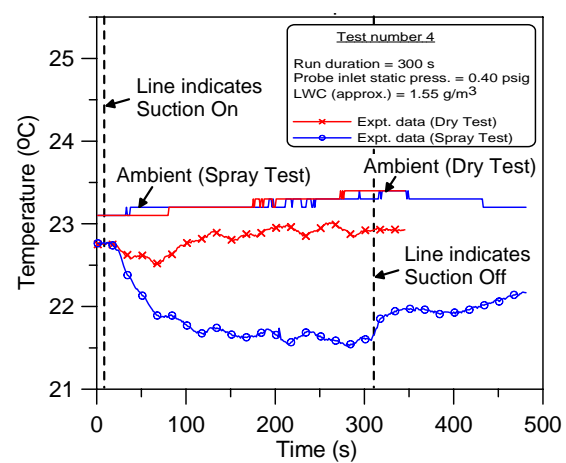
(b) Relative Humidity Distribution



(b) Relative Humidity Distribution



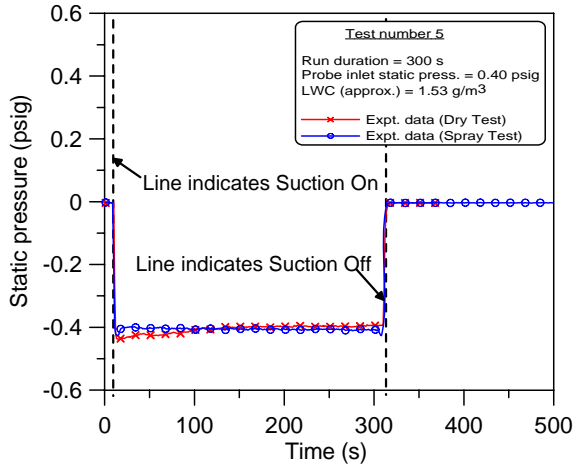
(c) Temperature Distribution



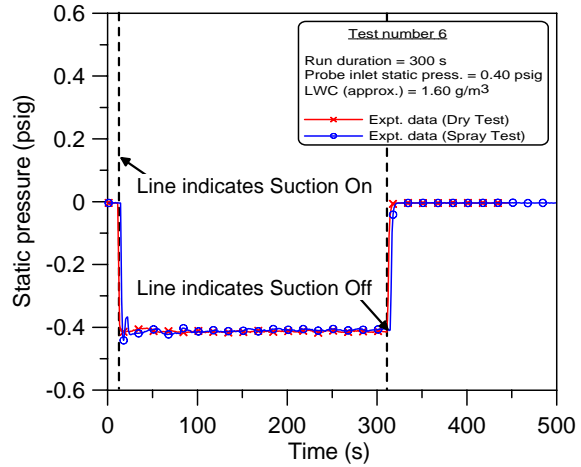
(c) Temperature Distribution

FIGURE E-3. RESULTS FOR TEST 3

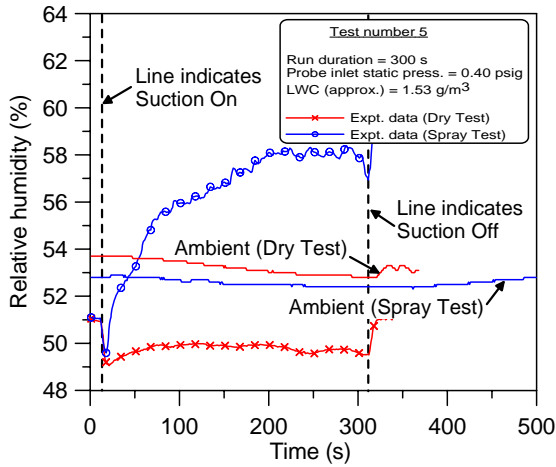
FIGURE E-4. RESULTS FOR TEST 4



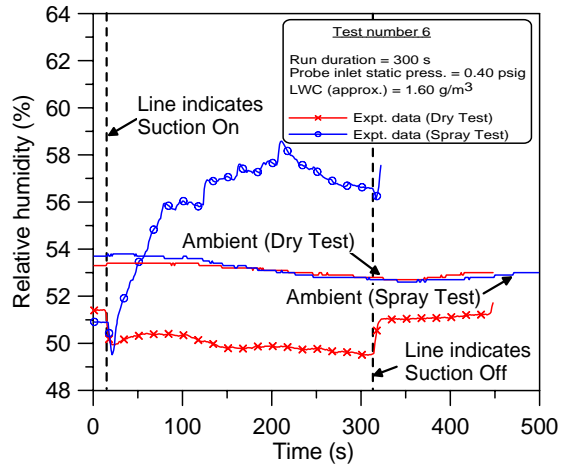
(a) Static Pressure Distribution



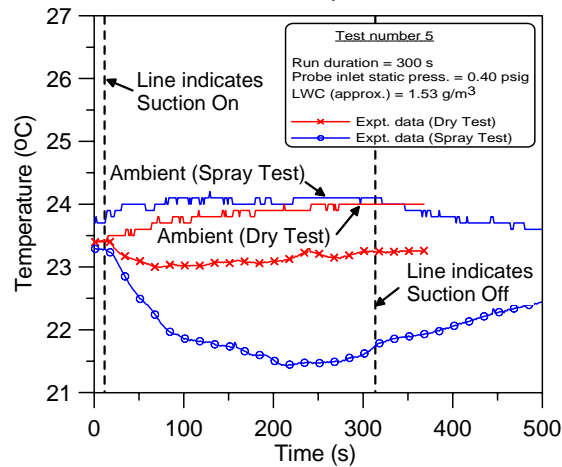
(a) Static Pressure Distribution



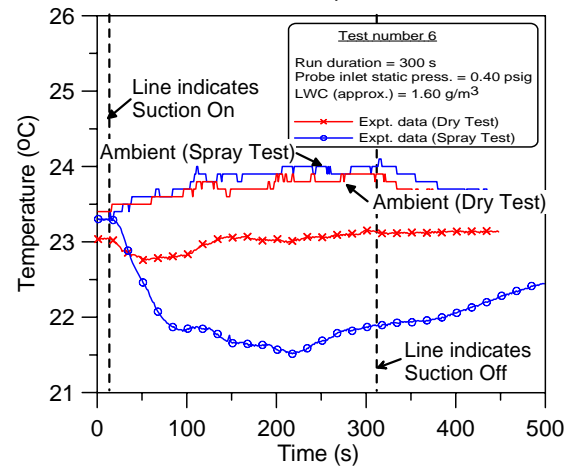
(b) Relative Humidity Distribution



(b) Relative Humidity Distribution



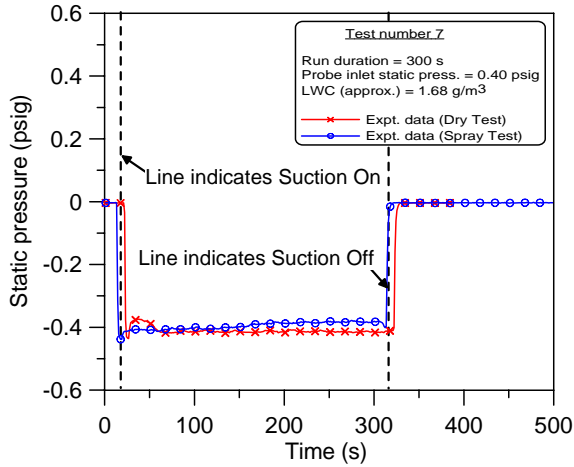
(c) Temperature Distribution



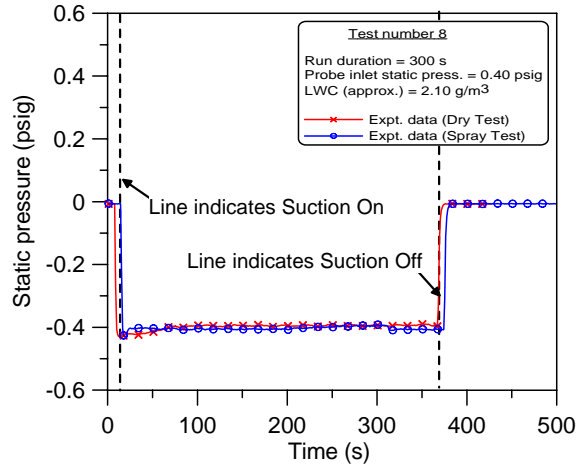
(c) Temperature Distribution

FIGURE E-5. RESULTS FOR TEST 5

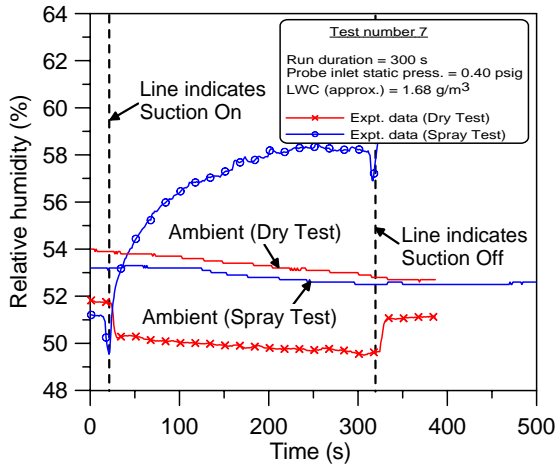
FIGURE E-6. RESULTS FOR TEST 6



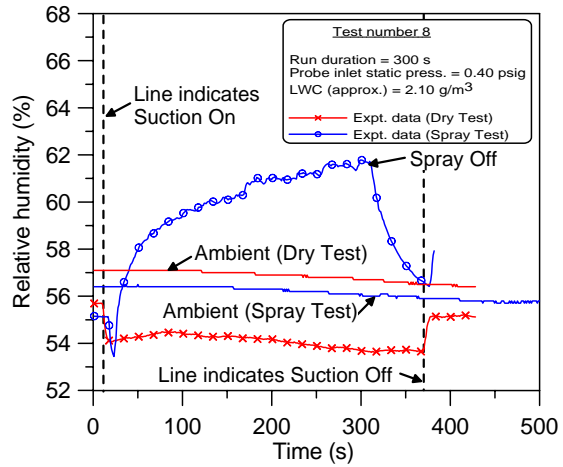
(a) Static Pressure Distribution



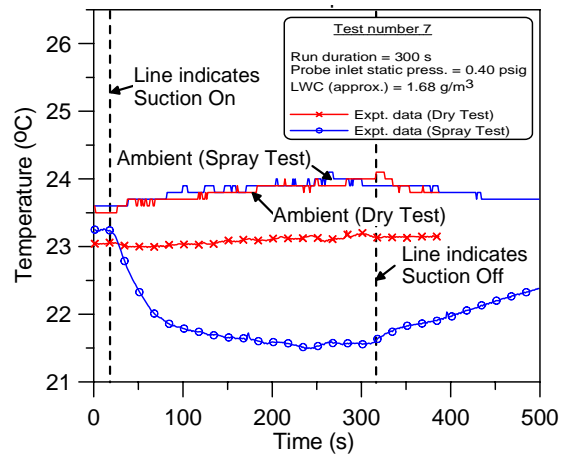
(a) Static Pressure Distribution



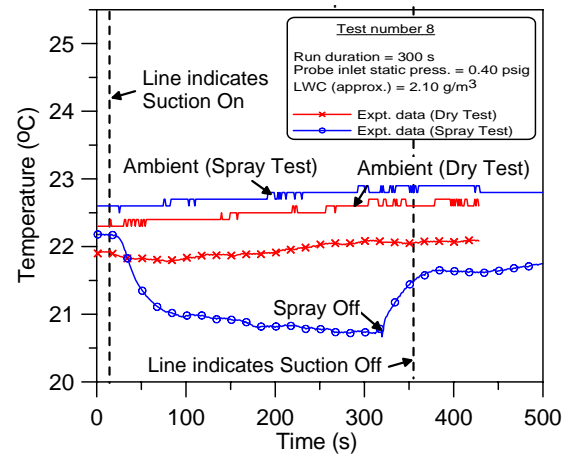
(b) Relative Humidity Distribution



(b) Relative Humidity Distribution



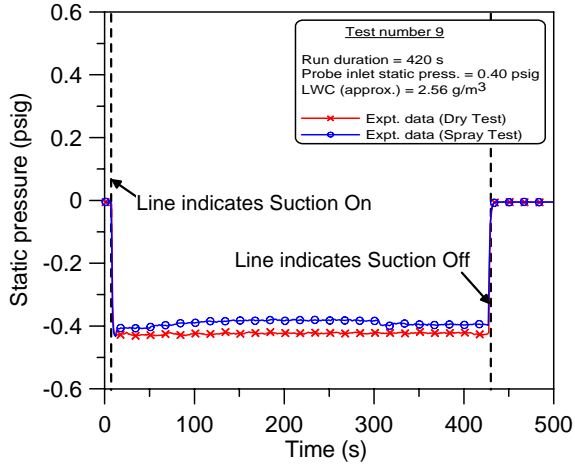
(c) Temperature Distribution



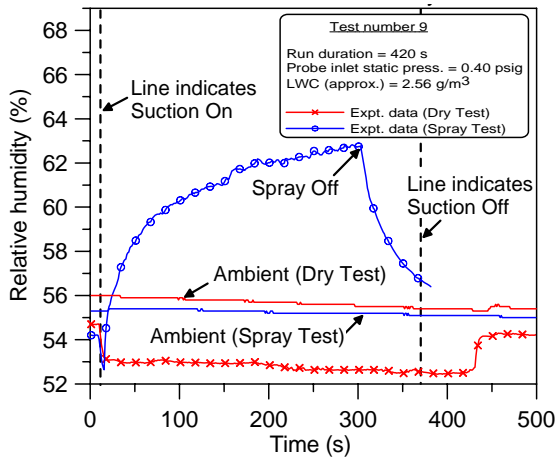
(c) Temperature Distribution

FIGURE E-7. RESULTS FOR TEST 7

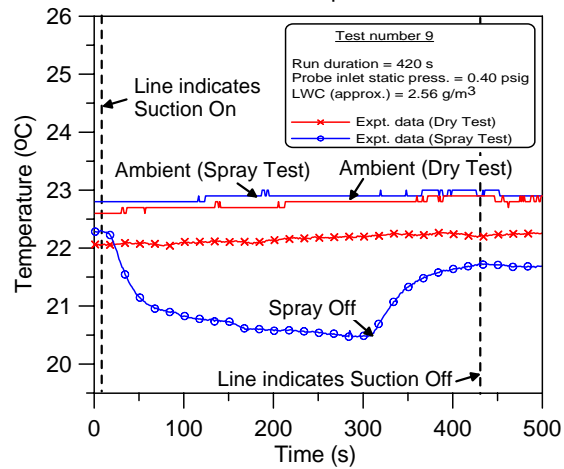
FIGURE E-8. RESULTS FOR TEST 8



(a) Static Pressure Distribution



(b) Relative Humidity Distribution



(c) Temperature Distribution

FIGURE E-9. RESULTS FOR TEST 9

## APPENDIX F—FUNDAMENTAL HUMIDITY EQUATIONS

The following describes the humidity relationships that were used to calculate the amount of evaporated water that had entered the reference probe (also known as ingress water). They are written as follows:

$$RH = E_v / E_{sat}(T) \quad (F-1)$$

$$W = M_v / M_d = (R_v / R_L) \{E_v / (P - E_v)\} \quad (F-2)$$

$$RH_{sp} = M_v / M_h \quad (F-3)$$

Defining

$$M_h = (M_v + M_d) \quad (F-4)$$

Therefore

$$\begin{aligned} M_h / M_d &= (M_v + M_d) / M_d \\ &= (M_v / M_d) + 1 \end{aligned} \quad (F-5)$$

Substituting equation F-2 gives

$$= W + 1 \quad (F-6)$$

Rewriting equation F-3 and substitute equation F-4 gives

$$RH_{sp} = (M_v / M_d) / (M_h / M_d) = W / (W + 1) \quad (F-7)$$

Hence,

$$M_v = RH_{sp} \times M_h \quad (F-8)$$

where,

$RH$  = relative humidity (recorded by humidity sensor)

$E_v$  = vapour pressure (contributed by the ambient vapor and/or evaporated mass from a spray cloud)

$E_{sat}(T)$  = saturated vapor pressure at a given temperature

$W$  = mixing ratio (grams of water vapor/grams of dry air)

$(R_v/R_L)$  = ratio of gas constant of water vapor and dry air (= 0.622)

$P$  = ambient pressure

$RH_{sp}$  = specific humidity (ratio of the mass of water vapor (g) to the mass of humid air (g))

$M_v$  = mass of water vapor (contributed by the ambient vapor and/or evaporated mass from a spray cloud)

$M_h$  = mass of humid air (environmental air consisted of water vapor and dry air)

$M_d$  = mass of dry air